

# The Higgs Boson in the Standard Model

---

## From LEP to LHC: Expectations, Searches, and Discovery of a Candidate

S. Dittmaier and M. Schumacher

Physikalisches Institut, Albert-Ludwigs-Universität Freiburg,  
Hermann-Herder-Strasse 3, 79104 Freiburg im Breisgau, Germany

March 28, 2013

### Abstract

The quest for the Higgs boson of the Standard Model, which was a cornerstone in the physics programme at particle colliders operating at the energy frontier for several decades, is the subject of this review. After reviewing the formulation of electroweak symmetry breaking via the Higgs mechanism within the Standard Model, the phenomenology of the Higgs boson at colliders and the theoretical and phenomenological constraints on the Standard Model Higgs sector are discussed. General remarks on experimental searches and the methodology of statistical interpretation are followed by a description of the phenomenology of Higgs-boson production and the corresponding precise predictions. The strategies of the experimental searches and their findings are discussed for the Large Electron Positron Collider (LEP) at CERN, the proton–antiproton collider Tevatron at Fermilab, and the proton–proton Large Hadron Collider (LHC) at CERN. The article concludes with the description of the observation of a Higgs-like boson at the LHC.

# Contents

<b>1</b>	<b>Introduction</b>	<b>3</b>
<b>2</b>	<b>The Standard Model Higgs boson</b>	<b>4</b>
2.1	The gauge structure of the Standard Model . . . . .	4
2.2	Electroweak symmetry breaking and the Higgs mechanism . . . . .	5
2.3	Yukawa couplings and fermion masses . . . . .	7
2.4	From input parameters to predictions for collider experiments . . . . .	8
2.5	Theoretical and phenomenological constraints on the Higgs sector . . . . .	11
2.6	Higgs-boson decays . . . . .	16
<b>3</b>	<b>General considerations for Higgs-boson searches</b>	<b>20</b>
3.1	Challenges . . . . .	20
3.2	Statistical interpretation of search results . . . . .	22
<b>4</b>	<b>Higgs-boson production at <math>e^+e^-</math> colliders</b>	<b>27</b>
<b>5</b>	<b>Searches at LEP</b>	<b>30</b>
5.1	The LEP1 era . . . . .	30
5.2	The LEP2 era . . . . .	34
<b>6</b>	<b>Higgs-boson production at hadron colliders</b>	<b>39</b>
6.1	Higgs-boson production mechanisms and cross-section overview . . . . .	39
6.2	Survey of precision calculations . . . . .	42
6.3	Towards couplings analyses after discovery . . . . .	46
<b>7</b>	<b>Searches at Tevatron</b>	<b>47</b>
7.1	Overview of search channels . . . . .	48
7.2	Searches for $H \rightarrow b\bar{b}$ . . . . .	49
7.3	Searches for $H \rightarrow W^+W^- \rightarrow \ell^+\nu\ell^-\bar{\nu}$ . . . . .	51
7.4	Preliminary combined results . . . . .	52
<b>8</b>	<b>Searches at the LHC</b>	<b>54</b>
8.1	Search with data collected in 2010 . . . . .	55
8.2	Searches with data collected in 2011 and up to June in 2012 . . . . .	55
8.3	Excluded mass ranges . . . . .	62
8.4	Observation of a new particle . . . . .	64
8.5	Anatomy of the new particle . . . . .	65
<b>9</b>	<b>Conclusions and outlook</b>	<b>66</b>
	<b>References</b>	<b>68</b>

# 1 Introduction

## Electroweak history in a nutshell

More than 40 years ago the standard theory of electroweak interaction [1], the Glashow–Salam–Weinberg model, emerged from a longer theoretical development, starting from the old Fermi theory in the 1930s, being generalized to a phenomenological model of intermediate massive vector bosons, and finally receiving the form of a spontaneously broken gauge theory in the 1960s. In those days the last bottleneck in the mathematically consistent construction of the electroweak theory was the merge of the successful Yang–Mills structure for the interaction of vector bosons with fermions with the experimental fact that the weak vector bosons possess mass. A historical milestone in this development was laid with the realization that a spontaneous breakdown of the gauge symmetry, driven by a self-interacting scalar field, can lend mass to gauge bosons—an idea nowadays known as the “Englert–Brout–Higgs–Guralnik–Hagen–Kibble (EBHGHK) mechanism” or simply “Higgs mechanism”.

In the early 1960’s it was realized by Nambu, Goldstone, Salam and Weinberg [2] that the spontaneous breakdown of a *global* continuous symmetry necessarily leads to the existence of a massless scalar (“Goldstone”) particle—a statement known as “Goldstone’s theorem”. This fact prevented theorists from associating the postulated massive weak vector bosons with a broken symmetry, because no corresponding Goldstone bosons had been observed. Later it was realized by Brout, Englert [3], Higgs [4], and Guralnik, Hagen, Kibble [5] that a spontaneous breakdown of a *local* continuous symmetry does not require Goldstone bosons, but rather their degrees of freedom deliver the longitudinal polarization modes of the gauge bosons that become massive. The understanding of this phenomenon, called the EBHGHK or Higgs mechanism, lead to the mathematical formulation of the class of spontaneously broken gauge field theories. In his second paper [4] P.W. Higgs stated “It is worth noting that an essential feature of the type of theory which has been described in this note is the prediction of incomplete multiplets of scalar and vector bosons.” It seems that it is this statement on the particle structure of such models that finally gave the Higgs particle its name.

The qualitative picture of the Higgs mechanism is that all massive elementary particles<sup>1</sup> interact with the vacuum, which is characterized by a non-vanishing expectation value of the *Higgs field*. This interaction with the vacuum prevents massive particles from acquiring the speed of light, in analogy to light rays proceeding through matter. At the same time, the Higgs field itself admits quantum-mechanical excitations which appear as new scalar particle types, the *Higgs bosons*.

Based on the understanding of the Higgs mechanism to lend masses to gauge bosons, Weinberg and Salam successfully completed Glashow’s model for the unified electroweak interaction to the spontaneously broken  $SU(2)\times U(1)$  gauge theory that still represents the heart of the electroweak part of our Standard Model (SM) of particle physics today. The remaining part of the SM is the gauge theory of strong interactions, known as quantum chromodynamics [6], which is based on the unbroken  $SU(3)$  colour gauge symmetry. The final breakthrough of gauge theories in particle physics came in the early 1970’s with the proof of their renormalizability, both for unbroken and broken symmetries by ’t Hooft, Veltman [7], Lee and Zinn-Justin [8]. This step raised gauge theories generally to the level of mathematically consistent quantum field theories, a fact that serves as our basis to work out predictions for collider experiments at a level of precision that is essentially only limited by our technical capabilities to evaluate higher orders in perturbation theory. Of course, some non-perturbative input is needed, such as parton distribution functions for hadronic collisions, but conceptually there is a solid field-theoretical basis.

---

<sup>1</sup>Here we understand that “elementary” means “point-like” and thus non-composite particles, because the mass of the latter typically receives large contributions from their binding energy. In the case of nucleons, the binding energy even comprises the major part of the mass.

## From theory to Higgs phenomenology and searches

The particle content of the SM comprises three charged leptons, three corresponding neutrinos, and six quarks in the sector of fermions. These “matter fermions” interact via the exchange of gauge bosons—the photon  $\gamma$  for electromagnetic interaction, the weak gauge bosons  $Z$  and  $W^\pm$ , and the eight gluons of the strong interaction. Apart from this particle content, which is experimentally established after the discoveries of the top quark at the Fermilab Tevatron in 1995 and of the  $\tau$  neutrino at the Fermilab DONUT experiment in 2000, there is just one postulated electrically neutral Higgs boson in the SM which is the phenomenological footprint of the Higgs mechanism. Since masses play the role of coupling strengths between particles and the vacuum, and Higgs bosons appear as “vacuum excitations”, the coupling of the Higgs boson to any other particle is predicted to be proportional to the particle’s mass term in the field equations. A phenomenological confirmation of the Higgs mechanism, thus, requires finding the Higgs boson(s), measuring its/their quantum numbers such as spin and electrical charge, and finally verifying the proportionality of the Higgs coupling to the mass of the attached particle. Once a value for the hypothetical Higgs-boson mass is assumed, the profile of the SM Higgs boson is completely fixed, and precision predictions are possible for production and decay rates and signal process kinematics. Based on these precise predictions experimental searches have been performed for the signature of the SM Higgs boson at colliders operating at the energy frontier. It took 25 years after the formulation of the Higgs mechanism until a significant mass range could be probed with the start of the operation of the Large Electron Positron Collider (LEP) at CERN in 1989. The search was continued at the Tevatron proton–antiproton collider from 2002 to 2011 at Fermilab. In 2010 the Large Hadron Collider (LHC) started to take data in proton–proton collisions at unprecedented CM energies with a primary goal of finally answering the question of whether a SM Higgs boson is realized in nature or not.

## 2 The Standard Model Higgs boson

Before we enter a thorough discussion of the phenomenology of the Higgs boson in the SM of particle physics, we briefly review the general structure of the model. Here we focus on the features of the SM that are most relevant for Higgs-boson phenomenology and refer to standard textbooks such as Refs. [9–13] for more details and theoretical background.

### 2.1 The gauge structure of the Standard Model

The Lagrangian  $\mathcal{L}_{\text{SM}}$  of the SM can be divided into four different parts,

$$\mathcal{L}_{\text{SM}} = \mathcal{L}_{\text{YM}} + \mathcal{L}_{\text{ferm}} + \mathcal{L}_{\text{H}} + \mathcal{L}_{\text{Yuk}}, \quad (1)$$

which will be discussed one by one in the following. We start with the first two, which contain the dynamics of the gauge bosons and matter fermions as predicted by the unbroken gauge symmetry, before we turn to the latter two which involve the Higgs field.

The Yang–Mills part  $\mathcal{L}_{\text{YM}}$  describes the genuine dynamics of the gauge fields, i.e. their free propagation as well as their self-interactions,

$$\mathcal{L}_{\text{YM}} = -\frac{1}{4}W_{\mu\nu}^i W^{i,\mu\nu} - \frac{1}{4}B_{\mu\nu} B^{\mu\nu} - \frac{1}{4}G_{\mu\nu}^a G^{a,\mu\nu}, \quad (2)$$

where

$$\begin{aligned} W_{\mu\nu}^i &= \partial_\mu W_\nu^i - \partial_\nu W_\mu^i - g\epsilon^{ijk}W_\mu^j W_\nu^k, & i, j, k &= 1, 2, 3, \\ B_{\mu\nu} &= \partial_\mu B_\nu - \partial_\nu B_\mu, \\ G_{\mu\nu}^a &= \partial_\mu G_\nu^a - \partial_\nu G_\mu^a - g_s f^{abc}G_\mu^b G_\nu^c, & a, b, c &= 1, \dots, 8, \end{aligned} \quad (3)$$

are the field-strength tensors of the gauge fields  $W_\mu^i$  for the  $SU(2)_I$  group of the weak isospin  $I_w^i$ ,  $B_\mu$  for the  $U(1)_Y$  of weak hypercharge  $Y_w$ , and  $G_\mu^a$  for the  $SU(3)_c$  of colour. The respective gauge couplings of these groups are denoted  $g$ ,  $g'$ , and  $g_s$ , and the structure constants of the non-abelian groups  $SU(2)$  and  $SU(3)$  are  $\epsilon^{ijk}$  and  $f^{abc}$ , following the usual notation.

The interaction of the gauge fields with the fermions is encoded in

$$\mathcal{L}_{\text{ferm}} = i\bar{\Psi}_L \not{D}\Psi_L + i\bar{\psi}_{\ell_R} \not{D}\psi_{\ell_R} + i\bar{\Psi}_Q \not{D}\Psi_Q + i\bar{\psi}_{u_R} \not{D}\psi_{u_R} + i\bar{\psi}_{d_R} \not{D}\psi_{d_R}, \quad (4)$$

where  $L = (\nu_{\ell_L}, \ell_L)^T$  are the left-handed  $SU(2)_I$  doublets of charged leptons  $\ell = e, \mu, \tau$  and neutrinos  $\nu_\ell = \nu_e, \nu_\mu, \nu_\tau$ ,  $Q = (u_L, d_L)^T$  the left-handed  $SU(2)_I$  doublets of up-type quarks  $u = u, c, t$  and down-type quarks  $d = d, s, b$ , and  $\ell_R, u_R, d_R$  are the respective right-handed  $SU(2)_I$  singlets.<sup>2</sup> The actual interaction is contained in the covariant derivative

$$D_\mu = \partial_\mu + igI_w^i W_\mu^i + ig' \frac{Y_w}{2} B_\mu + ig_s T_c^a G_\mu^a, \quad (5)$$

where  $I_w^i$ ,  $Y_w$ , and  $T_c^a$  are the generators of the respective gauge groups in the representation of the fermions they act on, i.e.  $I_w^i = \sigma^i/2$  ( $\sigma^i =$  Pauli matrices) for the left-handed  $SU(2)_I$  doublets and  $I_w^i = 0$  for the right-handed singlets, the weak hypercharge  $Y_w$  (= numbers) is related to the relative electric charge  $Q$  by the Gell-Mann–Nishijima relation  $Q = I_w^3 + Y_w/2$ , and  $T_c^a = \lambda^a/2$  ( $\lambda^a =$  Gell-Mann matrices) for  $SU(3)_c$  quark triplets and  $T_c^a = 0$  for the leptons. The requirement that the coupling structure of the photon is parity blind and proportional to  $Q\bar{\psi}A\psi$ , as in quantum electrodynamics, identifies the photon field  $A_\mu$  and the Z-boson field  $Z_\mu$  by the rotation

$$\begin{pmatrix} Z_\mu \\ A_\mu \end{pmatrix} = \begin{pmatrix} c_w & -s_w \\ s_w & c_w \end{pmatrix} \begin{pmatrix} W_\mu^3 \\ B_\mu \end{pmatrix} \quad (6)$$

with the weak mixing angle  $\theta_w$  and electric unit charge  $e$  fixed by

$$\cos \theta_w = c_w = \sqrt{1 - s_w^2} = \frac{g}{\sqrt{g^2 + (g')^2}}, \quad e = \frac{gg'}{\sqrt{g^2 + (g')^2}}. \quad (7)$$

Once the photon is identified among the gauge fields, it is easy to see that the fields

$$W_\mu^\pm = (W_\mu^1 \mp iW_\mu^2)/\sqrt{2} \quad (8)$$

correspond to the charged weak gauge bosons  $W^\pm$  of charge  $\pm e$ .

Note that the part of the SM described so far, encoded in  $\mathcal{L}_{\text{YM}} + \mathcal{L}_{\text{ferm}}$ , does not involve any mass terms. Naive gauge-boson mass terms, such as  $W_\mu^i W^{i,\mu}$  for the W bosons, obviously violate gauge invariance. Since left- and right-handed fermions transform differently under  $SU(2)_I \times U(1)_Y$  gauge transformations, naive fermion mass terms  $\propto (\bar{\psi}_{f_L} \psi_{f_R} + \bar{\psi}_{f_R} \psi_{f_L})$  for a fermion  $f$  are also ruled out by gauge invariance. The introduction of particle masses, while still maintaining the gauge invariance of the dynamics of the model, requires extensions of the theory.

## 2.2 Electroweak symmetry breaking and the Higgs mechanism

The Higgs part

$$\mathcal{L}_H = (D_\mu \Phi)^\dagger (D^\mu \Phi) - V(\Phi) \quad (9)$$

of the Lagrangian extends the experimentally well established particle content of the SM by the complex scalar  $SU(2)_I$  doublet  $\Phi = (\phi^+, \phi^0)^T$  of weak hypercharge  $Y_{w,\Phi} = 1$ , so that  $\phi^+$  carries charge  $+e$  and

---

<sup>2</sup>Right-handed neutrinos are omitted, since they do not play any role at high-energy colliders.

$\phi^0$  is neutral. In total  $\Phi$  involves four real degrees of freedom. The self-interaction of  $\Phi$  is described by the potential

$$V(\Phi) = -\mu^2(\Phi^\dagger\Phi) + \frac{\lambda}{4}(\Phi^\dagger\Phi)^2, \quad (10)$$

whose form is constrained by gauge invariance and renormalizability of the model. The latter is guaranteed by the polynomial structure of degree four in the field components, the former by the  $\Phi$  dependence via the combination  $\Phi^\dagger\Phi$ , leaving only the two real free parameters  $\mu^2$  and  $\lambda$  in  $V$ . While  $\lambda > 0$  is required by vacuum stability, the sign of  $\mu^2$  is deliberately taken positive in order to force a non-vanishing vacuum expectation value (vev)  $\Phi_0$  of  $\Phi$ . Minimizing  $V$  yields the condition

$$\Phi_0^\dagger\Phi_0 = \frac{v^2}{2}, \quad v = 2\sqrt{\frac{\mu^2}{\lambda}}. \quad (11)$$

Requiring that the vev is electrically neutral, forces the upper component of  $\Phi_0$  to vanish, i.e.  $\Phi_0$  is fixed up to a phase, with the usual choice  $\Phi_0 = (0, v/\sqrt{2})^T$ . This freedom in choosing the vev  $\Phi_0$  of  $\Phi$  reflects the spontaneous breakdown of the  $SU(2)_I \times U(1)_Y$  symmetry down to the remaining electromagnetic  $U(1)_{\text{em}}$  invariance. Splitting off the vev from  $\Phi$ ,

$$\Phi = \begin{pmatrix} \phi^+ \\ \phi^0 = (v + H + i\chi)/\sqrt{2} \end{pmatrix}, \quad (12)$$

we reparametrize  $\Phi$  in terms of the real physical Higgs field  $H$  and the unphysical would-be Goldstone boson fields  $\phi^+$  and  $\chi$ , which are complex and real, respectively. The fact that  $\phi^+$  and  $\chi$  do not correspond to physical states can already be seen by the fact that they are connected to the vev by gauge transformations; in fact one can always find a gauge, known as the ‘‘unitary gauge’’, in which  $\phi^+$  and  $\chi$  vanish. Making use of this gauge and inserting the parametrization (12) of  $\Phi$  and the covariant derivative (5) with  $I_{w,\Phi}^i = \sigma^i/2$ ,  $Y_{w,\Phi} = 1$ ,  $T_{c,\Phi}^a = 0$  into the Higgs Lagrangian (9), we find

$$\mathcal{L}_{\text{H,U-gauge}} = \frac{1}{2}(\partial H)^2 + \frac{g^2}{4}(v + H)^2 W_\mu^+ W^{-,\mu} + \frac{g^2}{8c_w^2}(v + H)^2 Z_\mu Z^\mu + \frac{\mu^2}{2}(v + H)^2 - \frac{\lambda}{16}(v + H)^2, \quad (13)$$

which in particular contains bilinear terms in the gauge fields  $W^\pm$ ,  $Z$  and in the Higgs field  $H$ , i.e. mass terms for the corresponding weak gauge bosons  $W^\pm$  and  $Z$  as well as for the Higgs boson  $H$ . Identifying these masses according to

$$M_W = \frac{gv}{2}, \quad M_Z = \frac{M_W}{c_w}, \quad M_H = \sqrt{2\mu^2}, \quad (14)$$

we can eliminate the parameters  $\mu^2$ ,  $\lambda$ ,  $v$  completely and get

$$\begin{aligned} \mathcal{L}_{\text{H,U-gauge}} &= \frac{1}{2}(\partial H)^2 - \frac{1}{2}M_H^2 H^2 + M_W^2 W_\mu^+ W^{-,\mu} + \frac{1}{2}M_Z^2 Z_\mu Z^\mu \\ &\quad + gM_W H W_\mu^+ W^{-,\mu} + \frac{g^2}{4}H^2 W_\mu^+ W^{-,\mu} + \frac{gM_Z}{2c_w} H Z_\mu Z^\mu + \frac{g^2}{4c_w^2} H^2 Z_\mu Z^\mu \\ &\quad - \frac{gM_H^2}{4M_W} H^3 - \frac{g^2 M_H^2}{32M_W^2} H^4 + \text{const.}, \end{aligned} \quad (15)$$

where we have not spelled out an irrelevant constant. In summary, the SM makes the following important phenomenological predictions in the Higgs sector which can be tested experimentally:

- Associated to the Higgs field  $H$ , a physical neutral, spinless particle of mass  $M_H$  is postulated—the Higgs boson. Since it can be viewed as some kind of vacuum excitation, it carries the quantum

numbers of the vacuum and is thus even with respect to CP symmetry. Note that  $M_H$  is the only free SM parameter that is tied to a property of the Higgs boson, while the other parameters are fixed by the weak-gauge-boson masses and the gauge couplings. Theoretical and phenomenological constraints of  $M_H$  are discussed below.

- The ratio  $\rho = M_W^2/(c_w^2 M_Z^2)$  [14]<sup>3</sup> is equal to one, which is a non-trivial relation among the weak-gauge-boson masses and the gauge couplings  $g = e/s_w$  and  $g' = e/c_w$ . While  $\rho = 1$  in this form is used to define  $c_w = M_W/M_Z$  in the process of renormalization to all orders, it nevertheless has important phenomenological consequences. For instance, on top of the Z-boson resonance, as measured at LEP and SLD via  $e^+e^- \rightarrow Z \rightarrow f\bar{f}$ , an effective weak mixing angle can be defined for each fermion species  $f$ , usually quantified via  $\sin^2 \theta_{\text{eff}}^f$ , which can be measured from various asymmetries. The ratios  $\rho_f = M_W^2/(\cos^2 \theta_{\text{eff}}^f M_Z^2)$  thus are predicted to be equal to one up to radiative corrections, a fact that is experimentally confirmed at a level of better than  $10^{-3}$  [15].

The lowest-order property  $\rho = 1$  is not shared by all possible scalar sectors that can be employed to lend masses to the  $W^\pm$  and Z bosons. If not accidental or forced by fine-tuned parameters, it is rather a consequence of a ‘‘custodial symmetry’’ [16] of the scalar sector. In the SM this is an SO(4) symmetry of  $\mathcal{L}_H$  with respect to the exchange of the four real components of  $\Phi$ , which holds up to  $U(1)_Y$  gauge interactions and differences in the fermion masses within  $SU(2)_I$  doublets, both inducing custodial-symmetry-breaking effects, however, only in higher orders.

- The model predicts couplings of the Higgs boson to a massive weak gauge boson  $V = W, Z$  proportional to  $M_V^2/v$ , because the  $HV^\dagger V$  couplings originate from the factor  $(1 + H/v)^2$  multiplying the gauge-boson mass term in  $\mathcal{L}_H$ . Owing to the square in this factor, quartic couplings of two Higgs bosons and two gauge bosons are also predicted, which are proportional to  $M_V^2/v^2$ .
- Finally, triple and quartic Higgs-boson self-interactions are predicted, both scaling with  $M_H^2$ . Since these couplings are in one-to-one correspondence with the shape of the Higgs potential that drives electroweak (EW) symmetry breaking, an experimental reconstruction of these couplings from an analysis of scattering processes would be part of an ultimate phenomenological confirmation of the Higgs mechanism. However, since the relevant processes involve multi-Higgs-boson final states with very low cross sections, the LHC will at best be able to give qualitative results here.

## 2.3 Yukawa couplings and fermion masses

Renormalizability and gauge invariance of the SM Lagrangian allow for so-called Yukawa couplings of the Higgs doublet  $\Phi$  to all fermions. The most general form of these interactions is

$$\mathcal{L}_{\text{Yuk}} = -\bar{\Psi}_L G_\ell \psi_{\ell_R} \Phi - \bar{\Psi}_Q G_u \psi_{u_R} \tilde{\Phi} - \bar{\Psi}_Q G_d \psi_{d_R} \Phi + \text{h.c.}, \quad (16)$$

where ‘‘h.c.’’ means hermitian conjugate and  $\tilde{\Phi} = i\sigma^2 \Phi^* = ((\phi^0)^*, -\phi^-)^T$  denotes the charge-conjugate Higgs doublet with quantum numbers opposite to  $\Phi$ . The matrices  $G_f$  ( $f = \ell, u, d$ ) represent arbitrary complex  $3 \times 3$  matrices, i.e. at first sight  $\mathcal{L}_{\text{Yuk}}$  involves a large number of free parameters. However, most of them turn out to be not physically relevant and can be transformed to canonical values or eliminated by appropriate field redefinitions. We first note that each term in  $\mathcal{L}_{\text{Yuk}}$  involves terms that are bilinear in the fermion fields because  $\Phi$  and  $\tilde{\Phi}$  contain a constant piece in the form of the vev  $v$ . More precisely, the non-diagonal elements of  $G_f$  mix the left- and right-handed parts of the different generations of fermion type  $f = \ell, u, d$ , where  $\ell$  generically stands for charged leptons,  $u$  for up-type quarks, and  $d$  for down-type quarks. Owing to these mixing terms, a fermion of flavour  $f_i$  ( $i = 1, 2, 3$ ) of the  $i$ th generation oscillates into  $f_j$  of the other generations ( $j \neq i$ ) even during a free propagation in space and

---

<sup>3</sup>The ratio  $\rho$  is called  $\beta$  in Ref. [14].

time. This oscillation can be removed upon transforming the existing “flavour basis”  $(\psi_{f\tau,1}, \psi_{f\tau,2}, \psi_{f\tau,3})$  of left- and right-handed fields ( $\tau = \text{L, R}$ ) into a “mass basis”  $(\hat{\psi}_{f\tau,1}, \hat{\psi}_{f\tau,2}, \hat{\psi}_{f\tau,3})$  with a unitary matrix  $U$ ,

$$\hat{\psi}_{f\tau,i} = U_{ij}^{f\tau} \psi_{f\tau,j}, \quad f = \ell, u, d, \quad \tau = \text{L, R}, \quad (17)$$

where in this process the matrices  $G_f$  receive a diagonal form,

$$U^{f\text{L}} G_f (U^{f\text{R}})^\dagger = \frac{\sqrt{2}}{v} \text{diag}\{m_{f_1}, m_{f_2}, m_{f_3}\}. \quad (18)$$

The diagonal value  $m_{f_i}$ , which can be chosen non-negative by convention, is the mass of the fermion  $f_i$ . For completeness we mention that the left-handed neutrino fields are transformed with the same unitary matrix as their charged counterparts; this is possible as long as we work in the approximation of three massless (i.e. mass-degenerate) neutrinos. The effect of this field redefinition on the whole SM Lagrangian can be summarized easily: (i) The coupling matrices  $G_f$  are replaced by their diagonal form (18); (ii) all fermion fields  $\psi_{f\tau,i}$  are replaced by their counterparts  $\hat{\psi}_{f\tau,i}$  of the mass basis; (iii) the only remnant of the  $U$  matrices is the appearance of the Cabibbo–Kobayashi–Maskawa matrix  $V = U^{u\text{L}}(U^{d\text{L}})^\dagger$  in fermion chains of type  $\hat{\psi}_{u\text{L}} \dots V \hat{\psi}_{d\text{L}}$  and of  $V^\dagger$  in  $\hat{\psi}_{d\text{L}} \dots V^\dagger \hat{\psi}_{u\text{L}}$ . In other words, only charged-current interactions receive modifications by  $V$ , while neutral currents remain unchanged. In the following we adopt the common convention to omit the clumsy hats on fermionic fields and assume the use of the mass basis.

In the unitary gauge, where the would-be Goldstone fields are absent, the Yukawa Lagrangian takes the simple final form

$$\mathcal{L}_{\text{Yuk,U-gauge}} = - \sum_f m_f (\bar{\psi}_{f\text{L}} \psi_{f\text{R}} + \bar{\psi}_{f\text{R}} \psi_{f\text{L}}) \left(1 + \frac{H}{v}\right), \quad (19)$$

where the sum over  $f$  runs over all fermion flavours of all generations. This form shows a distinctive footprint of the Higgs mechanism in the fermionic sector: The Higgs boson couples to each fermion  $f$  of mass  $m_f$  with the strength  $y_f = m_f/v$ . Moreover, the coupling is the one of a pure scalar, i.e. the coupling to fermions does not have any pseudo-scalar admixture proportional to  $\gamma_5$ . Testing these features offers a possibility to empirically tell a potential Higgs candidate from scalar particles predicted by other models. Alternative models with non-minimal Higgs sectors often predict new pseudoscalars as well, or even scalar particles without definite CP quantum numbers. Moreover, the strict proportionality of the Yukawa coupling strength to the fermion masses might be broken, as it is for instance the case in (type-II) Higgs doublet models, where the proportionality factor between  $y_f$  and  $m_f$  is different for up- and down-type fermions.

## 2.4 From input parameters to predictions for collider experiments

### Running parameters and renormalization scale

Like any gauge-field theory, the SM involves ultraviolet (UV) divergences that are removed in the process of renormalization which ties the input parameters of the theory to measurable quantities at some renormalization scale  $\mu_{\text{R}}$ . The input parameters, which are taken from experiment, in this sense depend on the arbitrary value of  $\mu_{\text{R}}$  as well as on more details that fix the actual procedure, thereby defining the *renormalization scheme*. The fact that predicted physical observables, on the other hand, cannot depend on  $\mu_{\text{R}}$  is expressed in terms of renormalization group equations (RGE) for each scheme (if it allows for a flexible renormalization scale). Solving these RGE for any field-theoretical quantity naturally involves the concept of running, i.e.  $\mu_{\text{R}}$ -dependent, parameters, such as the famous strong coupling  $\alpha_s(\mu_{\text{R}})$ . The running of each parameter from one scale to another can be predicted



in perturbation theory. In actual predictions of observables, thus, there is an *explicit* and an *implicit* dependence on  $\mu_R$ , which compensate each other order by order in perturbation theory—the former resulting from the renormalization of the considered observable at the scale  $\mu_R$ , the latter from the input values matched to renormalized quantities at  $\mu_R$ . A residual  $\mu_R$  dependence arises from orders of perturbation theory that are not completely taken into account. If an observable involves a typical scale  $Q$ , such as a scattering cross section at energy  $Q$ , it is advisable to fix  $\mu_R$  in the vicinity of  $Q$ , since this minimizes potentially large missing corrections that involve powers of logarithms  $\ln(Q/\mu_R)$ . If a process involves many different scales, the benefit of adjusting  $\mu_R$  is limited. For the precise mathematical formulation of this concept we refer to standard literature on quantum field theory such as Refs. [9–13].

## The input parameters of the SM

As is obvious from the construction of the model, the free input parameters of the SM are the gauge couplings  $g$ ,  $g'$ ,  $g_s$ , the parameters  $\mu^2$  and  $\lambda$  of the Higgs sector, the fermion masses  $m_f$ , and the CKM matrix  $V$ . For phenomenology it is much more convenient to take instead the following parameters as input: the electromagnetic coupling  $\alpha = e^2/(4\pi)$ , the strong couplings constant  $\alpha_s = g_s^2/(4\pi)$ , the weak gauge-boson masses  $M_W$  and  $M_Z$ , the Higgs-boson mass  $M_H$ , and finally  $m_f$  and  $V$ . The masses can all be defined as *pole masses*, defined from the locations of the particle poles in the respective propagators, but for the heavy quarks it is often useful to switch to a running mass at some appropriate scale. For Higgs physics, the CKM matrix plays a minor role. The couplings  $\alpha$  and  $\alpha_s$ , however, have to be chosen thoughtfully. The strong coupling is usually defined as running coupling  $\alpha_s(\mu_R)$  in the so-called  $\overline{\text{MS}}$  scheme. Very often the value of  $\alpha_s$  at the Z pole,  $\alpha_s(M_Z)$ , is used as numerical input and transferred to some other value  $\mu_R$  using the RGE.

For the electromagnetic coupling  $\alpha$  basically the choice is between three different values: the fine-structure constant  $\alpha(0) \approx 1/137$ , the effective value  $\alpha(M_Z) \approx 1/129$ , where  $\alpha(0)$  is evolved via RGE from zero-momentum transfer to the Z pole, and an effective value derived from the Fermi constant  $G_\mu$  leading to  $\alpha_{G_\mu} = \sqrt{2}G_\mu M_W^2(1 - M_W^2/M_Z^2)/\pi \approx 1/132$ , defining the so-called “ $G_\mu$ -scheme”. The various values of  $\alpha$  differ by 2–6%. Very often the actual value of  $\alpha$  can be adjusted in such a way that large universal EW corrections are already absorbed into the lowest-order prediction. Even different values of  $\alpha$  can be appropriate in one calculation, but care has to be taken that the same choice is taken within gauge-invariant subsets of diagrams. An external photon (virtuality  $Q^2 = 0$ ) always effectively couples with  $\alpha(0)$ , while internal photons with virtuality  $Q^2$  at a high energy scale effectively couple with  $\alpha(Q)$ , which is much closer to  $\alpha(M_Z)$ . On the other hand, the couplings of W and Z bosons should be parametrized with  $\alpha_{G_\mu}$ , which does not only take into account the running from  $Q = 0$  to the EW scale, but also universal effects from the  $\rho$ -parameter. Following these rules, in particular, avoids perturbative instabilities due to the appearance of light-quark masses, as e.g. discussed in Ref. [17].

## Predictions for hadronic collisions and factorization scale

Hadronic collisions are treated within the *QCD-improved parton model*, whose full description is beyond the scope of this review (see e.g. the standard textbooks [11–13]). In this framework hadronic cross sections are calculated in the factorized form

$$\sigma_{h_1 h_2} = \sum_{a,b} \int_0^1 dx_1 \int_0^1 dx_2 f_{a/h_1}(x_1, \mu_F) f_{b/h_2}(x_2, \mu_F) \int d\hat{\sigma}_{a_1 a_2}(x_1 P_1, x_2 P_2, \mu_F), \quad (20)$$

where the parton distribution functions (PDFs)  $f_{a_i/h_i}(x_i, \mu_F)$  are generalized probability densities for finding a parton  $a_i$  (quarks, antiquarks, gluons, photons) with momentum  $p_i = x_i P_i$  in the hadron  $h_i$  which has momentum  $P_i$ . The PDFs comprise the soft physics, which is dominated by small energy scales and not accessible by perturbation theory, and are process independent. The partonic cross sections  $d\hat{\sigma}_{a_1 a_2}$ , on the other hand, contain the full information on the hard scattering reaction of the partons

into a specific final state and can be calculated within perturbation theory. The separation of the soft and hard domains is performed at the *factorization scale*  $\mu_F$ , which effectively is the upper bound on transverse momenta up to which outgoing hadronic particles are considered as parts of the struck hadron. Similar to  $\mu_R$ , the scale  $\mu_F$  is arbitrary to a large extent, and predictions—if calculated to arbitrary precision—cannot depend on it. In  $d\hat{\sigma}_{a_1 a_2}(x_1 P_1, x_2 P_2, \mu_F)$  the value of  $\mu_F$  can be trivially changed, in the PDFs the change of  $\mu_F$  is governed by the so-called Dokshitzer–Gribov–Lipatov–Altarelli–Parisi (DGLAP) evolution, which ensures the  $\mu_F$ -independence of observables. Again a truncation of the perturbative series for  $d\hat{\sigma}_{a_1 a_2}$ , however, leads to some residual  $\mu_F$  dependence of observables, which is part of the intrinsic uncertainty in predictions.

The PDFs cannot be calculated from first principles, but are fitted to a large variety of data resulting from lepton–hadron and hadron–hadron collisions. State-of-the-art PDF sets are provided by several groups: CT10 [18], MSTW2008 [19], NNPDF2.1 [20], ABKM11 [21], GJR08 [22], and HERA-PDF1.5 [23]. Generally, there is good agreement between predictions, e.g. for the LHC, based on those PDF sets, in particular between CT10, MSTW2008, and NNPDF2.1, and differences between the PDF sets are continuously analyzed. More details and references on PDFs and their application to Higgs physics at the LHC can be found in Refs. [24–26]. In practice, each perturbative order requires its own set of PDFs for consistency, i.e. a LO cross section  $\sigma_{\text{LO}}$  has to be evaluated with LO PDFs and the corresponding one-loop running  $\alpha_s(\mu)$ ,  $\sigma_{\text{NLO}}$  with NLO PDFs and two-loop  $\alpha_s(\mu)$ , etc. In this context, QCD corrections are often quantified by the *K-factor*

$$K = \frac{\sigma^{(\text{N})\text{NLO}}}{\sigma_{\text{LO}}}, \quad (21)$$

resulting from the cross sections consistently calculated in different orders. While up-to-date PDF sets are available in LO, NLO, and NNLO QCD, no current PDF set includes EW corrections, i.e. EW corrections are both missing in the PDF fit to data as well as in the  $\mu_F$ -evolution of the PDFs. The older PDF set MRST2004QED [27] includes these effects, but is outdated otherwise. It is, thus, more advisable to use up-to-date PDFs, since ignoring EW PDF corrections typically introduces uncertainties of the level of  $\lesssim 1\%$  only [28].<sup>4</sup>

## Parametric and theoretical uncertainties

*Parametric uncertainties* arise from the errors of the input parameters of the SM model. For observables that involve strongly interacting objects the largest errors usually originate from the uncertainties of the strong coupling constant  $\alpha_s$  and of the masses of the heavy quarks that are possibly directly involved. In observables based on the EW interaction often the uncertainty of the electromagnetic coupling  $\alpha$  becomes significant if it is derived from the value of the running coupling  $\alpha(Q^2)$  at high energies, such as  $\alpha(M_Z^2)$ . Parametric errors of different observables are usually correlated, which has to be respected when their effect is combined.

For hadronic collisions the PDFs are very often the largest source of parametric uncertainties, which are also correlated with  $\alpha_s$ . The various groups who deliver regular updates of PDFs fitted to data provide different “error sets” of PDFs whose spread quantifies the PDF uncertainty. These error PDFs also allow for a combined assessment of the PDF+ $\alpha_s$  error of observables. A proposal how to combine errors from PDFs of different groups can be found in the report of the PDF4LHC Working Group [24].

*Theoretical uncertainties* can be—to some extent—quantified by the “scale uncertainties” mentioned above. The compensation between explicit and implicit  $\mu_R$  and/or  $\mu_F$  dependences remains necessarily incomplete in perturbative calculations, because in practice not all (but only few) perturbative orders can be calculated completely. Thus, a residual scale dependence remains in predictions, and, if the scales

---

<sup>4</sup>Though outdated, the MRST2004QED PDF set is, however, the only one that provides a photon PDF and, thus, offers the opportunity to at least approximately calculate the effect from partonic channels involving initial-state photons.

are varied within a reasonable range, the corresponding variation in the result quantifies theoretical uncertainties originating from missing higher-order effects. One should, however, keep in mind that not all missing corrections are sensitive to the residual scale dependences. For instance, missing finite corrections depend on  $\mu_R$  only very weakly, but might be large. Thus, overdoing a minimization of the residual scale dependence does not remove the uncertainties, but rather tends to hide them.

Finally, parametric uncertainties and theoretical uncertainties have to be combined. Since theoretical uncertainties have no true statistical meaning that is safely tied to a probability distribution, the two errors should not be added in quadrature, but linearly. A possible procedure to do that for Higgs observables at the LHC was, e.g., proposed in Ref. [25].

## 2.5 Theoretical and phenomenological constraints on the Higgs sector

Although the mass  $M_H$  of the Higgs boson represents a free parameter of the SM, it cannot assume arbitrary values. In the following we briefly summarize the bounds on  $M_H$  from above and below that originate from theoretical considerations and phenomenological constraints.

### The heavy-Higgs limit of the SM

Before looking more closely into the phenomenology of Higgs bosons, it is interesting to discuss the behaviour of the model in the limit  $M_H \rightarrow \infty$ , which means that  $M_H$  is supposed to be much larger than any other mass or energy scale involved in the considered physical system. In this limit the Higgs boson is effectively removed from the physical particle spectrum, but its vev still delivers the masses to the weak gauge bosons and massive fermions. Formally the Higgs potential tends to a delta function proportional to  $\delta(\Phi^\dagger\Phi - \Phi_0^\dagger\Phi_0)$ , i.e. the absolute value of the Higgs doublet field is constrained to its vev. This constrained scalar sector is more conveniently described in the framework of non-linear representations of the doublet  $\Phi$ , where the physical Higgs boson plays the role of the radial excitation in the space of its four real components and gets fixed by the delta function.

To illustrate this, we first rephrase the Higgs Lagrangian (9) in matrix notation,

$$\mathcal{L}_H = \frac{1}{2}\text{tr}\{(D_\mu\Phi)^\dagger(D^\mu\Phi)\} - V(\Phi), \quad D_\mu\Phi = \partial_\mu\Phi + i\frac{g}{2}\sigma^i W_\mu^i\Phi - i\frac{g'}{2}\Phi\sigma^3 B_\mu, \quad (22)$$

where the hermitian matrix field  $\Phi$  is given by

$$\Phi = \frac{1}{\sqrt{2}}[(v+H)\mathbf{1} + i\phi^i\sigma^i] = \begin{pmatrix} (v+H-i\chi)/\sqrt{2} & \phi^+ \\ -\phi^- & (v+H+i\chi)/\sqrt{2} \end{pmatrix} = (\tilde{\Phi}, \Phi), \quad (23)$$

with  $\sigma^i$  again denoting the Pauli matrices and the real scalar fields  $\phi^i$ , which are defined by  $\phi^\pm = (\phi^2 \pm i\phi^1)/\sqrt{2}$  and  $\chi = -\phi^3$ . In this linear representation the Lagrangian and the meaning of the scalar field components are exactly the same as described before, only the bookkeeping is somewhat different. The non-linear representation of  $\Phi$  parametrizes the matrix field according to

$$\Phi = \frac{1}{\sqrt{2}}(v+H)U, \quad U = \exp\left\{\frac{i\sigma^i\phi^i}{v}\right\}, \quad (24)$$

which results from the linear parametrization upon a non-trivial field transformation. In this parametrization the field  $H$  is gauge invariant. Inserting the non-polynomial field  $\Phi$  into the Higgs Lagrangian (22), leads to a theory that is physically equivalent to the SM with the more common linear Higgs representation [29], i.e. the  $S$ -matrix is the same in the linear and non-linear representations, although the Green functions do not coincide. The new form of the Higgs Lagrangian is

$$\mathcal{L}_{H,\text{nl}} = \frac{1}{4}(v+H)^2\text{tr}\{(D_\mu U)^\dagger(D^\mu U)\} + \frac{1}{2}(\partial_\mu H)(\partial^\mu H) + \frac{\mu^2}{2}(v+H)^2 - \frac{\lambda}{16}(v+H)^4. \quad (25)$$

Note that here the fields  $\phi^i$  of the unphysical Goldstone bosons, which are contained in the matrix  $U$ , appear only in their dynamical part  $\propto \text{tr}|DU|^2$ , but not in the Higgs potential, where only  $(v + H)$  survives owing to the unitarity of  $U$ . For this reason this form is very attractive for the discussion of the heavy-Higgs-boson limit, even in gauges different from the unitary gauge, which corresponds to  $U = \mathbf{1}$ .

To lowest order of perturbation theory, the heavy-Higgs-boson limit of  $\mathcal{L}_{\text{H,nl}}$  is reached upon setting the Higgs field  $H$  to zero, since all Higgs propagators are suppressed by factors  $1/M_{\text{H}}^2$  in amplitudes—a suppression that cannot be compensated by the  $M_{\text{H}}^2$  factors in the Higgs self-couplings, since there are always more Higgs propagators than Higgs self-couplings in amplitudes without external Higgs bosons. In other words, a heavy Higgs boson decouples in tree-level amplitudes. The resulting theory without a Higgs field is called the *gauged non-linear sigma model* [30] and described by the scalar Lagrangian

$$\mathcal{L}_{\sigma,\text{nl}} = \frac{1}{4}v^2\text{tr}\{(D_\mu U)^\dagger(D^\mu U)\} = \mathcal{L}_{\text{H,nl}}(H = 0). \quad (26)$$

This model is equivalent to the SM in the unitary gauge without Higgs boson, but still represents an  $\text{SU}(2)_{\text{I}} \times \text{U}(1)_{\text{Y}}$  gauge theory. The model, though, is physically unsatisfactory, since it is neither renormalizable, nor does its  $S$ -matrix respect unitarity. In fact these two short-comings are closely related, as shown in Ref. [31].

Beyond leading order, a heavy Higgs boson does not decouple anymore in amplitudes, a fact that is visible in the different UV behaviour of the SM with and without Higgs boson—the latter being the gauged non-linear sigma model. While the SM with Higgs boson is renormalizable, i.e. closed in the UV sector, the gauged non-linear sigma model is non-renormalizable, i.e. incomplete in the UV sector and thus at best can serve as an effective field theory up to some finite energy. Thus, removing the Higgs boson from the SM particle content upon increasing its mass more and more,  $M_{\text{H}}$  effectively works as UV cutoff scale for the UV divergences of the gauged non-linear sigma model. Specifically, using regularization in  $D$  dimensions the uncanceled one-loop UV poles  $1/(D - 4)$  of the sigma model are in one-to-one correspondence with one-loop corrections involving  $\ln M_{\text{H}}$  in the heavy-Higgs SM. At one loop, these non-decoupling effects of a heavy Higgs boson have been quantified in terms of effective Lagrangians in the literature [32], keeping also finite terms that are not suppressed by powers of  $M_{\text{H}}$ . At higher loop orders, non-decoupling effects can even grow with powers of  $M_{\text{H}}^2$ , as e.g. seen in heavy-Higgs corrections  $\propto M_{\text{H}}^2$  and  $M_{\text{H}}^4$  to the  $\rho$ -parameter at the two-loop [33] and three-loop level [34], respectively, suggesting a scaling law of  $M_{\text{H}}^{2(L-1)}$  at  $L$ -loop order, possibly modified by powers of  $\ln M_{\text{H}}$ .

The SM is of course not the only possible “UV closure” of the non-renormalizable non-linear  $\sigma$ -model. Any renormalizable model containing it bears some dimensionful quantity  $\Lambda$ , such as a particle mass, that acts effectively as cut-off for UV divergences, like the Higgs-boson mass in the SM. In the limit of large  $\Lambda$ , the same structure of  $\ln \Lambda$  terms will, thus, show up as in the heavy-Higgs SM with  $M_{\text{H}}$  playing the role of  $\Lambda$ .

### Constraints on $M_{\text{H}}$ from unitarity arguments

The unitarity of the  $S$ -matrix implies bounds on the high-energy behaviour of partial waves of  $2 \rightarrow 2$  scattering processes, but a naive power counting of energy factors in amplitudes with longitudinally polarized weak gauge bosons  $V_{\text{L}} = W_{\text{L}}^\pm, Z_{\text{L}}$  suggests that these bounds do not hold. The leading high-energy term in the longitudinal polarization vector  $\varepsilon_{V_{\text{L}}}(k)$  of an external  $V_{\text{L}}$  with momentum  $k^\mu$ , which behaves  $\sim k^\mu/M_{\text{V}}$ , introduces a dangerous energy factor which seems to spoil the power counting. Unitarity is restored by cancellations that are governed by gauge invariance in the form of Slavnov–Taylor identities, which relate the  $k^\mu$  contraction of an external  $V_\mu$  leg of an amplitude to another amplitude in which  $V_{\text{L}}$  is replaced by the respective Goldstone-boson field  $\phi_{\text{V}}$ . Schematically an amplitude  $\mathcal{M}_{V_{\text{L}}\dots}$  behaves like

$$\mathcal{M}_{V_{\text{L}}\dots} = \varepsilon_{V_{\text{L}},\mu}(k) T_{V_{\text{L}}\dots}^\mu \underset{k^0 \gg M_{\text{V}}}{\sim} \frac{k_\mu}{M_{\text{V}}} T_{V_{\text{L}}\dots}^\mu = \mathcal{M}_{\phi_{\text{V}}\dots}, \quad (27)$$

where  $\mathcal{M}_{\phi_V\dots}$  is the “scattering amplitude” of  $\phi_V$  (defined with an appropriate phase) at high energies with a decent scaling law in the scattering energy, as demanded by unitarity. Equation (27) expresses the so-called Goldstone-boson equivalence theorem [31, 35], whose formulation to all orders requires some care [36].

It is interesting to note that the equivalence theorem can also be formulated within the gauged non-linear sigma model [37]. Since the non-polynomial structure of the Goldstone-boson Lagrangian (26) involves arbitrarily high powers of derivatives (momentum factors in amplitudes), however, the power-counting of energy factors in (27) does not lead to a decent high-energy behaviour of the amplitude  $\mathcal{M}_{V_L\dots}$ . Amplitudes  $\mathcal{M}_{V_L\dots}$  in fact potentially violate unitarity, both in the gauged non-linear sigma model and in the SM with a heavy Higgs boson,  $M_H \rightarrow \infty$ . In the unitary gauge, where no Goldstone-boson fields are present, the same conclusion is drawn from the “bad high-energy behaviour” of the W and Z propagators.

The violation of unitarity can already be observed in the SM with finite  $M_H$  if the  $M_H$  value is large enough. The larger  $M_H$ , the more delayed is the necessary unitarity cancellation for large  $k^0$ . If  $M_H$  is too large, the amplitude starts to “explode” before the damping due to Higgs-boson exchange sets in. In  $2 \rightarrow 2$  particle scattering, the most delicate unitarity cancellations occur in longitudinal vector-boson scattering  $V_L V_L \rightarrow V_L V_L$  whose tree-level amplitudes respect unitarity only if  $M_H \lesssim 1$  TeV [38]. Within pure perturbation theory it is not possible to give sharp unitarity limits on  $M_H$ , because the range around  $M_H \sim 1$  TeV represents the transition region where perturbation theory runs out of control in the Higgs sector due to the huge self-couplings.

### Triviality and vacuum-stability bounds

It is interesting to apply the concept of a running coupling to the Higgs-boson self-coupling  $\lambda$ . The running of  $\lambda(\mu_R)$  is mainly driven by loop corrections to the  $H^4$ -interaction involving the Higgs-boson self-couplings or top quarks with the largest Yukawa coupling. Present-day evaluations of  $\lambda(\mu_R)$  involve (at least) two-loop effects and RGE. The behaviour of the resulting running  $\lambda(\mu_R)$  at large values of  $\mu_R$  contains information on the scale  $\Lambda$  up to which the SM can exist as a self-consistent quantum field theory:

- For a large Higgs-boson mass the Higgs self-interactions drive  $\lambda(\mu_R)$  to larger values with increasing  $\mu_R$ , reflecting the lack of asymptotic freedom. Above some scale the coupling enters its non-perturbative domain, a fact that is most obvious at one-loop order where  $\lambda(\mu_R)$  even reaches a so-called Landau pole and diverges. At two-loop order the divergence is mitigated to a UV fixed-point, but at three-loop order a Landau pole is expected to appear again. More details on the running and matching issues can be found in Ref. [39]. Of course, the transition to the non-perturbative domain is a continuous process, so that only a generic scale  $\Lambda$  for the onset of this region can be given. The non-perturbative domain and the Landau pole could be avoided if the exchange of new particles (not part of the SM) in the loop corrections to the  $H^4$  interaction counterbalances the too rapid running induced by the graphs containing the Higgs self-couplings. Thus,  $\Lambda$  can be interpreted as a lower bound on the new-physics scale if the SM is supposed to stay in its perturbative regime. Being perturbative or non-perturbative is certainly not a physical criterion on a field theory. However, the appearance of a Landau pole does not only signal non-perturbativity, but also a mathematical inconsistency. Beyond the Landau pole the self-consistency of the field theory seems to require a scalar self-coupling  $\lambda$  that vanishes at all, leading to a *trivial* theory. The bound on  $\Lambda$  to avoid the Landau pole is, thus, also called the *triviality bound* [40]. We are not aware of a field-theoretical proof of the triviality of scalar field theories with  $\phi^4$  interactions, such as the SM, but the triviality hypothesis is supported by non-perturbative results from lattice field theory (see Ref. [41] and earlier references therein).

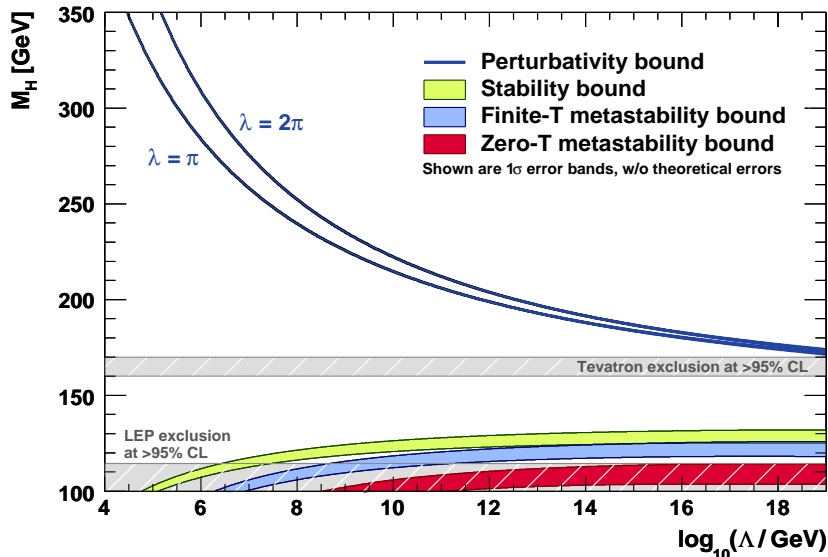


Figure 1: Perturbativity (triviality) upper bound and vacuum-stability lower bound on  $M_H$  as function of the scale  $\Lambda$  at which new physics has to appear (at the latest) in order to avoid the bounds (plot taken from Ref. [44]). The two different versions of the perturbativity bound reflects the intrinsic uncertainty of the limit, and the bands of the (meta)stability bounds reflect parametric uncertainties.

- For a small Higgs-boson mass the running of  $\lambda(\mu_R)$  is dominated by the top-quark loops which drive  $\lambda(\mu_R)$  even to negative values for large  $\mu_R$ . This fact has drastic consequences on the Higgs potential that determines the non-vanishing vev of the Higgs field. In lowest order the potential (10) still shows the asymptotics  $\propto \lambda H^4$ , but  $\lambda(\mu_R) < 0$  for large  $\mu_R$  indicates that higher-order effects bend the Higgs potential  $V$  over to negative values for large Higgs fields  $H$ , i.e. the potential is not bounded from below anymore. Thus, a stable vacuum does no longer exist, and the whole model becomes inconsistent. A thorough theoretical analysis of the vacuum structure goes beyond a pure running-coupling analysis and takes into account the leading static (for Higgs fields at zero momentum) all-order-resummed corrections to the Higgs potential  $V$ , leading to the so-called *effective Higgs potential*  $V_{\text{eff}}$  [42]. For small  $M_H$  the SM can escape the *vacuum-stability bound* [43] only if new-physics effects at some scale  $\Lambda$  modify the vacuum structure determined by  $V_{\text{eff}}$  in such a way that a stable vacuum exists. This results in a lower bound on  $M_H$  for a given value of  $\Lambda$ . The bound can be relaxed to some extent by assuming a metastable EW vacuum with a lifetime longer than the age of the Universe, where the vacuum decay may be mediated either by zero-temperature quantum fluctuations or thermal fluctuations.

Figure 1, which shows the results of the recent two-loop RGE analysis of Ref. [44], illustrates the upper and lower bounds on the SM Higgs-boson mass resulting from the hypothesis that the SM Higgs sector should be perturbative (and thus escapes the triviality bound) with a stable or at least metastable vacuum up to a potential new-physics scale  $\Lambda$ . A SM Higgs boson with  $M_H \lesssim 200$  GeV admits the SM to escape the non-perturbativity/triviality bound up to scales  $\Lambda \lesssim 10^{12}$  GeV, far above any energies reachable in collider experiments. On the other hand, the LEP exclusion limit  $M_H > 114.4$  GeV pushes the vacuum (meta)stability limit for the onset of new physics already to  $\Lambda \sim 10^6$  GeV, which is out of reach for colliders as well. For a Higgs boson within the mass window  $130 \text{ GeV} \lesssim M_H \lesssim 170 \text{ GeV}$  the SM would be surely consistent up to scales as high as the Planck scale  $\Lambda_{\text{Planck}} = 2 \times 10^{18}$  GeV, where gravity effects should become as large as the strong and EW interactions. Finally, interpreting the recent LHC discovery as a SM Higgs boson with  $M_H = 126$  GeV still allows the SM to be valid up to the Planck scale if our universe resides in a metastable phase.

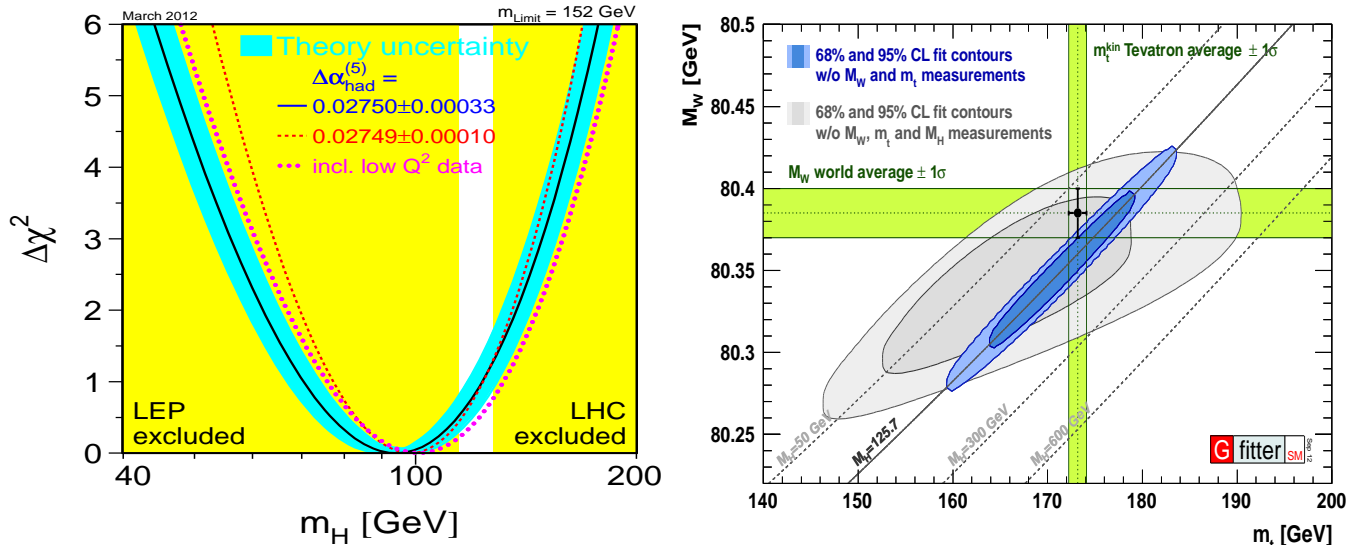


Figure 2: The “blueband plot” (left, taken from Ref. [45]) showing the result of a global  $\chi^2$  fit of the SM to precision data, projected onto the  $M_H$  axis and comparison of constraints on the top-quark and W-boson masses (right, taken from Ref. [46]) resulting from direct measurements and a global SM fit.

### Constraints from precision data

Experiments at LEP1, LEP2, SLC, and the Tevatron have performed a large variety of high-precision measurements, such as the determination of the W, Z, and top-quark masses and widths, measurements of cross sections and various asymmetries in the process  $e^+e^- \rightarrow \gamma^*/Z \rightarrow f\bar{f}$  at the Z pole, etc. These measurements characterize the past two decades as the era of EW precision physics. Parametrizing SM predictions as described in Section 2.4, thus, renders a fit of the complete SM to these data possible, which highly constrains the SM input parameters (with the exception of the CKM matrix, where dedicated observables from flavour physics are needed). Figure 2 shows, on the l.h.s., the status of March 2012 of such a fit projected on the Higgs-boson mass, together with the exclusion limits from the direct searches to be discussed later in detail. The blue band indicates theoretical uncertainties from missing higher-order corrections in the (numerous) underlying precision calculations, which were condensed into the state-of-the-art codes ZFITTER [47] and TOPAZ0 [48] (see also Ref. [49] for details and references). The best fit value together with its 68% CL limits for the Higgs-boson mass is  $M_H = 94_{-24}^{+29}$  GeV, being compatible with the open mass window  $122 \text{ GeV} < M_H < 127 \text{ GeV}$  (status July 2012, see Section 8.3) which is obtained from the 95% C.L. exclusion limits of the LHC from below and above, respectively. The r.h.s. of Figure 2 illustrates the SM overall fit, as obtained by the GFITTER [46]<sup>5</sup> collaboration, by its projection into the  $m_t - M_W$  plane and compares the preferred fit region with the directly measured values of the top-quark and W-boson masses. The shown SM prediction for  $M_W$  as function of  $m_t$  and  $M_H$  (diagonal lines for some fixed  $M_H$  values) is obtained from the measured muon lifetime (often translated into the Fermi constant  $G_\mu$ ). All these constraints on  $m_t$  and  $M_W$  are perfectly compatible with the recent observation of a Higgs-boson candidate of a mass around  $M_H = 126$  GeV, to be discussed in detail below.

<sup>5</sup>Similar results have been presented in Ref. [50].

## 2.6 Higgs-boson decays

The Higgs boson of the SM is unstable and predominantly decays into the heaviest particle–antiparticle pair that is kinematically possible depending on the available energy  $M_H$ . The search for the Higgs boson, which has to be reconstructed from its decay products in detectors, thus depends on the Higgs-boson mass, since the relevant final states strongly vary with  $M_H$ . Since the branching ratio  $\text{BR}(H \rightarrow X) = \Gamma_{H \rightarrow X}/\Gamma_H$ , which is the probability for the Higgs boson to decay into the final state  $X$ , weights the relevant Higgs-boson production cross section for the exclusive channel  $H \rightarrow X$ , theory has to provide precise predictions for all significant Higgs-boson decay widths—irrespective of whether the channel could be detected or not—since they all enter the total decay width  $\Gamma_H$ , which is the sum of all partial widths  $\Gamma_{H \rightarrow X}$ . To get the global picture we show the SM Higgs-boson branching ratios and the total decay width in Figures 3 and 4, where we separate the low- $M_H$  range that was accessible at the time of the  $e^+e^-$  collider LEP (Figure 3) from the  $M_H$  range that is challenged by the hadron colliders Tevatron and LHC (Figure 4). The relevant leading-order Feynman diagrams for the various decay channels are depicted in Figure 5. As anticipated above, the highest branching ratios typically correspond to decays into the heaviest particle–antiparticle pair that are kinematically allowed for a given value of  $M_H$ . However, as far as predictions are concerned, the regions where new channels become significant are theoretically delicate. For heavy-quark pairs the threshold regions are particularly sensitive to the heavy-quark masses whose proper perturbative treatment within QCD is highly non-trivial. For the Higgs-boson decays into the weak-gauge-boson pairs  $WW$  and  $ZZ$ , even the regions near and below the  $WW/ZZ$  thresholds become important which implies that the decays of the  $W/Z$  bosons have to be included in the predictions.

Owing to the proportionality of the Higgs couplings to the masses of the decay products, the total Higgs-boson width  $\Gamma_H$  stretches over many orders of magnitude, viz. from  $10^{-4}$  GeV for  $M_H \lesssim 10$  GeV to  $10^3$  GeV for  $M_H \sim 1$  TeV. Because of the finite energy resolution of detectors, the width of a light Higgs boson is too small to be resolved in invariant-mass distributions of its decay products. On the theoretical side this fact justifies the approach of dealing with stable, on-shell Higgs bosons in production processes and factorizing the subsequent decay from the production. For large invariant masses of the Higgs-boson decay products resulting from  $H \rightarrow VV$  ( $V = W, Z$ ), i.e. for  $M_{VV} \gtrsim 2M_V > M_H$ , off-shell effects can be quite large,  $\mathcal{O}(10\%)$ , but this region can be excluded by dedicated cuts [53]. On the other hand, a heavy Higgs boson would show up as an extremely broad resonance, whose width becomes of the same size as its mass for  $M_H \lesssim 1$  TeV. Theoretically this situation is very challenging, because production and decay processes do not factorize anymore from each other. Instead, a proper treatment of the broad resonance has to deal with the signal, consisting of Higgs-boson production, propagation, and decay, background, comprising non-resonant diagrams with the same final state as the Higgs-boson decay, and of interference effects between signal and background at the same time. Even the proper field-theoretical definition of mass and width of a heavy Higgs boson to parametrize the resonance becomes subtle. For more details about these issues, which are still under investigation, we have to refer to the literature (see e.g. Refs. [25, 26, 54, 55] and earlier references therein). In the following we put the emphasis on the Higgs-boson mass range  $100 \text{ GeV} < M_H < 200 \text{ GeV}$ , which is favoured by the overall fit of the SM to precision data and the results of the direct searches.

To deliver precise predictions for the Higgs-boson decay widths and branching ratios, a huge effort was made by many theorists. The decay channels that are most important for Tevatron and the LHC are:

- $H \rightarrow f\bar{f}$  (mainly  $f = \tau, b, t$ ) [56–68]

In describing a Higgs boson decaying into bottom (or even lighter) quarks it is essential to base the Yukawa coupling on the running quark mass at the relevant scale, which is set by the Higgs-boson mass. For instance, for  $M_H \gtrsim 100$  GeV the transition from the pole to the running bottom mass  $\bar{m}_b(M_H)$  reduces the  $H \rightarrow b\bar{b}$  partial decay width by  $\sim 60\%$  or more. Starting from this improved



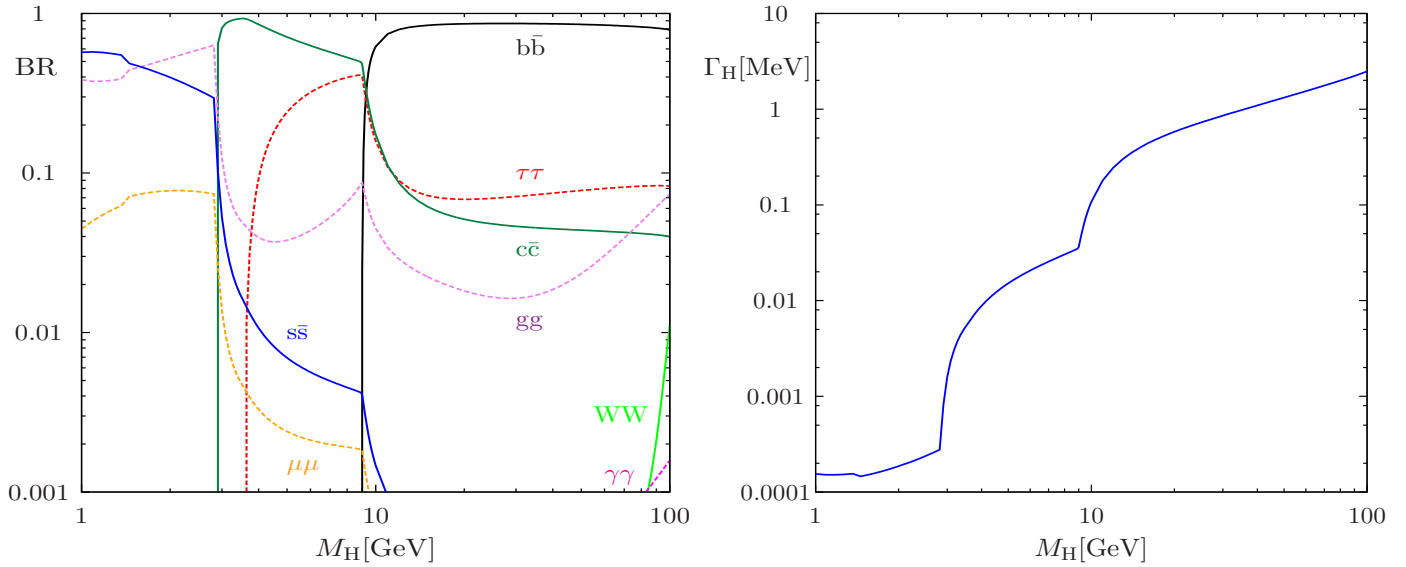


Figure 3: Branching ratios of the SM Higgs boson (left) and total decay width (right) for Higgs-boson masses accessible at LEP and before, calculated with the program HDECAY [51].

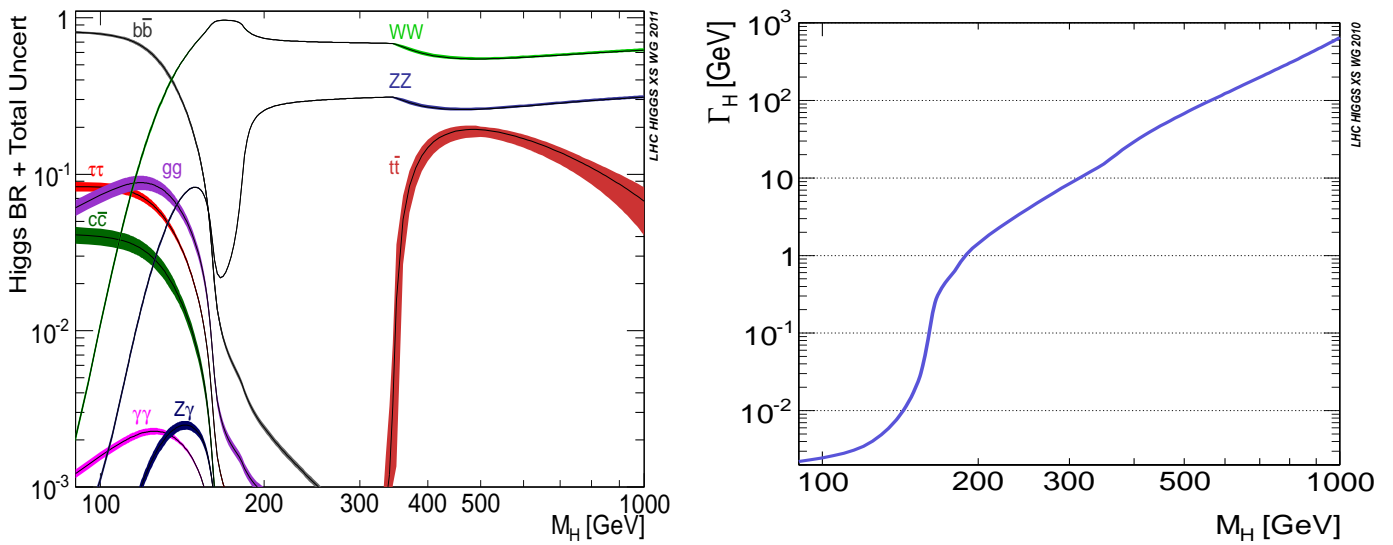


Figure 4: Branching ratios of the SM Higgs boson (left, taken from Refs. [26,52]), with the band widths illustrating the parametric and theoretical uncertainties, and total decay width (right, taken from Ref. [25]) in the Higgs-boson mass range accessible by the LHC.

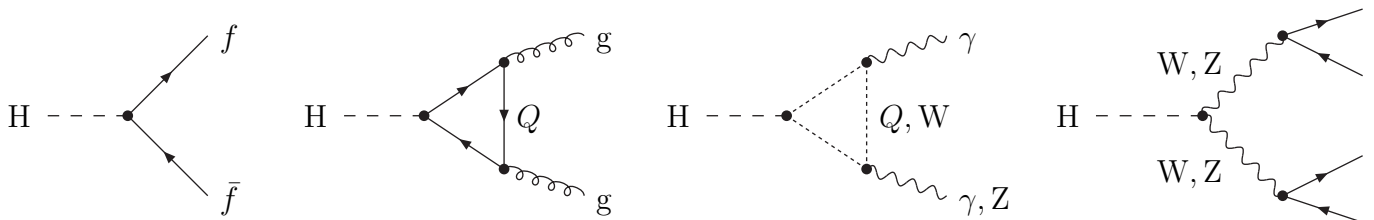


Figure 5: Leading-order diagrams for the various SM Higgs-boson decay channels, where  $Q$  denotes any heavy quark.

LO prediction, the perturbative QCD series, which is known in NLO [58] and beyond that even up to NNNNLO [60], shows nice convergence with a small residual scale uncertainty of  $\sim 0.1\%$ . Recently, the NNLO QCD corrections to  $H \rightarrow b\bar{b}$  became available for fully differential observables [61] as well. Generally, a proper treatment of the  $q\bar{q}$  threshold region deserves particular attention [59].

For the decay into top quarks, the full mass dependence of the  $t\bar{t}$  final state has to be included, and the issue of a running mass is not as pronounced as for the lighter quarks. The QCD corrections, which are available at NLO [58, 62] and NNLO [63], turn out to be moderate, but still  $\sim 5\%$  at NNLO. The decay of the top quarks should be taken into account in predictions as well, not only for precision, but also since it would offer the possibility to analyze the CP properties of a possible heavy-Higgs-boson candidate (see Refs. [64, 69] and references therein).

The theoretical structure of the NLO EW corrections [65, 66] to  $H \rightarrow f\bar{f}$  is very similar for all fermions, and their size is typical of the order of a few percent. Beyond NLO, some QCD and EW corrections that are enhanced by factors of  $G_\mu m_t^2$  are known [67] as well as the leading two-loop heavy-Higgs-boson effects  $\propto G_\mu^2 M_H^4$  [68] that reflect the failure of perturbation theory in the TeV range for  $M_H$ , where they are as large as their NLO counterparts.

- $H \rightarrow gg$  [70–76]

The NLO QCD (two-loop) corrections to the  $H \rightarrow gg$  decay were first calculated as an asymptotic expansion in  $M_H/m_t$  [71], which is applicable only for Higgs-boson masses below the  $t\bar{t}$  threshold ( $M_H < 2m_t$ ), and later generalized to the full mass dependence [72]. These corrections are very large, ranging from 70% to 40% for  $M_H = 100 \text{ GeV}$  to 1 TeV. QCD effects beyond NLO [73], which are known in the form of an expansion in small values of  $M_H$  valid up to  $M_H \lesssim m_t$ , add roughly another 20% to the partial decay width of a light Higgs boson to gluons. Electroweak NLO corrections are known with the full mass dependence and amount to  $\sim 5\%$  [74, 75]. Mixed QCD–EW beyond NLO corrections were calculated in the heavy-top limit, i.e. for light Higgs bosons, but found to be very small [76].

- $H \rightarrow \gamma\gamma/\gamma Z$  [56, 57, 72, 74, 75, 77–83]

Similar to the gluonic Higgs-boson decay, the NLO QCD corrections to the  $H \rightarrow \gamma\gamma$  decay were first calculated in the large-top-quark-mass limit [78] and later with the full mass dependence [72, 79]. For small  $M_H$  these corrections amount to only  $\lesssim 5\%$ , but for masses above the  $t\bar{t}$  threshold they can be as large as 50–100% around  $M_H \sim 600 \text{ GeV}$ , where the LO prediction receives some suppression due to a destructive interference between quark and W-boson loops. QCD effects beyond NLO are also known in the form of an expansion in small values of  $M_H$  [82]. NLO EW corrections, which were presented in Refs. [74, 75, 81], turn out to be of the order of a few percent. In the actual calculations, particular care has to be taken in the vicinity of the  $t\bar{t}$  and WW thresholds, where the finite decay widths of the top-quarks and W-bosons in the loop have to be taken into account [74, 75, 80].

Because of its lower phenomenological importance, the predictions to the decay  $H \rightarrow \gamma Z$  are much less advanced than in the  $\gamma\gamma$  case. The NLO QCD corrections, which turn out to be below 1%, can be found in Ref. [83]. Many leading higher-order corrections are very similar or even identical in the  $\gamma\gamma/\gamma Z$  cases.

- $H \rightarrow WW/ZZ \rightarrow 4f$  [65, 84–87]

Since the Higgs-boson decay channels into weak-gauge-boson pairs are also phenomenologically relevant in the WW/ZZ threshold region and below, i.e. for  $M_H \lesssim 2M_V$  ( $V = W, Z$ ), the W/Z decays have to be taken into account in precision calculations. Moreover, it was extensively discussed in the literature [84] that the kinematical details (energy, angular, and invariant-mass

Table 1: Estimated relative uncertainties of Higgs-boson branching ratios due to theoretical plus parametric errors for low and intermediate Higgs-boson masses, as given by the LHC Higgs Cross Section Working Group [26, 52].

$M_H$ [GeV]	$H \rightarrow b\bar{b}$	$\tau^+\tau^-$	$c\bar{c}$	gg	$\gamma\gamma$	WW	ZZ
120	3%	6%	12%	10%	5%	5%	5%
150	4%	3%	10%	8%	2%	1%	1%
200	5%	3%	10%	8%	2%	< 0.1%	< 0.1%

distributions) of the four-fermion final state offer the possibility to extract the spin and CP properties of a Higgs-boson candidate. Radiative corrections have first been calculated for on-shell W/Z bosons [65, 85], the results of which are only applicable for  $M_H > (2M_V + \text{some GeV})$ , and later including the full off-shell effects of the W/Z bosons [86] in the framework of the complex-mass scheme [88] for treating the W/Z resonances. For  $H \rightarrow WW/ZZ$  the heavy-Higgs-boson limit is of particular interest, because the dominating decay into longitudinal W/Z bosons leads to the above-mentioned rise  $\propto M_H^3$  of the total decay width  $\Gamma_H$ . The leading heavy-Higgs-boson corrections to  $\Gamma_{H \rightarrow WW/ZZ}$  are proportional to  $G_\mu M_H^2$  and  $G_\mu^2 M_H^4$  at the one- and two-loop level [87]. The fact that this two-loop term becomes as large as the one-loop correction for  $M_H \sim 1$  TeV signals again the onset of the non-perturbative regime for a heavy Higgs boson. The leading two-loop effect, which is negligible for  $M_H \lesssim 400$  GeV and amounts to  $\sim 4\%$  for  $M_H \sim 700$  GeV, can serve as an estimate for the theoretical uncertainty for large  $M_H$ . For  $100 \text{ GeV} < M_H < 200 \text{ GeV}$  the radiative corrections to the partial widths range from some percent to  $\lesssim 12\%$ , depending on the four-fermion final state and can be even much higher in distributions.

More details can be found in reviews or reports [25, 26, 69, 89].

State-of-the-art predictions can be obtained upon combining results from the two public programmes HDECAY [51] and PROPHECY4F [86]:

- HDECAY is designed to calculate all relevant Higgs-boson decay widths and branching ratios in the SM and its minimal supersymmetric extension. On the QCD side, all relevant known corrections are included, while the EW corrections, which are smaller for most of the channels, are approximated. Specifically, the EW (two-loop) corrections to  $H \rightarrow gg/\gamma\gamma$  are reconstructed via a numerical grid obtained from the full results of Ref. [74, 75], and the corrections to WW/ZZ (considered as two-body decays) are fitted to the corrections provided by PROPHECY4F.
- PROPHECY4F is a Monte Carlo event generator for all four-particle decays  $H \rightarrow WW/ZZ \rightarrow 4f$  that takes into account all interferences and all off-shell effects of the intermediate W/Z bosons, so that the obtained results are valid above, near, and below the gauge-boson pair thresholds. As an event generator, PROPHECY4F can simulate the four-body decays with its full kinematics with NLO QCD and EW corrections; for leptonic final states unweighted events can be produced as well. For large  $M_H$  the leading two-loop EW corrections from Ref. [87] are included as well.

All results shown in Figure 3 and all but the decay widths for  $H \rightarrow WW, ZZ$  in Figure 4 are based on HDECAY, while the results on  $H \rightarrow WW, ZZ$  are obtained upon summing over the relevant four-fermion final states in  $H \rightarrow WW/ZZ \rightarrow 4f$  whose decay widths are calculated with PROPHECY4F. More technical details about the calculations for Figure 4 can be found in Refs. [25, 26, 52] from which the plots are taken.

The bands in the prediction of the branching ratios shown in Figure 4 reflect the combined uncertainties due to missing higher-order effects in the calculations and parametric uncertainties in the input parameters, as assessed by the LHC Higgs Cross Section Working Group [26, 52]. Table 1 briefly summarizes the estimated total uncertainties for  $M_H$  values 120 GeV, 150 GeV, and 200 GeV, which are most interesting for SM Higgs physics at Tevatron and the LHC. It is important to note that the uncertainties of the branching ratios result from an interplay of the uncertainties of the corresponding partial decay width and the normalization to the total width  $\Gamma_H$ . The decay widths into hadronic final states ( $b\bar{b}$ ,  $c\bar{c}$ ,  $gg$ ) possess relatively large uncertainties via the parametric uncertainties from the heavy-quark masses and the strong coupling. As long as  $\Gamma_H$  is dominated by  $\Gamma_{H \rightarrow b\bar{b}}$  this uncertainty is mitigated in  $\text{BR}(H \rightarrow b\bar{b})$ , but feeds into the branching ratios of the other channels, as, e.g., clearly visible for  $H \rightarrow WW/ZZ$  at  $M_H = 120$  GeV. The opposite is observed at  $M_H = 200$  GeV, where  $\Gamma_H$  is dominated by  $\Gamma_{H \rightarrow WW/ZZ}$ , which are very precisely known, i.e. in this case the uncertainties of the other branching ratios entirely reflect the one of the respective partial widths. A similar estimate of the uncertainties of the branching ratios has been presented in Ref. [90] in the Higgs-boson mass range of  $M_H = 100\text{--}200$  GeV, where somewhat larger uncertainties are found, mainly due to larger assumed errors on the b- and c-quark masses.

For very low and very high Higgs-boson masses the theoretical uncertainties of the branching ratios become larger and larger and hard to quantify. Figure 3 shows the branching ratios without error bands, mainly because the predictions in the vicinity of the  $q\bar{q}$  thresholds, i.e. for  $M_H \lesssim 15$  GeV, become more of qualitative nature with uncertainties of 100%. This theoretical shortcoming was balanced experimentally by inclusive search strategies in the low- $M_H$  range, where the individual decay channels of the Higgs boson did not play a role. For large Higgs-boson masses the uncertainty of predictions increases more and more when the non-perturbative regime of  $M_H \sim 1$  TeV is approached.

## 3 General considerations for Higgs-boson searches

### 3.1 Challenges

The challenge in searches for the Higgs boson is to develop a selection that allows to increase the a priori very small signal-to-background ratio (see Figure 6) to a level of the order 1/1 to 1/10. In order to reach this goal, sophisticated selection strategies have been developed over the last decades at the experiments at LEP, Tevatron, and the LHC. In the beginning only simple rectangular cuts were used to separate the signal process from background processes. By now many search strategies make use of multivariate techniques such as likelihood ratios, artificial neural networks, or boosted decision trees.

The combination of production mechanisms and decay modes of the Higgs boson and the particles that are eventually produced in association with the Higgs particle yields a plenitude of final-state topologies which can be used to search for Higgs-boson production. The following considerations have to be taken into account when choosing the most promising search channels: sufficient a priori signal rate determined by cross section and branching ratios, means to trigger on signal events with high efficiency, means to suppress the background to an acceptable level, means to estimate the uncertainties in the background prediction, and in the case of exclusion also the uncertainties in the signal prediction. It is desirable to be able to construct a final discriminating variable to distinguish the two alternative hypotheses of background-only and signal+background in addition to simple event counting. An obvious choice is the reconstructed mass of the Higgs-boson candidate events. Depending on the final-state particles this is not always possible. Alternatively or in addition other powerful observables can be used, e.g. the response of a multivariate event classifier.

For the discovery of a new resonance, which means that the probability to observe the actual number of events is less than  $2.87 \times 10^{-7}$  under the background-only hypothesis, only the background prediction

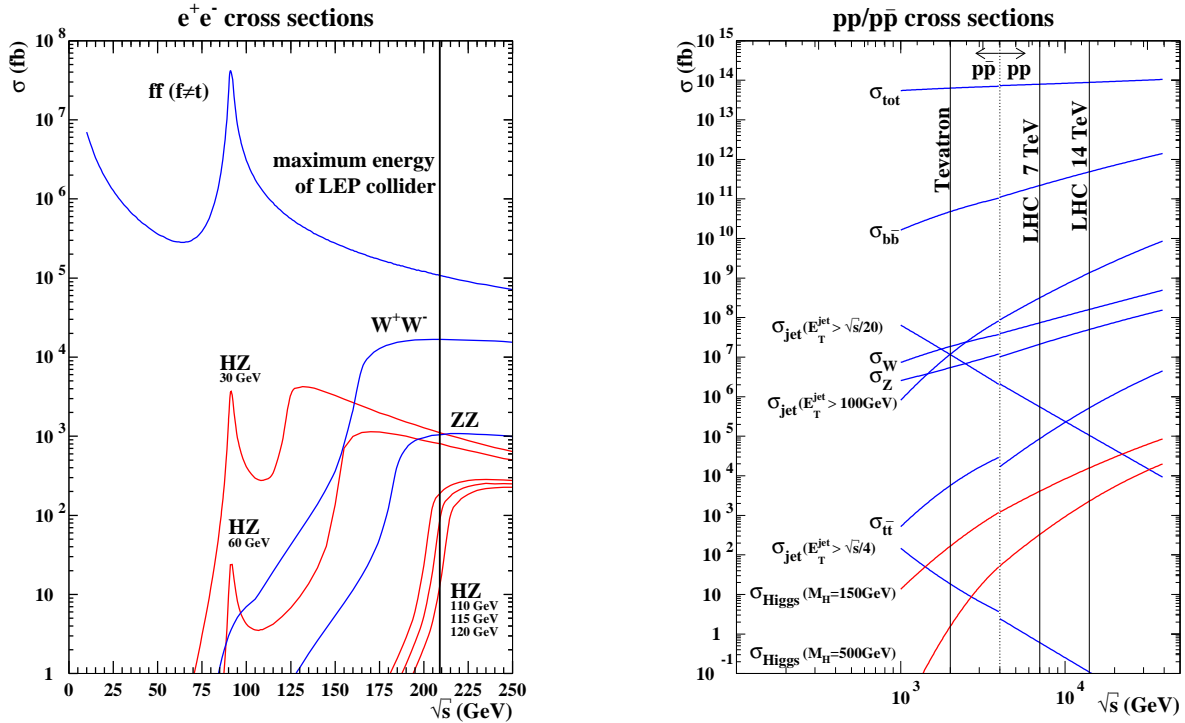


Figure 6: Signal and background cross sections at leading order (produced with PYTHIA [91, 92]) at  $e^+e^-$  colliders (left) and at hadron colliders (proton–antiproton and proton–proton colliders).

and its uncertainty need to be known. Wrong assumptions on the shape of discriminating observables for the signal process will lead to a reduced sensitivity. Hypothetically one observed event can yield the claim of discovery given the search is basically background free ( $\approx 3 \times 10^{-7}$  expected background events) with vanishing systematic uncertainty, which unfortunately is never the case in the environments at colliders. For the exclusion of a signal hypothesis, neglecting systematic uncertainties and performing a counting-only experiment with negligible background, a minimal signal yield of 3 expected events after application of the full selection chain is needed in order to exclude the signal+background hypothesis at the 95% confidence level, when using the Bayesian or “ $CL_S$ ” technique (see below). In this case the uncertainties on the signal rate and shape of the discriminating distributions will also influence the derived exclusion limits; for instance, a too optimistic assumption for the mass resolution for Higgs-boson candidates would yield a too stringent exclusion.

Although the Higgs mechanism had been incorporated in the electroweak theory in the late 1960s, it lasted until 1989, when LEP started its operation, before significant parts of the mass range of the SM Higgs boson could be investigated.<sup>6</sup> The particle data group in 1988 [94] concluded on Higgs-boson searches before the start of LEP “In summary, the only cast-iron constraint on the Higgs mass is  $M_H > 14 \text{ MeV}$ . A combination of theoretical arguments and bounds from  $B$ ,  $\Upsilon$ , and  $K$  decays probably excludes the range below  $4 \text{ GeV}$ .” Hence the mission of LEP was to probe the mass range of the SM Higgs boson starting from a zero mass to the highest possible mass values. For a discussion of Higgs-boson searches before the start of the LEP accelerator we, e.g., refer to Refs. [95–99]. In this article we review the most important results of the searches for the SM Higgs boson at the colliders LEP, Tevatron, and LHC. For details of the individual analyses, in particular identification criteria and

<sup>6</sup>A search carried out by the CDF experiment at Tevatron with up to  $4.4 \text{ pb}^{-1}$  at CM energy of  $1.8 \text{ TeV}$  excluded the mass ranges  $2m_\mu - 818 \text{ MeV}$  and  $846 \text{ MeV} - 2m_K$  at 90% CL [93]. However, in this mass range the prediction of the branching ratios have large theoretical uncertainties, as discussed in Section 2.6.

systematic uncertainties, the original literature should be consulted.

### 3.2 Statistical interpretation of search results

The result of a search for the Higgs boson after applying the whole selection algorithms is, in the simplest case, given by the observed event yield, and the expected event yield for the background processes and the signal process, which depends on the hypothetical Higgs-boson mass. Such analyses are often called “counting experiments”. Most of the searches performed during the LEP1 era were of this type. Very often the sensitivity of the search can be increased by using a final discriminating observable, which can be one-dimensional or, in rare cases, is chosen to be multi-dimensional. Here not only expected and observed event yields, but also the observed and expected shapes of the distributions in the final observable are used, when deriving the statistical interpretation of the results. This final discriminant is often given by the mass distribution of the Higgs-boson candidates, reconstructed from the decay products, or by the response of a multivariate event classifier (e.g. likelihood, artificial neural network, boosted decision tree). All searches during the LEP2 era, at Tevatron, and at the LHC use the distribution of a discriminating observable. Usually the expected event yields from signal and background processes as well as the shape of the distribution of the discriminating observable are affected by several systematic uncertainties, comprising, e.g., predictions of cross sections and acceptances due to kinematical requirements by theoretical calculations, knowledge of the detector performance in reconstruction and identification efficiencies, energy resolutions, and energy scales. Their influence on the signal and background expectations can be described by nuisance parameters  $\theta$ , which can be common in signal and background. The expected distribution for a Higgs-boson signal with SM strength  $s(M_H, \theta)$  depends on the Higgs-boson mass  $M_H$  and can either be given by a simple event count, a distribution of the final discriminant provided as a histogram, or an analytic function. In the following we will suppress the  $M_H$  dependence in the equations, but it should be kept in mind. The signal-strength parameter  $\mu = \sigma_H/\sigma_{H_{SM}}$  allows to describe a signal strength different from the SM expectation, where  $\mu = 1$  holds. In the same way the background expectation is given by  $b(\theta)$  and the data by  $n$ . The statistical interpretation uses the frequentist concept of hypothesis testing for claiming evidence or discovery. When setting exclusion limits either the concept of hypothesis testing is used as well, or the closely related frequentist derivation of an upper limit on the signal yield or signal-strength parameter  $\mu$ . For setting limits the Bayesian concept of providing a one-sided credibility interval or Bayesian upper limit is used as well. Below a partial overview of the main methods used at LEP, Tevatron, and the LHC is given. For more details we refer to the excellent review [100] and to the experiments’ publications. A general introduction into the topics of frequentist hypothesis tests, and Bayesian and frequentist limit setting and their interpretation can be found, e.g., in Ref. [101].

In a hypothesis test the consistency of the observed data with a given hypothesis, which one tries to falsify (null hypothesis  $H_0$ ), is evaluated via the so-called  $p$ -value. The null hypothesis is the opposite of the statement one is aiming at, because hypotheses can only be rejected, but not be approved: When looking for evidence or discovery, it is given by the existence of only background processes called “background-only” hypothesis (“ $b$ ”-only), whereas when excluding a signal, it is given by the “signal+background” hypothesis (“ $s + b$ ”). A test statistic  $t$  is constructed from the observed results (event yields and shapes of final discriminating observables), which is used to evaluate the consistency with the null hypothesis. Given that the probability density function  $f(t(\mu)|H_0)$  for the test statistic  $t$  under the null hypothesis is known, and knowing that small (large) values of  $t$  indicate consistency (inconsistency) with the null hypothesis the  $p$ -value for an actual observed value  $t_{\text{obs}}$  is defined by

$$p = \int_{t_{\text{obs}}}^{\infty} f(t(\mu)|H_0) dt. \quad (28)$$

The  $p$ -value is the probability to observe a value of the test statistic  $t$  at least as large as observed in data assuming the null hypothesis is realized in nature. Equivalently it quantifies the probability to

wrongly reject the null hypothesis, if it is actually true. The  $p$ -value can be translated into a so-called Gaussian significance  $Z$  via  $Z = \Phi^{-1}(1 - p)$ , where  $\Phi^{-1}$  is the inverse of the cumulative distribution for the standard Gaussian probability density function. For claiming discovery one requires the  $p$ -value to be less than or equal to  $2.87 \times 10^{-7}$  or equivalently the significance  $Z$  to be at least 5. For exclusion, when one wants to reject the signal+background hypothesis the  $p$ -value is usually required to be less than 0.05. The hypothesis is then called excluded with a confidence level  $\text{CL} = 1 - p$ . Alternatively one can determine the signal strength for which the  $p$ -value is exactly 0.05. This is equivalent to constructing a one-sided frequentist confidence interval for  $\mu$  or an upper limit on  $\mu$  called  $\mu_{95}$  to a confidence level  $\text{CL} = 95\%$ , which fulfills the condition

$$0.05 = 1 - \text{CL} = \int_{t_{\text{obs}}}^{\infty} f(t(\mu_{95})|H_0) dt, \quad \text{i.e.} \quad 0.95 = \text{CL} = \int_{-\infty}^{t_{\text{obs}}} f(t(\mu_{95})|H_0) dt. \quad (29)$$

All values of  $\mu$  larger than  $\mu_{95}$  are then excluded, i.e. the SM Higgs-boson hypothesis is excluded if  $\mu_{95} \leq 1$ . The Bayesian technique to derive a one-sided credibility interval or a Bayesian upper limit on  $\mu$  at credibility level  $\text{CL}$  relies on the likelihood function  $\mathcal{L}(\text{data}|\mu)$ , which gives the conditional probability to observe the data for a given value of  $\mu$ . Using Bayes' theorem the posterior probability for the degree of belief in a particular value of  $\mu$  in the light of the data is given by

$$p(\mu|\text{data}) = \text{const.} \times \mathcal{L}(\text{data}|\mu) \pi(\mu), \quad (30)$$

where  $\pi(\mu)$  is the a priori belief about the knowledge of  $\mu$  and *const.* is an irrelevant constant to normalize  $p(\mu|\text{data})$ . Very often and in all results discussed in this review,  $\pi(\mu)$  is chosen to be uniform for non-negative and hence physically meaningful values of  $\mu$  and zero otherwise. The Bayesian upper limit  $\mu_{95}$  to a credibility level  $\text{CL} = 95\%$  is then obtained via

$$0.95 = \frac{\int_{-\infty}^{\mu_{95}} p(\mu|\text{data}) d\mu}{\int_{-\infty}^{\infty} p(\mu|\text{data}) d\mu} = \frac{\int_0^{\mu_{95}} \mathcal{L}(\text{data}|\mu) d\mu}{\int_0^{\infty} \mathcal{L}(\text{data}|\mu) d\mu}. \quad (31)$$

The procedure described above is repeated for each hypothetical value of  $M_{\text{H}}$  in all approaches (frequentist hypothesis test, frequentist upper limit, and Bayesian upper limit).

Let us first consider a counting experiment as was done during the LEP1 era and partially at the beginning of the LEP2 era. The discussion will be restricted to rejecting the signal+background hypothesis and hence to the derivation of exclusion limits, as during that era no significant excess was observed. The background  $b$  is assumed to be known without uncertainties and the expected signal yield is given by  $s$ . The upper limits on the signal yield is denoted by  $s_{95} = \mu_{95}s$ . In the frequentist approach one has to specify the test statistic, which is chosen to be the number of observed events  $n$ , which in this case does not depend on the signal hypothesis. The probability density function for  $n$  under the signal+background hypothesis is simply the Poisson probability  $f(n|\mu s + b) = e^{-(\mu s + b)}(\mu s + b)^n/n!$ . The likelihood function needed in the Bayesian approach is also given by the Poisson probability  $\mathcal{L}(\text{data}|\mu s + b) = e^{-(\mu s + b)}(\mu s + b)^n/n!$ , where  $n$  plays the role of "data". A low number of observed events indicates an inconsistency with the signal+background hypothesis. Hence the frequentist upper  $s_{95}$  limit is derived from

$$0.05 = \sum_{n=0}^{n_{\text{obs}}} e^{-(s_{95}+b)}(s_{95}+b)^n/n!. \quad (32)$$

The analytic solution of this equation for  $s_{95}$  gives

$$s_{95} = \frac{1}{2} F_{\chi^2}^{-1}(0.95; 2(n_{\text{obs}} + 1)) - b, \quad (33)$$

where  $F_{\chi^2}^{-1}$  denotes the inverse of the cumulative  $\chi^2$  probability density distribution evaluated for  $2(n_{\text{obs}} + 1)$  degrees of freedom. The Bayesian upper limit has to be derived from [102]

$$0.05 = \frac{\sum_{n=0}^{n_{\text{obs}}} e^{-(s_{95}+b)}(s_{95}+b)^n/n!}{\sum_{n=0}^{n_{\text{obs}}} e^{-b}b^n/n!}. \quad (34)$$

For zero background ( $b = 0$ ) the two approaches give identical results. For  $n_{\text{obs}} = 0$  (1) observed events the  $s_{95}$  is then given by 3.0 (4.7). These are the numbers that are used in the derivation of the final LEP1 exclusion limits, where all observed events were considered as candidate events or equivalently using  $b = 0$  in the above equations for  $s_{95}$ . A Higgs-boson mass hypothesis is excluded if the expected signal event yield for the value of  $M_{\text{H}}$  tested is larger than 3.0 (4.7) given 0 (1) events are observed in data. The expected signal event yields are decreased by their systematic uncertainty before the determination of  $s_{95}$  and its comparison with  $\mu s$ .

For non-vanishing background the frequentist approach due to the  $-b$  term can give arbitrarily small values  $s_{95}$ , e.g.  $s_{95} = 0$  for  $b = 3$  and  $n = 0$ , if the observed event yield is significantly lower than the one expected from background processes. In the Bayesian approach  $s_{95}$  can never get smaller than 3. Even if completely correct from a purely frequentist point of view, people felt uneasy with quoting a very small  $s_{95}$  in a situation where the average experiment has no sensitivity to exclude such a small signal yield, but excludes it due to a downward fluctuation of the observed event yield with respect to the background-only hypothesis. Such situations are avoided in the Bayesian approach. An alternative derivation of the Bayesian formula in a pseudo-frequentist ansatz and its interpretation are given in Ref. [103]. Formally the right-hand side of the Bayesian formula can be rewritten in the language of frequentist hypothesis tests as  $p_{\text{s+b}}/(1-p_{\text{b}})$ , where  $p_{\text{s+b}}$  and  $p_{\text{b}}$  denote the  $p$ -values under the signal+background and background-only hypotheses, respectively, keeping in mind that small (large) observed event yields mean inconsistency with the signal+background (background-only) hypothesis.

At LEP2 and later, multiple channels with different signal-to-background ratios were combined, and the distributions of the final discriminants were also used. At the beginning of the LEP2 era different techniques [104] were used for the construction of a test statistic that takes into account the different signal-to-background ratios in the various search channels and bins of the histograms of the final discriminants. The likelihood functions  $\mathcal{L}(\text{data}|\mu s + b)$  and  $\mathcal{L}(\text{data}|b)$  are given by the product of Poisson probabilities running over all channels and bins. Neglecting systematic uncertainties, the optimal test statistic is given, according to the Neyman–Pearson lemma [105], by the ratio of the two likelihoods to observe the data under the signal+background hypothesis and background-only hypothesis, its reciprocal, or any monotonic function of it. This is the statistic

$$Q = \mathcal{L}(\text{data}|\mu s + b)/\mathcal{L}(\text{data}|b), \quad (35)$$

or its transform  $-2 \ln Q$  used at LEP. For a single-channel/single-bin counting experiment the Neyman–Pearson test statistic derived from the ratio of two Poisson probabilities is (setting  $\mu = 1$ )

$$Q = e^{-s}(1 + s/b)^n, \quad \text{i.e.} \quad -2 \ln Q = 2s - 2n \ln(1 + s/b). \quad (36)$$

Hence as  $Q$  is monotonic in  $n$ ,  $n$  is the optimal test statistic for a simple counting experiment in one channel. Each observed event enters the calculation of  $-2 \ln Q$  with a weight of  $\ln(1 + s/b)$  which takes into account the local  $s/b$  ratio. Large values of  $-2 \ln Q$  are obtained for “b-only”-like data and small values for “s+b”-like data. The median of the  $-2 \ln Q$  distribution is positive under the background-only hypothesis, whereas the median is negative under the signal+background hypothesis. The probability density functions for  $-2 \ln Q$  under the signal+background hypothesis and background-only hypothesis are obtained from simulation of toy MC experiments.

Translating the Bayesian formula in the interpretation of Ref. [103] to the test statistic  $-2 \ln Q$  yields the so-called “CL<sub>S</sub>” technique [106,107], which avoids exclusion without sensitivity. The  $p$ -values for the LEP test statistic  $-2 \ln Q$  are calculated according to:

$$p_{\text{s+b}} = \int_{-2 \ln Q_{\text{obs}}}^{\infty} f(-2 \ln Q|s + b) d(-2 \ln Q) \quad (37)$$

and

$$p_{\text{b}} = \int_{-\infty}^{-2 \ln Q_{\text{obs}}} f(-2 \ln Q|b) d(-2 \ln Q). \quad (38)$$



The “CL<sub>S</sub>” value is then calculated as

$$\text{CL}_S = p_{s+b}/(1 - p_b). \quad (39)$$

A Higgs-boson mass hypothesis is called excluded at least to 95% CL if  $\text{CL}_S \leq 0.05$ . The probability to reject the signal+background hypothesis, if it is true, is less than 5%, as the “ad hoc” correction in the denominator destroys the strict frequentist interpretation. Even if not proven in a mathematically rigorous way, good agreement has been found between the Bayesian approach and “CL<sub>S</sub>” technique in practice at LEP, Tevatron, and the LHC. Systematic uncertainties (denoted by  $\theta$ ) were incorporated at LEP in the hybrid frequentist–Bayesian approach described in Ref. [108], which results in modified probability density functions for the unchanged test statistic  $-2 \ln Q$ ,

$$f(-2 \ln Q|s + b) = \int f(-2 \ln Q|s + b, \theta)\pi(\theta) d\theta \quad \text{and} \quad f(-2 \ln Q|b) = \int f(-2 \ln Q|b, \theta)\pi(\theta) d\theta, \quad (40)$$

which is a so-called marginalization with respect to the parameters  $\theta$  with a priori probabilities  $\pi(\theta)$ . The explicit choice of  $\pi(\theta)$  is specific to the sources of the systematic uncertainties and thus depends on the analysis.

At Tevatron the Neyman–Pearson test statistic was modified to include the parameters  $\theta$ , describing the systematic uncertainties, in the likelihood, which yields a better discrimination between signal+background and background-only hypotheses in the presence of systematic uncertainties compared to LEP. The likelihood function now reads  $\mathcal{L}(\text{data}|\mu s(\theta) + b(\theta))\pi(\theta)$ , with a priori probabilities  $\pi(\theta)$  for the nuisance parameters  $\theta$ , and the test statistics LLR, in the Tevatron convention, is given by ratio of two profiled likelihoods

$$\text{LLR} = -2 \ln \left( \frac{\mathcal{L}(\text{data}|\mu s(\hat{\theta}) + b(\hat{\theta}))\pi(\hat{\theta})}{\mathcal{L}(\text{data}|b(\hat{\theta}))\pi(\hat{\theta})} \right). \quad (41)$$

The  $\hat{\theta}$  and  $\hat{\theta}$  are, respectively, the conditional maximum-likelihood estimators of two fits performed (i) under the signal+background hypothesis in the numerator and (ii) under the background-only hypothesis in the denominator. The best fit values  $\hat{\theta}$  and  $\hat{\theta}$  for  $\theta$  are usually different under the two hypotheses. The determination of the probability density functions for LLR and of the “CL<sub>S</sub>” value proceeds as was done at LEP. The primary choice for deriving upper limits on  $\mu$ , which is called  $R$  in the Tevatron analyses, in the latest Tevatron combinations is the use of the Bayesian method with the posterior probabilities for  $\mu$  given by

$$p(\mu|\text{data}) = \text{const.} \times \int \mathcal{L}(\text{data}|\mu s(\theta) + b(\theta))\pi(\theta)\pi(\mu) d\theta. \quad (42)$$

Again a uniform prior for positive  $\mu$  is used and a marginalization with respect to the  $\theta$  is performed. For deriving  $p$ -values under the background-only hypothesis and calculating significances, a fit of  $\mathcal{L}(\text{data}|\mu s(\theta) + b(\theta))\pi(\theta)$  to the data is performed, and the best fit value  $\hat{\mu}$  for the signal-strength parameter  $\mu$  is used as the test statistic. The probability density functions for  $\hat{\mu}$  are derived again from toy MC experiments.

At the LHC two different test statistics are used for the two cases, setting limits and claiming evidence for discovery [109]. The likelihood function is the same as at Tevatron,  $\mathcal{L}(\text{data}|\mu s(\theta) + b(\theta))\rho(\tilde{\theta}|\theta)$ , but the a priori probabilities for the nuisance parameters  $\pi(\theta)$  are reinterpreted or replaced by conditional probabilities  $\rho(\tilde{\theta}|\theta)$  to observe a value  $\tilde{\theta}$  in an auxiliary measurement given the value  $\theta$ . For setting limits, i.e. testing a signal strength  $\mu$ , the test statistic is given by

$$\tilde{q}_\mu = -2 \ln \left( \frac{\mathcal{L}(\text{data}|\mu s(\hat{\theta}) + b(\hat{\theta}))\rho(\tilde{\theta}|\hat{\theta})}{\mathcal{L}(\text{data}|\hat{\mu} s(\hat{\theta}) + b(\hat{\theta}))\rho(\tilde{\theta}|\hat{\theta})} \right). \quad (43)$$

In the numerator the likelihood under the signal+background hypothesis with fixed signal strength  $\mu$ , to be tested, is evaluated, while in the denominator (in contrast to Tevatron) the likelihood is evaluated after fitting also for the best signal strength consistent with the data  $\hat{\mu}$ . The range for  $\hat{\mu}$  is restricted to  $0 \leq \hat{\mu} \leq \mu$ , as  $\hat{\mu} < 0$  is unphysical and as a one-sided hypothesis test is performed, where  $\hat{\mu} > \mu$  is considered as being consistent with the signal+background hypothesis (see Ref. [109] for details). The value of the test statistic  $\tilde{q}_\mu$  is restricted to the range between zero and infinity. In order to be able to define a one-sided hypothesis test, the value of  $\tilde{q}_\mu$  is set to zero for  $\hat{\mu}$  values larger than  $\mu$ . Background-like data yield large values of  $\tilde{q}_\mu$ , whereas “ $s + b$ ”-like data accumulate at low values of  $\tilde{q}_\mu$ . The advantage of not fixing  $\mu$  to 0 in the denominator, as done at LEP and Tevatron, is that the probability density function for  $\tilde{q}_\mu$  in the limit of large event yields are known analytically due to Wilks’ [110] and Wald’s [111] theorems (see Ref. [109] for the approximative analytic expressions). The determination of frequentist upper limits proceeds as at LEP and Tevatron via the “CL<sub>S</sub>” technique.

For testing the background-only hypothesis, when looking for discovery or evidence at the LHC, the test statistic is calculated as a different ratio of profiled likelihoods:

$$q_0 = -2 \ln \left( \frac{\mathcal{L}(\text{data}|b(\hat{\theta}))\rho(\tilde{\theta}|\hat{\theta})}{\mathcal{L}(\text{data}|\hat{\mu}s(\hat{\theta}) + b(\hat{\theta}))\rho(\tilde{\theta}|\hat{\theta})} \right). \quad (44)$$

Now  $\mu$  is fixed in the numerator under the null hypothesis (background-only) and is determined via a fit to the data  $\hat{\mu}$  in the denominator. The range for  $\hat{\mu}$  is restricted to  $\geq 0$ , as  $\mu < 0$  is unphysical and as a one-sided hypothesis test is performed, where  $\hat{\mu} < 0$  is considered as being consistent with the background-only hypothesis (see Ref. [109] for details). The values of  $q_0$  are restricted to the range between zero and infinity. In order to be able to define a one-sided hypothesis test, the value of  $q_0$  is set to zero for  $\hat{\mu} < 0$ . Now “ $b$ -only”-like data accumulate at low values of  $q_0$ , whereas “ $s + b$ ”-like data yield large values of  $q_0$ . Again the test statistic  $q_0$  has the advantage that its probability density function is known analytically due to Wilks’ and Wald’s theorems, i.e.

$$f(q_0|b) = \frac{1}{2}\delta(q_0) + \frac{1}{2}f_{\chi^2}(q_0; 1), \quad (45)$$

by a combination of  $\frac{1}{2}\delta$ -function and  $\frac{1}{2}\chi^2$ -probability density function with 1 degree of freedom (see Ref. [109] for details). The  $\frac{1}{2}\delta$ -function is due to the fact that  $q_0$  is set to 0 for  $\hat{\mu} < 0$ . Hence any observed  $q_0 \neq 0$  yields a maximal  $p$ -value of 0.5.

So far in the likelihood functions that enter the construction of test statistics used for testing the background-only hypothesis ( $-2 \ln Q$  at LEP,  $\hat{\mu}$  at Tevatron,  $q_0$  at the LHC) the Higgs-boson mass hypothesis  $M_H$  is fixed under the alternative signal+background hypothesis. The corresponding  $p$ -values are hence called *local*  $p$ -values. It gives the probability to observe such a fluctuation for a fixed  $M_H$  value. The so-called *global*  $p$ -value denotes the probability to find such an excess anywhere in the mass spectrum or more precisely for arbitrary Higgs-boson mass hypothesis under the alternative hypothesis within a certain  $M_H$  range. The relation between the two  $p$ -values is given by  $p_{\text{global}} = f_{\text{trial}} p_{\text{local}}$ . The trial factor  $f_{\text{trial}}$  can be interpreted as the effective number of independent searches performed. This enhancement in the  $p$ -value is commonly called the “look-elsewhere effect”. A technique to derive approximate global  $p$ -values and trial factors used at the LHC can be found in Ref. [112], and in Ref. [113] for Tevatron.

Often expected limits on the signal strength, expected  $p$ -values, and significances are quoted. These are the median values for those quantities derived under the alternative hypothesis: *Expected limit* is the median limit under the background-only hypothesis, *expected significance* is the median significance under the signal+background hypothesis.

A subtle difference should be noted when generating toy MC experiments at Tevatron and the LHC. The central values of the nuisance parameters, which are used as input to the MC experiments, are

fixed to the a priori best values at Tevatron and are extracted from a fit to the data at the LHC (see Ref. [114] for details).

In the following, all limits are given to 95% CL, if not stated otherwise.

## 4 Higgs-boson production at $e^+e^-$ colliders

At  $e^+e^-$  colliders the importance of the various Higgs production mechanisms strongly depends on the centre-of-mass (CM) energy of the collider and to some extent also on the Higgs-boson mass. Figure 7 illustrates the production channels by some representative lowest-order diagrams. Up to LEP energies,  $\sqrt{s} \lesssim 209$  GeV, ZH production via ‘‘Higgs-strahlung’’ with a variety of Higgs and Z-boson decays was the main search channel. Some events from  $H\gamma$  production were expected in spite of a very small cross section; owing to the extremely suppressed electron Yukawa coupling the leading order of the channel is loop-induced by massive-fermion and W-boson loops. At future  $e^+e^-$  linear colliders, such as the ILC or CLIC, two additional types of production channels become relevant: the fusion of W or Z bosons and the associated production with  $t\bar{t}$  pairs. For instance, the cross section of W-boson fusion at an ILC with a CM energy  $\sqrt{s} = 500$  GeV exceeds the one of Higgs-strahlung off Z bosons for Higgs-boson masses larger than  $\sim 160$  GeV. While the HZ production cross section falls off  $\propto 1/s$ , like any typical  $s$ -channel process, the  $t$ -channel-like W/Z-fusion processes receive contributions that grow like  $\ln(s/M_H^2)/M_W^2$  for large energies. Above the  $t\bar{t}H$  production threshold,  $\sqrt{s} > 2m_t + M_H$ , Higgs production in association with  $t\bar{t}$  pairs offers the possibility to directly measure the top-quark Yukawa coupling with good precision. Figure 8 (r.h.s.) presents an overview over the various cross sections as function of the collider energy  $\sqrt{s}$ , covering the range from LEP energies to the TeV region of potential future colliders. The theoretical preparation of the LEP analysis is described in detail in Refs. [115, 118], and a more detailed survey of both the physics potential of linear colliders and features of the predictions can be found in Refs. [69, 119].

Figure 8 is based on lowest-order predictions, but state-of-the-art calculations include higher-order improvements as well. Collinear photonic initial-state radiation (ISR) generically delivers corrections at the level of 10% or more, which are particularly pronounced in region where cross sections or distributions show strong variations, as it is, e.g., the case near kinematical thresholds. The by far dominating part of ISR is of universal origin and consists of logarithmically enhanced terms  $\alpha^n \ln^m(m_e/Q)$  with ( $m \leq n$ ), where  $Q$  is a typical scale of the process. This important effect can be taken into account by structure functions, which are known to quite high order (see, e.g., Ref. [120] and references therein). The full inclusion of NLO corrections in predictions, however, require dedicated calculations:

- *Higgs-boson–photon production*  $e^+e^- \rightarrow H\gamma$  [121, 122]

The production of a Higgs boson in association with a photon mainly proceeds via top-quark and W-boson loops, where a significant destructive interference occurs. At LEP energies,  $H\gamma$

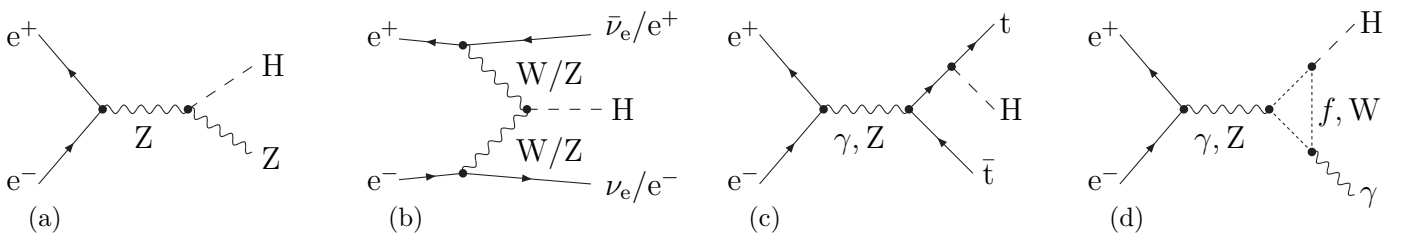


Figure 7: Representative lowest-order diagrams for the main SM Higgs-boson production channels at  $e^+e^-$  colliders: (a) Higgs-strahlung, (b) vector-boson fusion, (c) top-quark associated production, (d)  $H\gamma$  production.

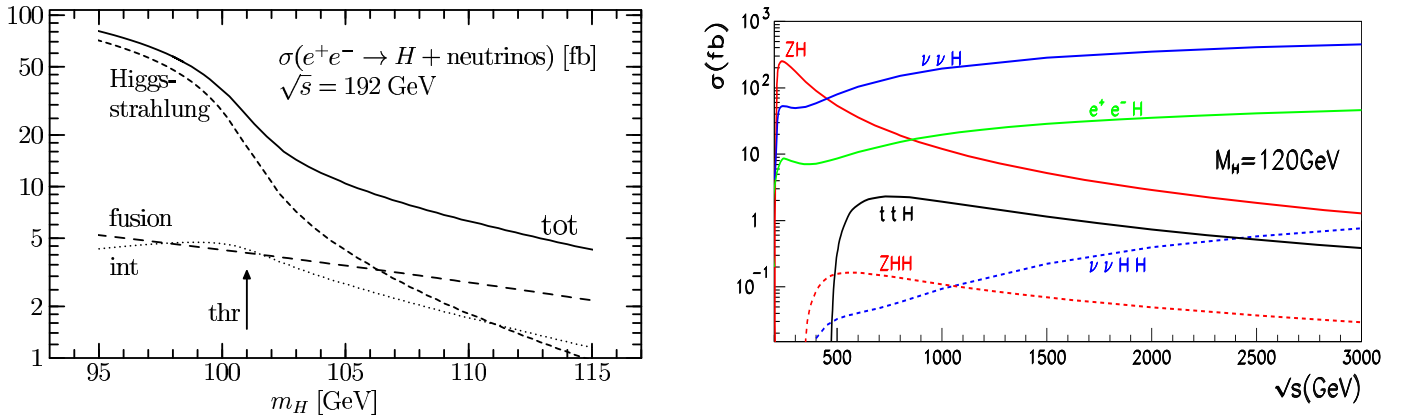


Figure 8: Left: cross section for  $e^+e^- \rightarrow H\nu\bar{\nu}$  for a typical LEP2 energy and its breakup into Higgs-strahlung, W-fusion, and interference contribution (taken from Refs. [115, 116]); right: cross sections for the various SM single-Higgs-boson and Higgs-boson pair production channels for a future  $e^+e^-$  linear collider (taken from Ref. [117]).

production only contributed in the search for a light Higgs boson with a mass well below the Z-boson mass, i.e.  $H\gamma$  production was mainly treated as potential decay mode of the Z boson [121]. At a high-luminosity  $e^+e^-$  linear collider  $H\gamma$  should, however, also be observable at energies far above the Z resonance [122], where  $e^+e^- \rightarrow H\gamma$  is a true  $2 \rightarrow 2$  scattering process. Since this rare process is already loop induced, full NLO predictions would require a two-loop calculation with multiple scales that is technically still out of reach with present calculational techniques. On the other hand, taking into account the universal ISR effects most likely will also be sufficient to match the expected experimental precision at a future collider.

- *Higgs-strahlung*  $e^+e^- \rightarrow HZ$  [57, 123–125]

The actual Higgs-strahlung signal that was searched for at LEP was mainly based on the  $H \rightarrow b\bar{b}$  decay and various Z-boson decays  $Z \rightarrow f\bar{f}$ . Higher-order effects from ISR lead to relevant corrections of 10–20% at LEP energies and have been taken into account in the LEP analyses. The remaining genuine weak corrections, which comprise weak-boson exchange etc., have been first calculated in the approximation of on-shell Z and Higgs bosons [124] and amount to 1–2% only at LEP energies. Later the EW corrections have also been evaluated including the leading off-shell effects of  $Z \rightarrow \mu^+\mu^-$  and  $H \rightarrow b\bar{b}$  [125], which will be relevant at possible precision studies at a future linear collider. The EW corrections become more and more relevant with increasing collider energy.

- *W fusion*  $e^+e^- (WW) \rightarrow H\nu\bar{\nu}$  [116, 123, 126–131]

Actually the physically observable process involves a sum over all three neutrino species in the final state. While W fusion is only possible for  $\nu_e\bar{\nu}_e$  pairs in the final state, all three  $\nu\bar{\nu}$  channels receive contributions from  $s$ -channel HZ production with  $Z \rightarrow \nu\bar{\nu}$  decays; for  $H\nu_e\bar{\nu}_e$   $t$ - and  $s$ -channel interfere. The l.h.s. of Figure 8 illustrates the interplay of HZ ( $\rightarrow \nu\bar{\nu}$ ) production and W fusion for a typical LEP2 energy near the HZ threshold region where W fusion becomes significant. For  $\sqrt{s} \lesssim M_H + M_Z$  the HZ production process can only proceed via off-shell Z bosons (the Higgs boson is too narrow to get off shell for the  $M_H$  values relevant at LEP). Sufficiently above the HZ threshold ( $\sqrt{s} \gtrsim M_H + M_Z + 100$  GeV for  $M_H \sim 100$ –200 GeV), which is an interesting region for future linear colliders, W fusion dominates (see r.h.s. of Figure 8). The NLO corrections are of pure EW origin and known [130, 131]. Owing to the dominating  $t$ -channel kinematics, which prefers forward/backward-produced (anti)neutrinos and low-virtuality intermediate W bosons,

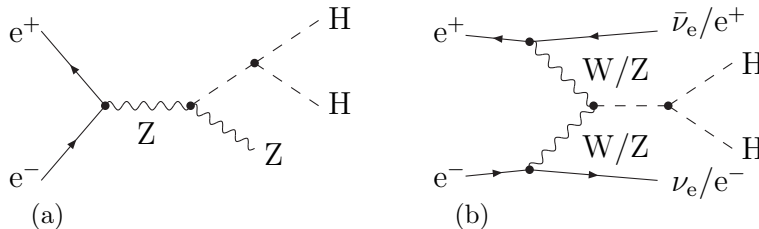


Figure 9: Lowest-order diagrams for Higgs-boson pair production at  $e^+e^-$  colliders: (a) Higgs-strahlung, (b) W/Z-boson fusion.

the corrections to W fusion can be described within few percent by an approximation based on universal ISR (with appropriate scale  $Q$ ) and a simple constant correction factor from heavy top loops [131].

- *Z fusion*  $e^+e^-(ZZ) \rightarrow H^+e^-$  [127–129, 132]

The Z-fusion cross section is suppressed with respect to the one of W fusion by roughly a factor of 10 as a mere consequence of the different size of the charged- and neutral-current couplings of the electron. However, Z fusion bears the advantage that it also would be observable at the  $e^-e^-$  variant of a linear collider. Similar to  $H\nu\bar{\nu}$  production,  $H^+e^-$  production receives contributions from  $s$ -channel  $HZ$  production diagrams and  $t$ -channel Z fusion graphs, where the logarithmic rise of the latter dominates at high energies. The EW corrections [132] again receive only small contributions  $\lesssim 5\%$  beyond ISR.

- *$t\bar{t}$  associated production*  $e^+e^- \rightarrow t\bar{t}H$  [133–140]

A precise measurement of the top-quark Yukawa coupling represents the main motivation to analyze  $t\bar{t}H$  production in the clean environment of an  $e^+e^-$  collider [134]. Assuming, for instance,  $M_H = 120$  GeV the Yukawa coupling could be measured with an accuracy of  $\sim 5\%$  at a linear collider operating at the energy of 800 GeV after collecting the integrated luminosity of  $1 \text{ ab}^{-1}$  [135]; in combination with other measurements even a higher accuracy is possible [136]. Owing to the  $t\bar{t}$  pair in the final state, the  $t\bar{t}H$  cross section receives both QCD [137] and EW corrections [138] at the NLO level, which are completely known. Sufficiently above the  $t\bar{t}$  threshold the generic size of QCD, photonic, and remaining electroweak corrections is 5–10% on the cross section, but the effect on kinematical distributions can be much larger. In particular, the QCD correction in the  $t\bar{t}$  threshold region deserves particular attention, since it is dominated by the Coulomb singularity. A careful treatment of these long-distance effects within non-relativistic QCD [139] reveals corrections of  $\sim 70\%$  relative to the NLO cross section for slowly moving  $t\bar{t}$  pairs. For a Higgs boson with  $M_H = 120$  GeV at a 500 GeV collider this pushes the NLO  $K$  factor of 1.7 further up to 2.4.

On the other hand, a realistic, precise description of the process has to include the top-quark and Higgs-boson decays, leading to a 10-particle final state already at LO, assuming the Higgs-boson decay into  $b\bar{b}$  pairs. Corresponding multi-particle Monte Carlo simulations are described in Ref. [140].

A future  $e^+e^-$  linear collider could also allow for a determination of the triple Higgs-boson self-coupling via Higgs-boson pair production [117, 141–143] if the collider energy is high enough. As illustrated in Figure 9, the promising production channels are Higgs-strahlung and W fusion, where diagrams with triple Higgs couplings compete with other pair production diagrams. Figure 8 includes the corresponding Higgs pair production cross sections for a linear collider up to energies in the few-TeV range. Similar to single-Higgs-boson production, the Higgs-strahlung mechanism delivers the largest production cross section for Higgs-boson pairs for energies directly above the  $HHZ$  threshold, but this

cross section decreases  $\propto 1/s$ . W fusion again shows a logarithmic rise with increasing energy and takes over the leading role for energies  $\sqrt{s} \gtrsim 1$  TeV for  $M_H = 120$  GeV. It should be noted, however, that for a low Higgs-boson mass the cross sections are  $\lesssim 0.2 \text{ fb}^{-1}$  for  $\sqrt{s} \lesssim 1$  TeV and get even more suppressed for larger  $M_H$ . Thus, a determination of the triple-Higgs coupling to  $\sim 20\%$  for  $M_H = 120\text{--}180$  GeV requires a high-luminosity linear collider ( $L \sim 1 \text{ ab}^{-1}$ ) operating at TeV energies [142]. The EW corrections both to HHZ production [143] and to W fusion to Higgs-boson pairs [117] are known. The results resemble the qualitative features of their single-Higgs counterparts, but the size of the effects get somewhat larger. In addition to the obligatory large ISR effects, the genuine weak corrections are at the generic level of 5–10%. For  $s$ -channel HHZ production the weak corrections show the tendency to grow negative with increasing energy, while the weak corrections to  $t$ -channel W fusion hardly depend on the energy sufficiently above the HH threshold.

A direct experimental investigation of the quartic Higgs self-coupling via triple Higgs production processes seems out of reach, since the cross sections are too much suppressed and are not very sensitive to the  $H^4$  coupling.

## 5 Searches at LEP

### 5.1 The LEP1 era

From autumn 1989 to summer 1995 the LEP accelerator was operated at CM energies in the vicinity of the mass of the Z boson, and in total 15.5 million hadronic Z-boson decays  $Z \rightarrow q\bar{q}$  and 1.7 million leptonic decays  $Z \rightarrow \ell^+\ell^-$  were collected by the four experiments ALEPH, DELPHI, L3, and OPAL. At the end of LEP1 data taking a peak luminosity of  $2 \times 10^{31} \text{ cm}^{-2}\text{s}^{-1}$  was reached, corresponding to approximately 1000 Z bosons being recorded per hour by each experiment. Even for very low Higgs-boson masses very efficient triggering of the final states of interest was possible and did not impose a severe problem for the analysis.

As detailed in Section 4, the dominant production mode for the Higgs boson is the rare decay  $Z \rightarrow Z^*H$ . The total expected event rate for the decay  $Z \rightarrow Z^*H \rightarrow \mu\mu H$  for one million of hadronic Z decays is approximately 75 (12, 0.4) for a Higgs-boson mass of 10 (30, 60) GeV (see Figure 10, left). For a Higgs-boson mass of roughly 60 GeV the event rates in  $Z \rightarrow Z^*H \rightarrow \mu\mu H$  and  $Z \rightarrow \gamma H$  are of comparable size (see Figure 10, left). However, considering also the decay of the  $Z^*$  into electrons and neutrinos increases the rate in accessible final states arising from  $Z \rightarrow Z^*H$  by a factor of eight. In addition to the smaller rate for  $Z \rightarrow \gamma H$  the background from  $f\bar{f}\gamma$  was also more severe for this final state. Hence no dedicated search for the decay  $Z \rightarrow \gamma H$  was performed, as the contribution to the sensitivity is negligible given the integrated luminosity collected at LEP1 of up to approximately  $160 \text{ pb}^{-1}$ . At LEP1 the Higgs-boson mass range from 0 to approximately 65 GeV could be probed.<sup>7</sup> The a priori signal-to-background ratio corresponds to  $10^{-2}$  for low masses and  $10^{-6}$  at the edge of the mass sensitivity (see also Figure 6). The kinematics in Higgs-boson production and decay is characterized by the average values of the Higgs-boson momentum and the opening angle of the H- and Z-boson decay products, which are shown in Figure 10 (middle and right) as function of the Higgs-boson mass.

Three Higgs-boson mass ranges can be roughly distinguished: (a)  $0 \leq M_H \leq 2m_\mu$ , (b)  $2m_\mu \leq M_H \leq 3 \text{ GeV}$ , and (c)  $M_H \geq 3 \text{ GeV}$ . These mass ranges differ in the dominant Higgs-boson branching ratios and the robustness of their theoretical predictions, the kinematics and topology, the composition of the dominant backgrounds, and the search strategies applied.

- For  $2m_\mu \leq M_H \leq 3 \text{ GeV}$  a perturbative description of the Higgs-boson decay, the prediction of the branching ratios, and hence the estimation of the detection efficiencies have large uncertainties.

---

<sup>7</sup>In parallel to the start of LEP a search for light Higgs bosons, performed in an electron beam-dump experiment, was published, which unambiguously excludes the mass range 1.2–52 MeV [144].

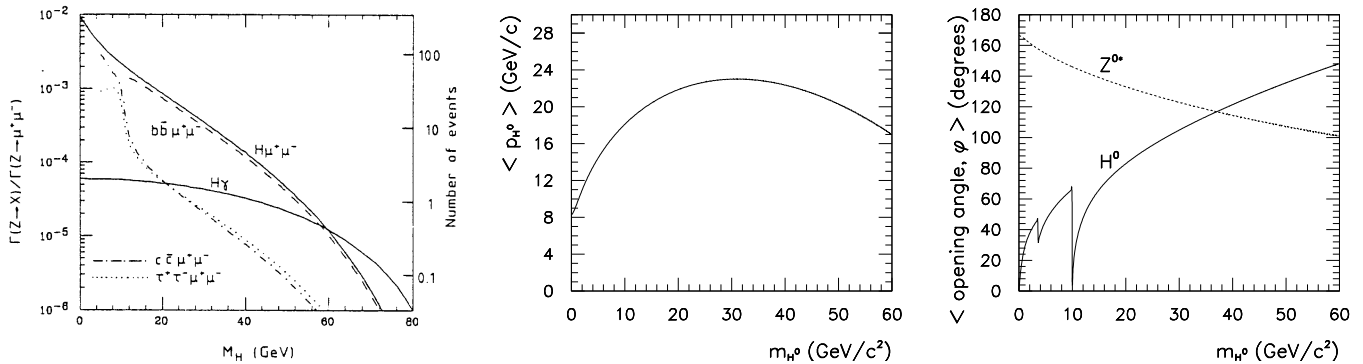


Figure 10: Relative decay rates for  $Z \rightarrow Z^*H \rightarrow \mu\mu H$  and  $Z \rightarrow \gamma H$  and number of expected events per  $10^6$  hadronic  $Z$  decays [145] (left), average momentum of the Higgs boson (middle), and average opening angle of the  $Z^*$  and  $H$ -boson decay products [98] (right) as a function of the hypothetical Higgs-boson mass.

The Higgs boson decays dominantly into several hadrons (e.g. a pair of pions, kaons, etc.) and for  $2m_\mu \leq M_H \leq 2m_\pi$  into a pair of muons. Different approaches were used by the four experiments to cover this mass range. ALEPH [146] and DELPHI [147] extended their standard searches in the lepton  $Z^* \rightarrow \ell^+\ell^-$  and missing energy  $Z^* \rightarrow \nu\bar{\nu}$  final states (see below) to the mass range below 3 GeV, allowing only two tracks being assigned to the Higgs-boson candidate. They relied on some modelling of Higgs-boson decays in this non-perturbative regime. In addition, for mass values below 2 GeV the decay  $Z^* \rightarrow q\bar{q}$  was considered by asking for three- or four-jet events and assigning the jet with the lowest track multiplicity to the Higgs-boson candidate, which is only allowed to have two tracks. L3 [148] only utilized the decay  $Z^* \rightarrow \ell^+\ell^-$  with two energetic acoplanar leptons and considered Higgs-boson decays to a least one track, covering the decay into muons and hadrons. OPAL [149] performed a decay-mode-independent search by two complementary analyses: (a) acoplanar leptons with vetoing on  $H \rightarrow$  “electromagnetic”  $e^+e^-/\gamma\gamma/\pi^0\pi^0$  decays, which is also sensitive to a long-lived Higgs boson decaying outside the detector, and (b) a dedicated search  $H \rightarrow$  “electromagnetic” decays accompanied by missing energy from  $Z^* \rightarrow \nu\bar{\nu}$ . The OPAL approach does not rely on the prediction of branching ratios and details of modelling the hadronic Higgs-boson decay in the non-perturbative regime, and hence is almost model independent.

- For  $M_H \leq 2m_\mu$  the dominant decay is to a pair of electrons, and for  $M_H \leq 2m_e$  only the loop-induced decay to a pair of photons is possible. In this mass range the Higgs boson gets long-lived (average decay length of 1 (100) meter(s) for  $M_H = 100$  (10) MeV), and a significant fraction of Higgs bosons decay outside the detector, leaving an invisible Higgs-boson decay as signature. ALEPH [146, 150] and DELPHI [151] extended the above searches in the  $Z^* \rightarrow q\bar{q}$  and  $Z^* \rightarrow \nu\bar{\nu}$  final states and performed a dedicated analysis, which looked for a  $V^0$  signature (i.e. a displaced vertex with two tracks) accompanied by any decay mode of the  $Z^*$  boson. The di-track invariant mass of the  $V^0$  candidate should not be consistent with that of a long-lived hadron ( $K_s^0$ ,  $\Lambda$ , etc.), and the tracks should be not identified as hadrons. L3 [152] used the acoplanar lepton search from the  $2m_\mu \leq M_H \leq 3$  GeV range allowing also for  $H \rightarrow e^+e^-$  decays. OPAL [153] looked for  $Z^* \rightarrow \nu\bar{\nu}$  and  $H \rightarrow e^+e^-/\gamma\gamma$  decays with at least one energy deposit in the electromagnetic calorimeter, to which tracks can be assigned, and not much additional detector activity. All experiments complemented this analysis by a search for invisible Higgs-boson decays in the acoplanar lepton topology with no other significant activity in the detector. A combination of the “invisible Higgs-boson” search and the other ones discussed above exclude all mass values down to 0.

- For  $M_H \geq 3 \text{ GeV}$  the perturbative description of the Higgs-boson decay is more reliable (apart from the mass values corresponding to  $b\bar{b}$  and  $c\bar{c}$  bound states). For low Higgs-boson masses ( $M_H \leq 10\text{--}15 \text{ GeV}$ ) the Higgs-boson decay products build a mono-jet topology due to the large Lorentz boost. For larger Higgs-boson masses the topology tends to two separated jets, which have an opening angle less than 180 degree in space (“acollinearity”) and also in the projection into the plane perpendicular to the beam axes (“acoplanarity”). The final state with largest sensitivity is the decay  $Z \rightarrow Z^*H \rightarrow \nu\bar{\nu}H$ , where for  $M_H$  larger than 15 GeV the decay into a pair of b-quarks is dominant. A production rate that is smaller by a factor three is provided by the decays  $Z \rightarrow Z^*H \rightarrow \mu^+\mu^-H/e^+e^-H$ . This ratio of three is roughly retained at the end of the event selections. Together the two final states cover approximately 25% of the Higgs-boson production rate. Final states involving tau leptons,  $Z^*H \rightarrow \tau^+\tau^-q\bar{q}$ ,  $Z^*H \rightarrow q\bar{q}\tau^+\tau^-$ ,  $Z^*H \rightarrow \ell^+\ell^-\tau^+\tau^-$ , and  $Z^*H \rightarrow \nu\bar{\nu}\tau^+\tau^-$ , have either a small production rate or a quite low selection efficiency. The expected signal event yields after the full selection are approximately one order of magnitude smaller than that expected in the  $Z^*H \rightarrow \nu\bar{\nu}H$  search. Hence final states with tau leptons only contribute marginally to the combined sensitivity. All collaborations investigated final states with tau leptons [150, 154–156] at intermediate stages of the Higgs-boson search at LEP1, but not included them in the analysis providing the final mass limit. Fully hadronic final states from  $Z \rightarrow Z^*H$  are not considered due to the overwhelming background.

The  $Z \rightarrow Z^*H \rightarrow \nu\bar{\nu}H$  topology is characterized by missing energy, missing (transverse) momentum, and the detector activity from the Higgs-boson decay. With increasing Higgs-boson mass the particle multiplicity from the Higgs-boson decay is increased. Due to the smaller Lorentz boost the topology changes from a mono-jet to an acollinear and acoplanar di-jet final state. At the same time the missing energy and missing mass decrease, as the  $Z^*$  boson has to be more off shell. Almost no irreducible backgrounds exist, and the background contributions are mostly of instrumental nature due to mismeasurements, wrong identification of final-state particles, and incomplete detector coverage. The dominant background for large Higgs-boson masses is due to  $Z \rightarrow q\bar{q}$  decays, where missing energy arises from neutrinos produced in heavy-flavour decays and mismeasurements, and from four-fermion production via  $Z^* \rightarrow Z^*\gamma^* \rightarrow \nu\bar{\nu}q\bar{q}$  and  $e^+e^- \rightarrow e^+e^-\gamma^*\gamma^* \rightarrow e^+e^-q\bar{q}$ . The four-fermion processes are characterized by a low mass of the hadronic system and hence are mostly relevant for small Higgs-boson masses, and events of the  $e^+e^-q\bar{q}$  channel typically show small (missing) transverse momentum. The mass resolution for the hadronic system is of the order of 10%. DELPHI also applied b-tagging for the final analysis exploiting the large branching ratio  $H \rightarrow b\bar{b}$ .

The  $Z \rightarrow Z^*H \rightarrow \ell^+\ell^-H$  topology is characterized by two isolated leptons, whose acollinearity and acoplanarity increase with increasing Higgs-boson mass, and a recoiling hadronic system. The mass of the Higgs-boson candidate can be reconstructed from the four-momenta of the leptons using energy–momentum conservation (“recoil mass technique”) with a precision of 1–2%. The dominant background from four-fermion production has either a small mass of the leptonic or of the hadronic system. The  $Z \rightarrow q\bar{q}$  background with leptonic heavy-flavour decays possesses a large mass of the hadronic system, and the leptons do not originate from the primary collision vertex. For the final analysis performed at LEP1 most experiments exploited b-tagging to further discriminate the signal especially from four-fermion background processes.

The event selections were mostly designed in such a way that the expected background was at the level of one event or less at the edge of the Higgs-boson mass sensitivity for a given data set. With increased integrated luminosities this required more sophisticated and refined analyses and tighter identification and isolation requirements to exploit the above-mentioned differences between signal and background topologies and their dependence on the Higgs-boson mass. Hence the selection efficiency for signal events at the sensitivity edge dropped from roughly 60% or higher



Table 2: Excluded Higgs-boson mass ranges from LEP1 searches: experiment, excluded mass range, number (in thousands) of recorded hadronic Z decays, integrated luminosity, years of data taking and references. The entry “–” indicates that the information is not available.

Experiment	excluded $M_H$ range	$10^3 Z \rightarrow q\bar{q}$	int. lumi. [ $\text{pb}^{-1}$ ]	data from year	Ref.
ALEPH	0.032–15 GeV	12	0.5	89	[146]
	11–24 GeV	25	1.2	89	[161]
	0–57 MeV	23	1.2	89	[162]
	< 41.6 GeV	100	–	89–90	[150]
	< 48 GeV	185	–	89–90	[163]
	< 58.4 GeV	1233	–	89–92	[164]
	< 63.9 GeV	4500	–	89–95	[157]
DELPHI	$2m_\mu$ –14 GeV	11	0.5	89	[147]
	0– $2m_\mu$	119	–	90	[151]
	< 38 GeV	119	–	90	[154]
	< 55.7 GeV	1000	34.6	91–92	[158]
L3	2–32 GeV	50	–	90	[148]
	0–2 GeV	70	–	90	[152]
	< 41.8 GeV	111	5.3	90	[165]
	< 52 GeV	408	17.5	90–91	[155]
	< 57.7 GeV	1062	39.0	90–92	[166]
	< 60.2 GeV	3000	114	91–94	[159]
OPAL	3–19.3 GeV	–	0.8	89	[167]
	0– $2m_\mu$	25	1.2	89	[153]
	3–25.3 GeV	25	1.2	89	[168]
	3–44 GeV	170	8	89–90	[156]
	0–11.3 GeV	–	6.8	90	[149]
	< 56.9 GeV	1900	78	90–93	[169]
	< 59.6 GeV	5000	160	89–95	[160]

in the first searches to a level of 30% in the final LEP1 searches. Only a few events survived all selection requirements in agreement with expectations from background processes.

All observed events are considered as Higgs-boson candidates and the expected signal yields are reduced by their systematic uncertainty. In summary, the searches performed by the four experiments allowed to exclude all Higgs-boson mass hypotheses below 63.9 GeV (ALEPH [157]), 55.7 GeV (DELPHI [158]), 60.2 GeV (L3 [159]), and 59.6 GeV (OPAL [160]), as shown in Figure 11 and in Table 2. The relative contribution to the sensitivity of the missing energy and leptonic final states can be deduced from Figure 11. In ALEPH and L3 the mass resolution of candidates close to the edge of the excluded mass range is taken into account following the technique described in Ref. [170], whereas OPAL did not apply such a technique. No official combination of the findings of the four LEP experiments was performed. Owing to the exponential decrease of the Higgs-strahlung cross section with increasing Higgs-boson mass, the excluded mass range only extended slowly with collected integrated luminosity

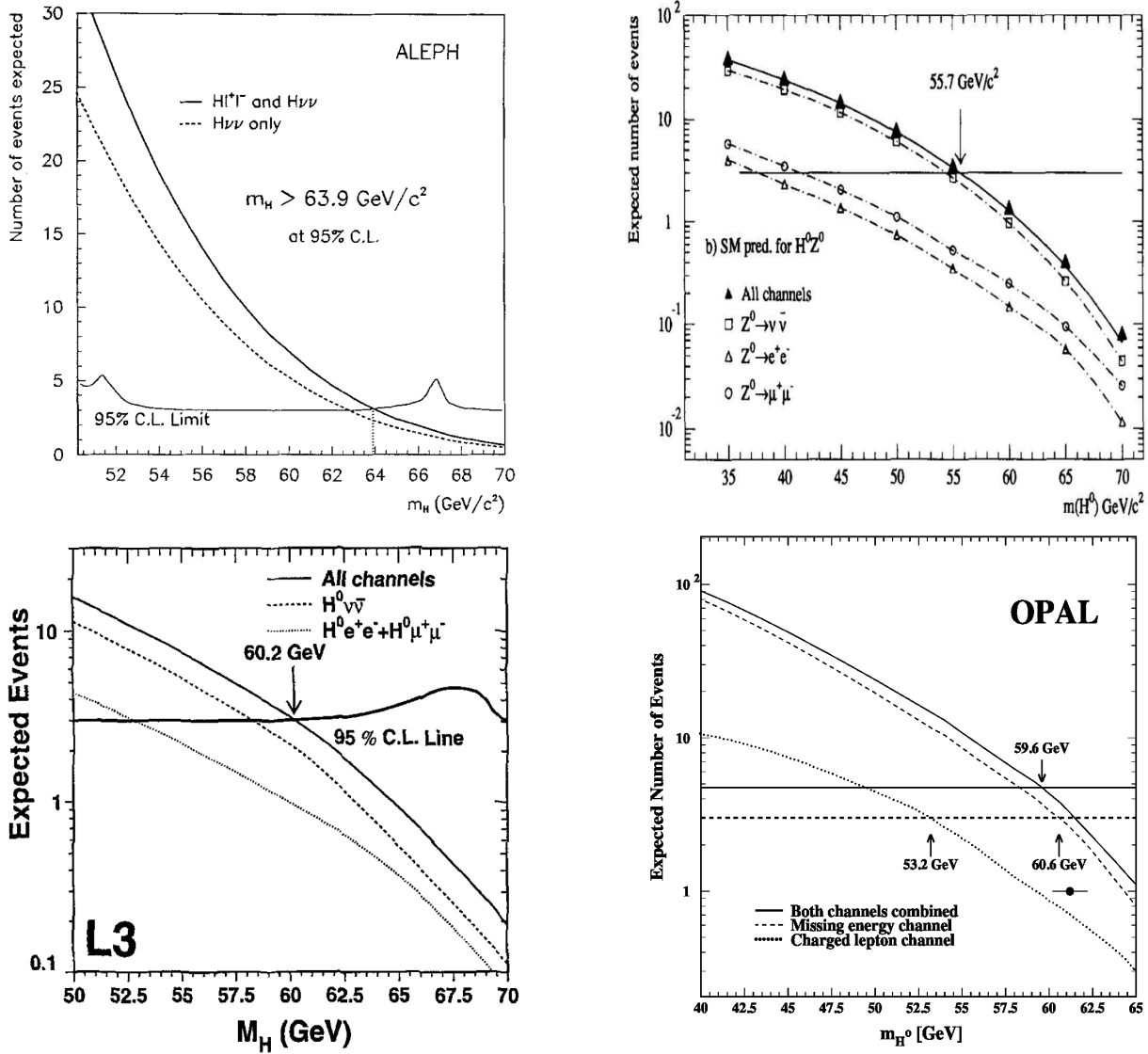


Figure 11: Excluded and expected event yields for Higgs-boson production at LEP1 by ALEPH (top-left) [157], DELPHI (top-right) [158], L3 (bottom-left) [159], and OPAL (bottom-right) [160].

(see Table 2). Hence an extension of data taking at LEP1 would not have significantly increased the mass reach of the searches, which for the first time excluded a significant fraction of the allowed Higgs-boson mass range in an unambiguous way.

## 5.2 The LEP2 era

Starting in summer 1995 at 130/136 GeV, the CM energy of the LEP collider was continuously increased over the next years up to 209 GeV in 2000. The data taken at 130/136 GeV were not used for SM Higgs-boson searches. A summary of the data sets recorded at different CM energies used for SM Higgs-boson searches during the LEP2 programme is given in Table 3. Approximately 0.5 (2.5)  $\text{fb}^{-1}$  at CM energies in excess of 206 (189) GeV were collected in total by the four experiments ALEPH, DELPHI, L3, and OPAL. At LEP2 CM energies the dominant production process is again Higgs-strahlung. But in contrast to LEP1 the Z boson in the final state is dominantly produced on its mass shell. The difference in the  $M_H$  dependence of  $e^+e^- \rightarrow Z \rightarrow Z^*H$  at LEP1 and  $e^+e^- \rightarrow Z^* \rightarrow ZH$  at LEP2 is shown in Figure 12 (left). Additional contributions from the vector-boson-fusion processes  $e^+e^- \rightarrow e^+e^-Z^*Z^* \rightarrow e^+e^-H$  and

Table 3: CM energies and integrated luminosities collected in each experiment at LEP2. Numbers in brackets give the luminosity-weighted CM energy of the corresponding year. The luminosity ranges are caused by the different data-taking efficiencies in the four experiments.

year	1996	1997	1998	1999	2000
CM energy [GeV]	161/170/172	183	189	192–202(198)	202–209(206)
int. luminosity [ $\text{pb}^{-1}$ ]	10–11/1/9–10	54–57	158–176	228–237	217–224

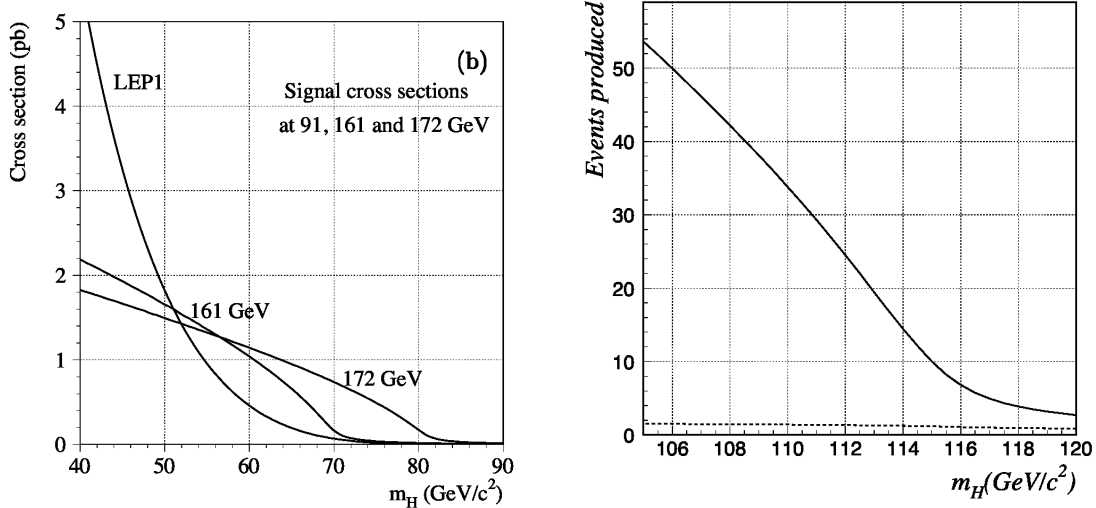


Figure 12: Comparison of Higgs-strahlung production cross sections at LEP1 and at the beginning of LEP2 (left from Ref. [171]). Number of expected Higgs-boson events per experiment produced in 2000 data taking from Higgs-strahlung (full line) and from vector-boson fusion and interference (dashed line) (right from Ref. [172]).

$e^+e^- \rightarrow \nu\bar{\nu}W^*W^* \rightarrow \nu\bar{\nu}H$  and their interference with the respective final states from Higgs-strahlung are at the level of maximally 10–20% (see Figure 8) at the sensitivity edge, which is approximately given by  $\sqrt{s} - M_Z - \text{few GeV}$ . The contribution to the total event yield (per experiment) for the production of a hypothetical Higgs boson in 2000 data is shown in Figure 12 (right). No dedicated searches for production in vector-boson fusion were performed. Signal cross sections were calculated and signal event were generated with HZHA [173].

In contrast to LEP1, now the hadronic decays of the Z boson can be utilized in the search, as the a priori signal-to-background ratio is larger by two to three orders of magnitude compared to LEP1 (see l.h.s. of Figure 10) at the sensitivity edge. Furthermore the mass constraint of two jets to stem from the decay  $Z \rightarrow q\bar{q}$  helps to discriminate the signal process from background processes. This new channel delivers the largest contribution to the sensitivity at LEP2. At LEP1 the background was mostly reducible, at least in principle, and caused by mismeasurements and hence difficult to model in all details. After crossing the thresholds for WW and ZZ production at the LEP2 CM energies of 161 GeV and 183 GeV, respectively, the dominant backgrounds are due to di-boson production and to a large extent irreducible. These could reliably be predicted via simulation.

Searches were performed in the “four-jet channel”  $ZH \rightarrow q\bar{q}b\bar{b}$  ( $ZH \rightarrow q\bar{q}q\bar{q}$ ), “missing-energy channel”  $ZH \rightarrow \nu\bar{\nu}b\bar{b}$  ( $ZH \rightarrow \nu\bar{\nu}q\bar{q}$ ), “tau channels”  $ZH \rightarrow q\bar{q}\tau^+\tau^-$  and  $ZH \rightarrow \tau^+\tau^-b\bar{b}$  ( $ZH \rightarrow \tau^+\tau^-q\bar{q}$ ), and “lepton channels”  $ZH \rightarrow e^+e^-b\bar{b}$  and  $ZH \rightarrow \mu^+\mu^-b\bar{b}$  ( $ZH \rightarrow e^+e^-q\bar{q}$  and  $ZH \rightarrow \mu^+\mu^-q\bar{q}$ ). Those final states together cover approximately 80% of the total production rate (see Table 4) for a Higgs boson

Table 4: Fraction of production rates in the different search channels at LEP2. The number outside (inside) brackets correspond to  $H \rightarrow q\bar{q}$  ( $H \rightarrow b\bar{b}$ ) decays.

Channel	$M_H = 60 \text{ GeV}$	$M_H = 115 \text{ GeV}$
four jets	64(60)%	57(50)%
missing energy	18(17)%	16(14)%
taus	9(9)%	6(5)%
leptons	6(6)%	8(8)%
sum	97(91)%	87(77)%

with a mass of 115 GeV, when only taking into account the decay  $H \rightarrow b\bar{b}$ . Given the long time intervals between bunch crossings of  $22 \mu\text{s}$ , the instantaneous luminosity of  $10^{32} \text{ cm}^{-2}\text{s}^{-1}$ , and the size of the total cross section, triggering on all signal topologies was not a problem. Due to the presence of irreducible backgrounds from pair production of weak gauge bosons, in particular for CM energies of 183 GeV and larger, it was not possible to design analyses that yield background expectations at the level of few events as at LEP1, while retaining a large fraction of the signal process. Extensive use was made of largely improved capabilities to identify b-flavoured jets in order to suppress backgrounds, in particular from WW production. The reconstruction of the mass of Higgs-boson candidates was greatly improved in many channels by kinematic fits which required energy and momentum conservation and often the consistency of a di-fermion mass with  $M_Z$ . Many analyses exploited the advantages of multivariate techniques, which were trained for various different Higgs-boson mass hypotheses. In several cases the mass-sensitive observables together with the response of the multivariate technique were combined in a final discriminant, which was used in the hypothesis tests.

Below the main characteristics of the four search channels, which are ordered by their sensitivity, and the most important means to discriminate them from the dominant backgrounds are discussed:

- “Four-jet channel”: The topology is characterized by four jets, two consistent with the decay  $Z \rightarrow q\bar{q}$  and two consistent with the decay  $H \rightarrow b\bar{b}$ . Requiring two jets to be identified as b-flavoured suppresses strongly backgrounds from WW production and partially from ZZ production, as the branching ratios for  $Z \rightarrow b\bar{b}$  of 15% is much smaller than the corresponding one for the Higgs boson. The sensitivity is enhanced by a precise reconstruction of the di-jet invariant mass of the jets assigned to the Higgs-boson decay. Exploiting energy and momentum conservation and constraining the other di-jet mass to  $M_Z$ , significantly improves the mass resolution. Contributions from  $e^+e^- \rightarrow Z/\gamma^* \rightarrow 4 \text{ jets}$  are small for CM energies beyond 183 GeV.
- “Missing-energy channel”: The topology is characterized by large missing energy, missing (transverse) momentum, and missing mass (derived from energy and momentum conservation) due to the decay  $Z \rightarrow \nu\bar{\nu}$ , two acoplanar b-flavoured jets from the decay of the Higgs boson, and no leptons being present. Requiring b-tagged jets greatly reduces backgrounds from  $WW \rightarrow q\bar{q}\ell\nu$ , where the charged lepton escapes detection, and partially helps to reduce the contribution from  $ZZ \rightarrow q\bar{q}\nu\bar{\nu}$ . The reconstruction of the mass of the Higgs boson candidate from the di-jet system is often significantly improved by exploiting energy and momentum conservation and constraining the missing mass to  $M_Z$ . The remaining background is dominated by di-boson production.
- “Lepton channels”: The topology is characterized by two acoplanar leptons consistent with the decay  $Z \rightarrow \ell^+\ell^-$  and two acoplanar b-flavoured jets from the decay of the Higgs boson. Requiring b-tagged jets reduces background from  $ZZ \rightarrow q\bar{q}\ell^+\ell^-$ . The mass of the Higgs-boson candidate is

Table 5: Excluded mass ranges in the individual experiments at various stages during the LEP2 programme: data set used, observed (expected) mass limit, and reference. The entry “–” indicates that this information is not published.

CM energy	ALEPH	DELPHI	L3	OPAL
$\leq 161$ GeV	–	–	–	65.0 (–) [174]
$\leq 172$ GeV	70.7 (–) [171]	66.2 (–) [175]	69.5 (–) [176]	69.4 (65) [177]
$\leq 183$ GeV	87.9 (85.3) [178]	85.7 (86.5) [179]	87.6 (86.8) [180]	88.3 (86.1) [181]
$\leq 189$ GeV	92.9 (95.9) [182]	94.6 (94.4) [183]	95.3 (94.8) [184]	91.0 (94.9) [185]
$\leq 202$ GeV	107.7 (107.8) [186]	107.3 (106.4) [187]	107.0 (105.2) [188]	–
$\leq 209$ GeV	111.1 (114.2) [172]	114.3 (113.5) [189]	–	109.7 (112.5) [190]
final	111.5 (114.2) [191]	114.1 (113.3) [192]	112.0 (112.4) [193]	112.7 (112.7) [194]

reconstructed as the recoil to the di-lepton system. In some cases kinematic fits exploiting energy and momentum resolution improve the sensitivity. For CM energies larger than 183 GeV the final background is, to a very large extent, due to ZZ production.

- “Tau channels”: The topology is characterized by two hadronic jets and two tau-lepton candidates, where one pair is assigned to the Z decay and the other to the H decay. The assignment to the  $ZH \rightarrow q\bar{q}\tau^+\tau^-$  or  $ZH \rightarrow \tau^+\tau^-\text{b}\bar{\text{b}}$  channels is based on the invariant masses of the tau and jet systems, and the quality of kinematic fits requiring energy and momentum conservation and applying the  $M_Z$  constraint. B-tagging improves the sensitivity in the  $ZH \rightarrow \tau^+\tau^-\text{b}\bar{\text{b}}$  final state. Selected background events are largely due to di-boson production.

After all selection requirement a typical signal-to-background ratio of the order between 2-to-1 and 1-to-1 could be achieved at the edge of the LEP sensitivity for masses of 115 GeV still retaining 30–60% of the eventually produced signal events depending on the final state. No significant deviations from the background-only hypothesis were observed in the data collected up to 1999 (see first four rows in Table 5). When comparing the sensitivity of the four experiments one should keep in mind that slightly different techniques for deriving the limits are used: for example ALEPH uses the technique discussed in Ref. [195] instead of the  $CL_S$  technique yielding a better expected limit by up to 0.5 GeV. Shortly after the end of data taking in 2000, ALEPH [172] reported an excess of events, dominated by the observation in the “four-jet channel”, with a minimal local  $p$ -value of  $1.5 \times 10^{-3}$  for  $M_H = 116$  GeV and stated that the observed rate would be compatible with Higgs-boson production for  $M_H = 114$  GeV. The other three experiments also published their initial findings based on 2000 data with focus on the mass range around 115 GeV. L3 [196] reported an excess with a  $p$ -value at  $M_H = 114.5$  GeV for the background-only hypothesis of 0.09 (for signal+background of 0.62). DELPHI and OPAL did not observe any excess. DELPHI [189] preferred the background-only hypothesis ( $p$ -value = 0.23) over the signal+background hypothesis ( $p$ -value = 0.03) for  $M_H = 115$  GeV, and OPAL [190] reported a similar  $p$ -value of 0.2 (0.4) for the background-only (signal+background) hypothesis. The corresponding observed and expected mass limits are shown in the fifth row of Table 5. The final LEP analyses (see last row of Table 5) used the latest and more accurate determinations of the LEP beam energies, better detector calibrations, a higher-statistics sample for simulated events and in some cases performed an optimization of the selection strategies for high  $M_H$ , whereas non-optimized analyses were used in the first analysis of the 2000 data.

The final mass distribution obtained from the combination of the four LEP experiments after tight selection requirements is shown in Figure 13 (top-left). The slight excess at large values is dominated

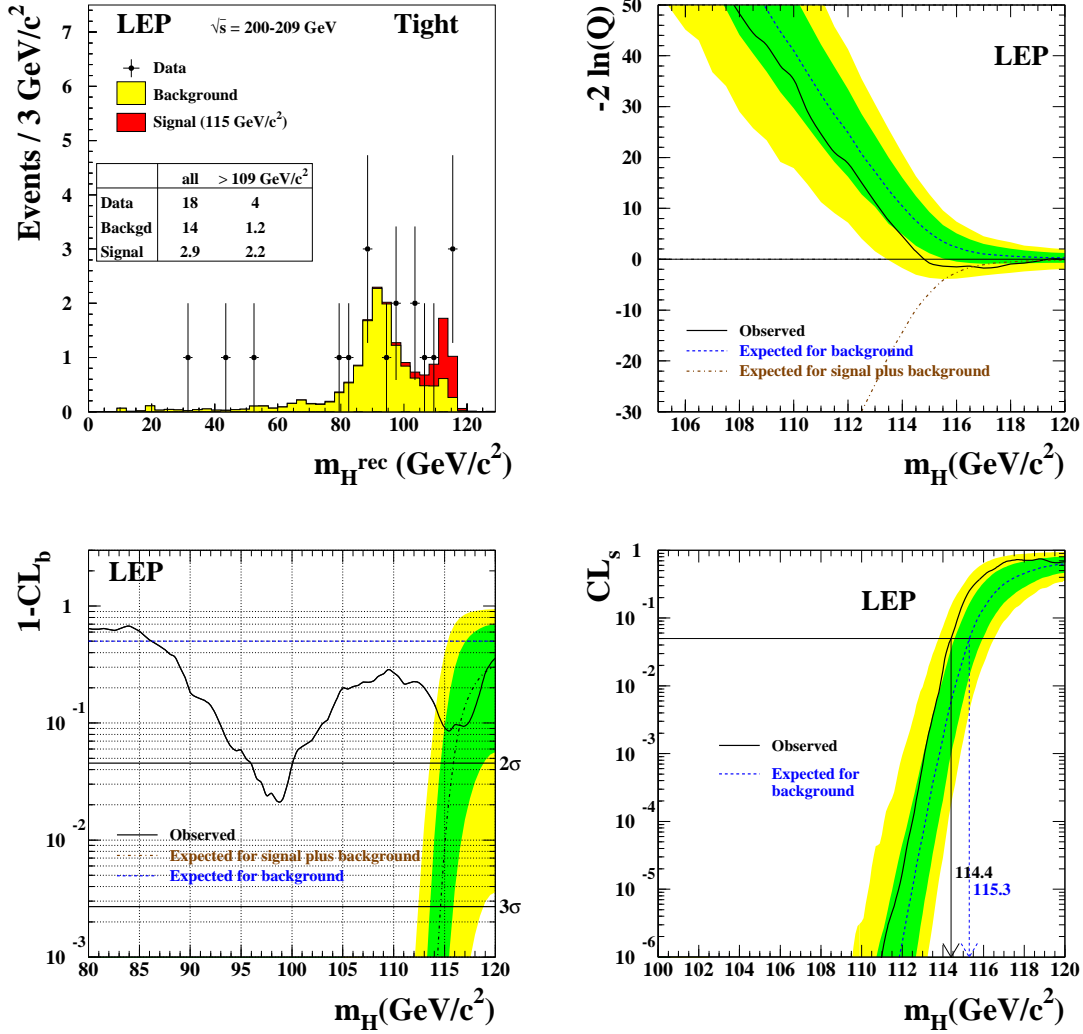


Figure 13: Final results of the Higgs-boson searches at LEP [197]: mass distribution of tightly selected Higgs-boson candidates compared to signal and background expectations (top-left), mean value of the test statistic  $-2 \ln Q$  as function of  $M_H$  for data and expectations from the signal+background hypothesis and the background-only hypothesis with 68% and 95% CL error bands (top-right), local  $p$ -values as function of  $M_H$  for data and expectations from the background-only hypothesis and signal+background hypothesis with 68% and 95% CL error bands (bottom-left),  $CL_s$ -values as function of  $M_H$  for data and expectations from the signal+background hypothesis and background-only hypothesis with 68% and 95% CL error bands (bottom-right).

by the “four-jet channel” in ALEPH. The expected and observed values of the test statistic  $-2 \ln Q$  depending on  $M_H$  (Figure 13, top-right), show the limited capabilities to distinguish the two hypotheses for large Higgs-boson masses. The two bands show the 68% and 95% probability bands for the background-only hypothesis. The final local  $p$ -values for the combination of all experiments are shown in Figure 13 (bottom, left) and detailed in Table 6 for the combination and the individual experiments. No significant excess is observed in the combination. The  $p$ -values for the two alternative hypotheses are very similar, indicating again the difficulty to discriminate the background-only and signal+background hypotheses for  $M_H = 115$  GeV. All SM Higgs-boson mass hypotheses below 114.4 GeV were excluded with at least 95% CL from the combination of the four experiments (see Figure 13, bottom-right) [197]. The expected combined limit was 115.3 GeV. The very small differences in the limits from the LEP

Table 6: Final results of the searches at LEP2: local  $p$ -values for the consistency with the background-only and signal+background hypotheses assuming  $M_H = 115$  GeV, expected and observed mass limits as derived in the LEP Higgs Working Group [197].

	$P_{b\text{-only}}$	$P_{s+b}$	exp. limit	obs. limit
LEP	0.09	0.15	115.3 GeV	114.4 GeV
ALEPH	$3.3 \times 10^{-3}$	0.87	113.5 GeV	111.5 GeV
DELPHI	0.79	0.03	113.3 GeV	114.3 GeV
L3	0.33	0.30	112.4 GeV	112.0 GeV
OPAL	0.50	0.14	112.7 GeV	112.8 GeV
four jets	0.05	0.44	114.5 GeV	113.3 GeV
all but four jets	0.37	0.10	114.2 GeV	114.2 GeV

Higgs Working Group for each individual experiment in Table 6 and the final ones published by each experiment, as shown in Table 5, are due to differences in the statistical methods applied.

At the beginning of the LEP programme no solid limit existed on the mass of the Higgs boson. The searches for the SM Higgs boson carried out by the four LEP experiments extended the sensitive range well beyond that anticipated at the beginning of the LEP programme. This is due to the higher energy achieved and to more sophisticated detectors and analysis techniques. The range below 114.4 GeV was and is difficult to probe at past and current hadron colliders.

## 6 Higgs-boson production at hadron colliders

### 6.1 Higgs-boson production mechanisms and cross-section overview

The four main production mechanisms for SM Higgs bosons at hadron colliders are illustrated by some representative LO diagrams in Figure 14. The size of the respective cross sections depends both on the type of colliding hadrons and on the collision energy. Figures 15 and 16 show the total cross sections of the various channels for the  $p\bar{p}$  collider Tevatron at its CM energy of  $\sqrt{s} = 1.96$  TeV and for the  $pp$  collider LHC at the two energies  $\sqrt{s} = 7$  TeV and 14 TeV. At the LHC, the energy increase from 7 TeV to 8 TeV leads to an increase of 20–30% in the Higgs-boson production cross sections for  $M_H \sim 100\text{--}200$  GeV. The transition from 7 TeV to 14 TeV in energy increases the cross sections even by a factor of about 3–4 for these Higgs-boson masses, with the exception of  $t\bar{t}H$  production, where

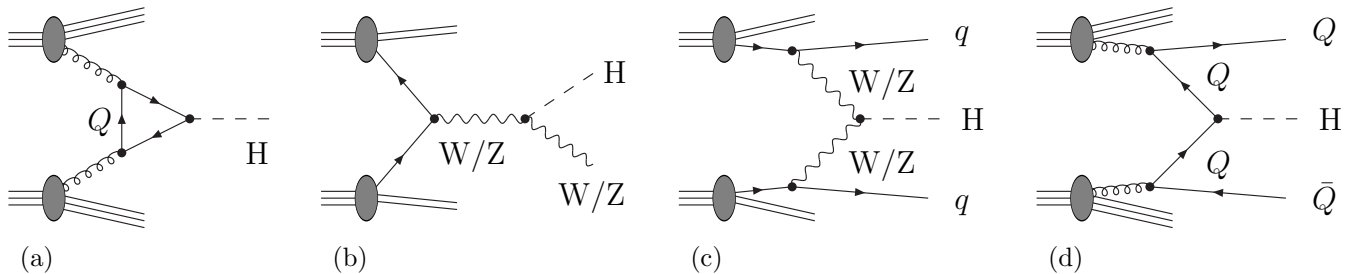


Figure 14: Representative leading-order diagrams for the main SM Higgs-boson production channels at hadron colliders, where  $q$  and  $Q$  denote light and heavy quarks, respectively: (a) gluon fusion, (b) Higgs-strahlung, (c) vector-boson fusion, (d) heavy-quark associated production.

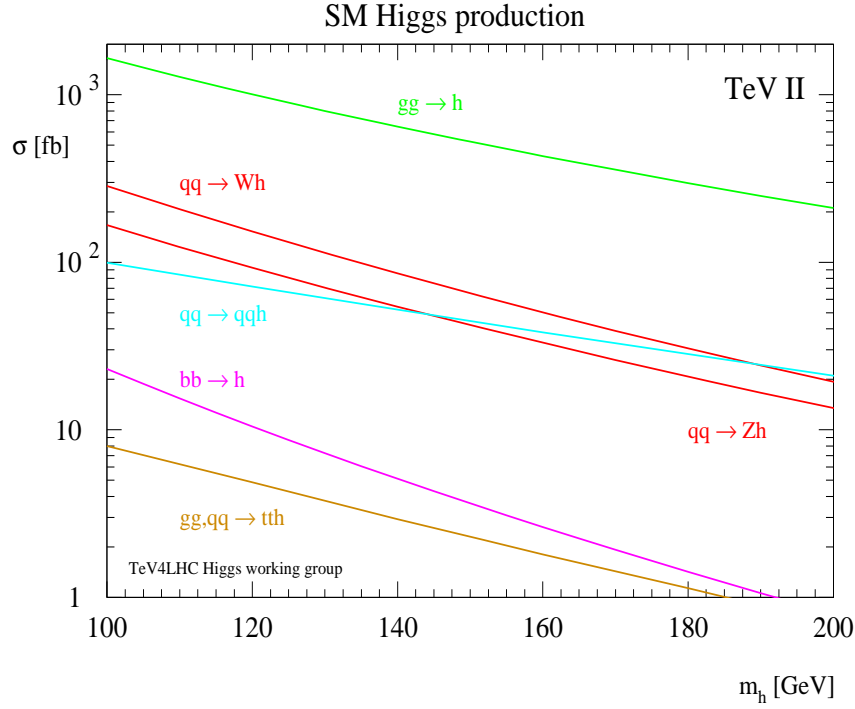


Figure 15: Cross sections for the various SM Higgs-boson production channels at Tevatron with a CM energy of 1.96 TeV, as predicted by the TeV4LHC Section Working Group [198].

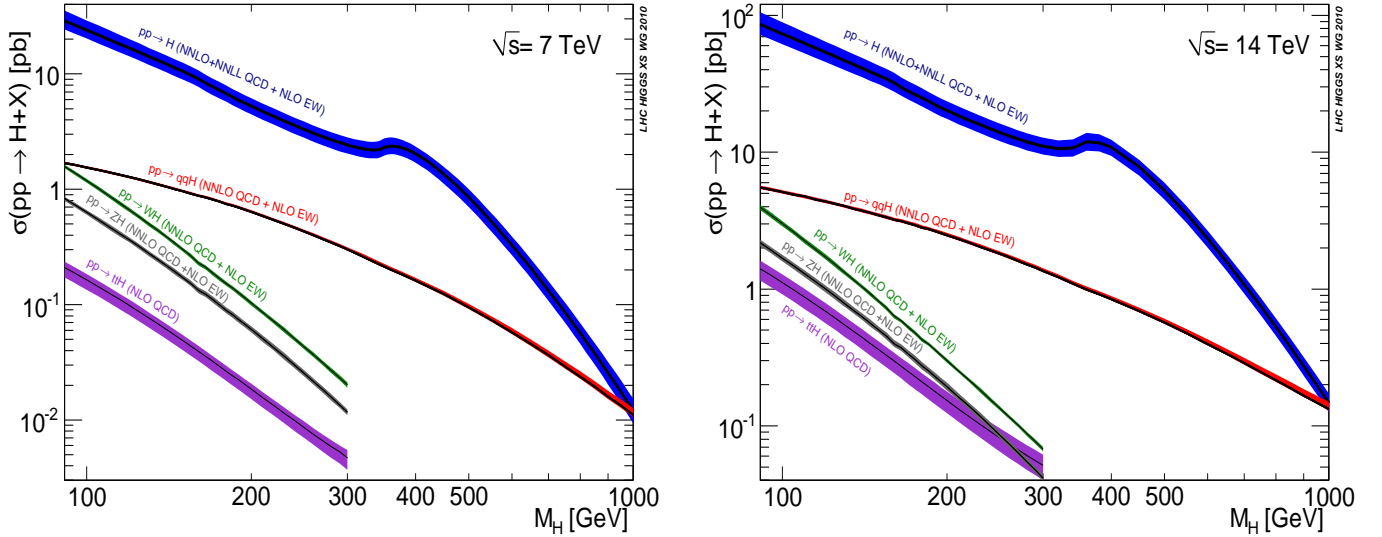


Figure 16: Cross sections and respective uncertainties, indicated by the band widths, for the various SM Higgs-boson production channels at the LHC with a CM energy of 7 TeV and 14 TeV, as predicted by the LHC Higgs Cross Section Working Group [25].

the factor is roughly 8. Globally, loop-induced Higgs-boson production via gluon fusion delivers the largest cross section owing to the large gluon flux in high-energy proton-(anti)proton collisions. The respective cross section is typically an order of magnitude or more larger than the remaining production cross sections. At the LHC, the vector-boson fusion (VBF) cross section competes in size with gluon fusion only for Higgs bosons as heavy as nearly 1 TeV. VBF delivers the second largest cross section, showing a much slower decrease with increasing Higgs-boson mass owing to its  $t$ -channel dominance, which leads to a logarithmic rise of its partonic cross section with increasing partonic CM energy  $\sqrt{\hat{s}}$ .



Table 7: Theoretical (THU) and parametric PDF+ $\alpha_s$  uncertainties (PU) for the total Higgs-boson production cross sections at the LHC with CM energies 7 TeV and 14 TeV, as assessed by the LHC Higgs Cross Section Working Group [25] employing the PDF4LHC [24] recipe for PU, as well as the typical size of radiative corrections of the strong (QCD) and electroweak (EW) interactions. The colour coding NLO/NNLO/NNLO+ refers to the respective perturbative order included in the predictions, where NNLO+ means that resummations beyond the fixed-order correction are included.

$M_H$ [GeV]	LHC @ $\sqrt{s} = 7$ TeV				LHC @ $\sqrt{s} = 14$ TeV			
	uncertainties		corrections		uncertainties		corrections	
	THU	PU	QCD	EW	THU	PU	QCD	EW
ggF < 500	6–10%	8–10%	$\gtrsim 100\%$	5%	6–14%	7%	$\gtrsim 100\%$	5%
VBF < 500	1%	2–7%	5%	5%	1%	3–4%	5%	5%
HW < 200	1%	3–4%	30%	5–10%	1%	3–4%	30%	5–10%
HZ < 200	1–2%	3–4%	40%	5%	2–4%	3–4%	45%	5%
ttH < 200	10%	9%	5%	?	10%	9%	15–20%	?

At Tevatron the Higgs-strahlung channels of HW/HZ production compete with VBF in size for Higgs masses  $M_H \lesssim 100\text{--}200$  GeV mainly due to the different combinations of PDFs. For a  $p\bar{p}$  initial state high-energy  $q\bar{q}$  collision, which is needed for Higgs-strahlung in LO, is preferred over  $qq$  scattering, since in this case the  $q\bar{q}$  channel can proceed via two valence quarks, which carry much more momentum than sea quarks on average. The total Higgs-strahlung cross section for HW production, where the sum over  $W^\pm$  is taken, is larger than the one for HZ production by roughly a factor of two. The smallest relevant cross section in all cases is provided by Higgs production in association with  $t\bar{t}$  pairs, whose suppression is mainly due to the large invariant mass required to produce the three-particle final state of heavy objects. Similar to pure  $t\bar{t}$  pair production,  $t\bar{t}H$  production is largely dominated by  $q\bar{q}$  annihilation at Tevatron, but by gg fusion at the LHC. In the transition from Tevatron to the LHC and with increasing LHC energy, the suppression of the  $t\bar{t}H$  cross section steadily decreases with respect to the other channels, since the phase-space suppression of the heavy  $t\bar{t}H$  final state is fading for larger collider energy. The main motivation to measure the  $t\bar{t}H$  cross section clearly rests in the direct access to the top Yukawa coupling, without contamination from other couplings; even a qualitative measurement at the LHC would be a great success.

Predictions for hadronic collisions in general involve several serious sources of uncertainties that are tied to the hadronic environment, as explained in more detail in Section 2.4. Perturbative corrections, especially of the strong interactions, have to be taken into account as much as possible, in order to minimize the uncertainties, and the residual uncertainties, which are due to missing higher-order effects and parametric errors have to be quantified carefully. Figure 16 illustrates the error estimate as assessed by the LHC Higgs Cross Section Working Group for the total cross sections at the LHC [25], comprising both theoretical and parametric errors (PDF+ $\alpha_s$ ). Table 7 gives a brief overview of theoretical and parametric PDF+ $\alpha_s$  uncertainties, for the latter following the recipe of the PDF4LHC Working Group [24]; the explicit numbers are based on the results given in Ref. [25]. For later reference, the table also illustrates the typical size of the known QCD and EW corrections. A similar, but rather conservative estimate of cross-section uncertainties for Tevatron can be found in Ref. [199].

The overview over the total cross sections shown in Figures 15 and 16 can only give a rough idea about the importance the respective production channels for Higgs-boson discovery or for later precision studies. The total cross sections provide the total production rates for Higgs bosons, but in practice the rates of potentially observable events is relevant. Moreover, the signatures left in the detectors are

rather different for the various production channels:

- Single-Higgs production in gg fusion strongly prefers Higgs bosons at low transverse momenta plus some hadronic activity recoiling against the Higgs boson. Owing to the overwhelming hadronic background it is impossible to access the  $H \rightarrow b\bar{b}$  decay channel here. Instead the  $H \rightarrow \gamma\gamma$  decay yields a promising signal at small Higgs-boson masses in spite of its small branching ratios. At higher values of  $M_H$  the decays  $H \rightarrow WW/ZZ \rightarrow 4$  fermions via weak gauge bosons lead to rather clean signatures, in particular in the “gold-plated” four-muon channel of the ZZ decay.
- VBF offers the possibility to tag on the two accompanying jets which strongly prefer the forward–backward directions owing to the  $t$ -channel topology. Colour exchange between the two colliding partons is largely suppressed also in higher orders, further pronouncing this signature. Special VBF selection cuts on the two jets exploit this feature to suppress background. Apart from the WW/ZZ decays, VBF offers the best possibility to search for Higgs-boson decays into  $\tau^+\tau^-$  pairs.
- Higgs-strahlung represents the main search channel for SM Higgs bosons near the LEP exclusion limit at  $M_H = 114$  GeV at Tevatron, but at the LHC the higher background rates pose serious problems. In order to make use of this channel, a sophisticated novel search technique is promising that first focuses on “fat jets” (with large cones) at large transverse momenta which show an internal structure with B mesons [200]. Heavy objects decaying into a  $b\bar{b}$  quark pair, such as a light SM Higgs boson, are very likely to fit into this selection pattern.
- $t\bar{t}H$  production seems at best to be accessible at very low Higgs-boson masses owing to the cross-section suppression, so that one is forced to search for the  $H \rightarrow b\bar{b}$  decay. This leads to the partonic final state  $t\bar{t}H \rightarrow WWb\bar{b}b\bar{b} \rightarrow 4f + 4b$ , where  $4f$  stands for a four-fermion final state of the type  $4\ell$ ,  $2\ell 2q$ , or  $4q$ . It turns out that it will be extremely difficult to establish a signal over the serious background created by  $t\bar{t}b\bar{b}$  and  $t\bar{t} + 2$  jet production. At present, here the hope again rests on a selection focusing on fat jets with a  $b\bar{b}$  substructure [201]. However, owing to these difficulties,  $t\bar{t}H$  production cannot contribute to the Higgs-boson discovery, but would be very interesting in later precision analyses to assess Higgs-boson couplings.
- Finally, according to the SM, Higgs-boson production with  $b\bar{b}$  pairs is most likely not accessible at hadron colliders owing to the overwhelming hadronic background at hadron colliders. However, it plays an important role in extensions of the SM where the  $Hb\bar{b}$  Yukawa coupling is enhanced, such as in supersymmetric or non-supersymmetric two-Higgs doublet models.

## 6.2 Survey of precision calculations

The features reviewed above make it clear that theoretical predictions have to account for kinematical details of the various production mechanisms and of the Higgs-boson decay channels, because many of the specific event selections heavily make use of those properties.

For the individual Higgs-boson production channels in the SM, theory predictions are accurate within 5–20%, depending in detail on the production mechanism:

- *Gluon fusion*  $pp/p\bar{p} \rightarrow H + X$  [72, 74, 81, 90, 199, 202–226]  
Higgs-boson production via gluon fusion is strongly dominated by top-quark loops in the SM and receives very large QCD corrections, which are mainly due to soft-gluon exchange and emission. The NLO corrections, which are known with their full quark-mass dependence [72, 203], increase the cross section by 80–100%. The NNLO QCD corrections, which were first evaluated in the large-top-mass limit [204] and later on refined by top-mass corrections [205], add another 25% to the cross section. The still significant scale uncertainty of the NNLO QCD cross section can be

reduced by soft-gluon resummation. The resummation effects, known up to the next-to-next-to-next-to-leading logarithmic ( $N^3LL$ ) level [206], add another 6–9% to the cross section at the LHC, leading to the 6–10%(6–14%) of residual scale uncertainties at 7(14) TeV quoted in Table 7. The seemingly bad convergence in the sequence LO→NLO→NNLO of fixed-order predictions can be cured by an analytical continuation of the cross-section result to an imaginary renormalization scale, which results in a resummation of large corrections  $\propto (\alpha_s\pi^2)^n$  [207]. However, the optimistic estimate of uncertainties in the effective-field theory prediction of Ref. [207], which is also accurate to the  $N^3LL$  level, is still under debate [25].

EW corrections, which are known at NLO [74, 81, 208, 209], turn out to be of the size of  $\sim 5\%$  (relative to LO) and strongly depend on the Higgs-boson mass. The extreme size  $\sim 100\%$  of the QCD corrections poses the question how to combine the NLO  $\mathcal{O}(\alpha_s)$  QCD and  $\mathcal{O}(\alpha)$  EW corrections: additively or in factorized form? An investigation of mixed QCD–EW corrections for small  $M_H$  clearly favours the factorized approach [210]. Electroweak corrections to Higgs+jet production [211] influence the total single-Higgs production cross section at the negligible  $\lesssim 1\%$  level, but become relevant at large Higgs-boson transverse momenta.

Finally, at the level of some percent, interference effects between Higgs-boson signal and irreducible background, and Higgs-boson off-shell effects should be taken into account, as studied for  $gg \rightarrow H \rightarrow WW/ZZ$  in Refs. [53, 54, 212].

Various predictions of total Higgs-boson production cross sections [90, 199, 207, 210, 213] were described and partially updated in the first review [25] of the LHC Higgs Cross Section Working Group, where many details, in particular, about the various error estimates can be found. The second review [26] summarizes differential cross sections, such as the Higgs-boson-transverse-momentum ( $p_{T,H}$ ) distribution, and related cut-based observables, such as cross sections with a jet veto or definite jet multiplicities—a broad subject where we can only make brief statements.

Predictions for the  $p_{T,H}$  distribution were first worked out in fixed-order NLO QCD [214] and were refined later by soft-gluon resummations [215, 216]. For high  $p_{T,H}$ , the application of the large-top-quark-mass limit in predictions becomes subtle, and calculations should include the full quark-mass dependence as far as possible; errors from missing corrections due to finite quark masses do not necessarily show up in the scale uncertainty. Moreover, differential  $K$ -factors [218, 219, 221], i.e. corrections to distributions, in general show significant variations over phase space or depend on cuts, clearly disfavoured the use of a simple uniform rescaling of distributions by global  $K$ -factors. Even for integrated quantities, in particular, if vetoes or cuts are involved, a naive scale variation can underestimate theoretical uncertainties significantly. For the jet multiplicities and jet vetoes the discussion of appropriate error estimates and resummations started in Ref. [26] and went on in the literature since then, with proposals for solutions based on traditional resummations [227] and effective-theory approaches [217].

Several public programmes that include higher-order corrections to Higgs-boson production via gluon fusion are used in the experimental analyses:

- HIGLU [72] for calculating the total NLO QCD cross section with the full mass dependence;
- MCFM [222, 224] for Higgs+2jet production at NLO QCD;
- FEHiP [218] and HNNLO [219] for differential quantities, based on the NNLO QCD calculation in the heavy-top limit, but supporting the full kinematical information on the Higgs-boson decays  $H \rightarrow \gamma\gamma$  and  $H \rightarrow WW/ZZ \rightarrow 4$  leptons;
- HQT [216] and HRES [221] for the NNLL resummation matched to NLO QCD for Higgs-transverse-momentum spectrum, where HRES supports the decays  $H \rightarrow \gamma\gamma$  and  $H \rightarrow WW/ZZ \rightarrow 4$  leptons;

- IHIXS [55, 220] for the inclusive Higgs-boson production cross section using state-of-the-art fixed-order results, i.e. QCD corrections to NNLO, EW, and mixed QCD–EW corrections, as well as quark-mass and finite width effects;
  - MC@NLO [225] and POWHEG [226] for differential predictions in NLO QCD properly matched to QCD parton showers.
- *Vector-boson fusion*  $pp/p\bar{p} \rightarrow H + 2\text{jets} + X$  [89, 128, 129, 223, 224, 228–240]

Higgs-boson production via VBF experimentally means Higgs-boson production in association with two hard jets which are forward–backward pointing with some rapidity gap and an appropriate central-jet veto, in order to drastically reduce background [229]. The VBF cuts suppress  $H + 2\text{jet}$  production via top-quark-loop-induced  $gg$  fusion [230] as well, which for  $M_H = 120\text{ GeV}$  contributes about 4–5% [231] to the cross section with a non-negligible residual NLO scale uncertainty of about 35% [223, 224]. While  $s$ -channel contributions from  $HW/HZ$  with hadronically decaying  $W/Z$  bosons deliver up to  $\sim 30\%$  to the total cross section at low  $M_H \sim 120\text{ GeV}$ , VBF cuts suppress this Higgs-strahlung contamination to  $\lesssim 0.6\%$ . Thus,  $H + 2\text{jet}$  production with VBF cuts is nearly a pure EW process proceeding via  $W$ - or  $Z$ -boson fusion to a Higgs boson with almost no colour exchange between two forward-scattered (anti)quark lines.

The suppressed colour exchange and the forward kinematics suggest that QCD corrections are small after an appropriate scale setting (to small scales of the order of  $M_W$ ) in the PDF redefinition of QCD factorization. In fact this expectation is confirmed by explicit NLO QCD [89, 232–234] and NNLO QCD [235–237] calculations, which are available for differential cross sections in the former case and for the total cross section in the latter. The NLO QCD corrections are of the order of 5–10%, depending in detail on the VBF cuts, with interferences between  $t$ - and  $u$ -channels—including gluon exchange between the (anti)quark lines at NLO—at the negligible level of  $\lesssim 0.1\%$  [234]. This suppression of colour exchange is also confirmed at NNLO, where large parts of the corrections with non-trivial colour flow were calculated or estimated [235, 237], so that the NNLO QCD corrections can be treated in the so-called structure-function approach as used in Refs. [236, 237] for the total cross section. Likewise, interference effects between amplitudes with top-quark-loop-induced  $ggH$  couplings and VBF amplitudes with one-loop gluon exchange turn out to be negligible as well [238]. The remaining scale uncertainty of the total cross section at NNLO QCD, which is at the percent level, turns out to be small as compared to the parametric PDF+ $\alpha_s$  uncertainty of 2–7%(3–4%) at the LHC at 7(14) TeV. For differential quantities, i.e. for cross sections with VBF cuts or for distributions, QCD corrections at fixed order are only known to NLO, but including the matching to QCD parton showers at this order [239].

The NLO EW corrections have been calculated for all  $t/u$ - and  $s$ -channel contributions, including all interferences, in Ref. [234] and for the  $t/u$ -channels in Ref. [240], where both calculations are valid for integrated and differential quantities. In the presence of VBF cuts, the approximation by  $t/u$ -channels only is sufficient. The EW corrections to integrated cross sections amount to 5–10% and are, thus, of the same generic size as the QCD corrections, but in distributions at high transverse momenta of the Higgs boson or the jets the EW corrections can even be larger. Similar to the situation in the related decays  $H \rightarrow WW/ZZ \rightarrow 4f$ , discussed in Section 2.6, the leading two-loop corrections of the order  $G_\mu^2 M_H^4$  [87] become of the same size as their one-loop counterpart of order  $G_\mu M_H^2$  at  $M_H \sim 700\text{ GeV}$ , signalling the breakdown of perturbation theory. For  $M_H \lesssim 500\text{ GeV}$ , on the other hand, perturbation theory is safely applicable.

The described state-of-the-art is widely available by public programmes. The fixed-order NLO QCD+EW predictions can be obtained with the Monte Carlo programmes VBF@NLO [233, 240, 241] and HAWK [234, 242], the former in the  $t/u$ -channel approximation, the latter including  $s$ -channels and all interferences as well. The (approximated) NNLO QCD corrections to the

total cross section can be obtained with the programme VBF@NNLO [236, 237, 243]. Presently, the best prediction for differential distributions should be obtained upon reweighting the parton-shower-improved NLO predictions of POWHEG [239] with the relative EW correction from HAWK or VBF@NLO.

- *Higgs-strahlung*  $pp/p\bar{p} \rightarrow HW/HZ + X$  [244–253]

As far as higher-order QCD corrections are concerned, Higgs-strahlung is very similar to the well-known Drell–Yan process. In LO there is just quark–antiquark annihilation to an off-shell weak gauge boson,  $q\bar{q} \rightarrow W^*/Z^* \rightarrow HW/HZ$ , and the structure and size ( $\sim 30\%$ ) of NLO QCD corrections [245] are identical to the Drell–Yan case. At NNLO QCD, the Drell–Yan-like corrections, which are known for the total HW/HZ cross sections [246] and the differential HW cross section [247], dominate, but there are additional corrections to Higgs-strahlung that have no counterparts in Drell–Yan production. Firstly, loop-induced gg fusion contributes to HZ production about 2–6%(4–12%) for CM energies of 7 TeV(14 TeV) at the LHC [246]<sup>8</sup>, and secondly diagrams involving Higgs couplings to top-quark loops correct the HW/HZ cross sections by another 1–3% [249]. As far as EW corrections are concerned, Higgs-strahlung is more involved than the Drell–Yan process. The NLO EW corrections to the total cross sections have been calculated in Ref. [250] and are of the order of  $-(5–10)\%$ , only weakly depending on the collider type and energy. The NLO EW corrections to differential cross sections, calculated in Ref. [251], can be significantly larger, in particular for the kinematics relevant in the “boosted-Higgs analysis” which requires large transverse Higgs momenta. For instance, the EW corrections to HW production with  $M_H = 120$  GeV are  $\sim -14\%$  for  $p_{T,H} \gtrsim 200$  GeV.

From Table 7 one can read off that theoretical uncertainties at the LHC are of the order of 1–2%(2–4%) and the PDF+ $\alpha_s$  uncertainties of the order of 3–4% for a CM energy of 7(14) TeV for the total HW/HZ cross sections (see Ref. [25] for details). Note, however, that the uncertainties for the scenario of a boosted Higgs boson ( $p_{T,H} \gtrsim 200$  GeV) are somewhat larger [26]. Specifically, the issue of final-state radiation off the Higgs-boson decay products deserves particular attention in the boosted-Higgs scenario [252]. The PDF uncertainties are estimated to  $\sim 5\%$ , and for HZ production, where differential QCD corrections are only known to NLO, the theoretical uncertainty is estimated to  $\sim 7\%$ ; a reduction of these theoretical uncertainties to the few-percent level requires the inclusion of NNLO QCD corrections.

To a large extent, the described precision calculations are available via public programmes. The NLO QCD corrections for total and differential cross sections can be calculated with V2HV [254] and MCFM [222], respectively, and the total cross section, including NNLO QCD and NLO EW corrections, with the programme VH@NNLO [253]. Finally, the NLO QCD+EW corrections to fully differential observables (with decaying W/Z bosons) can be computed with the Monte Carlo programme HAWK [242].

- *Associated Higgs-boson production with  $t\bar{t}$  pairs*  $pp/p\bar{p} \rightarrow t\bar{t}H + X$  [201, 255–258]

Both the total and differential cross sections to  $t\bar{t}H$  production are known to NLO QCD [256]. The size of the QCD corrections is moderate, i.e. typically 10–20% (positive at the LHC and negative at Tevatron), which holds also true for differential distributions if appropriate dynamical scales are used. Theoretical uncertainties from missing higher-order effects as well as PDF+ $\alpha_s$  uncertainties are estimated to be of the order of  $\sim 10\%$  for total cross sections at the LHC (see Table 7 and Ref. [25]). For differential distributions the theoretical uncertainty is somewhat larger (10–20%) and together with the parametric PDF+ $\alpha_s$  uncertainties can add up to 20–50% [26].

---

<sup>8</sup>These numbers, which were used also in Figure 16, are based on the LO one-loop diagrams of the gg channel. A recent evaluation [248] of the two-loop NLO corrections in the heavy-top limit, however, roughly doubles this contribution, i.e. in order to reach the precision tag of Table 7 these corrections should be taken into account.

The NLO QCD predictions were matched to parton showers, employing the MC@NLO [257] and POWHEG [258] concepts. The results obtained with the two shower variants typically agree to better than 10%. Electroweak corrections to  $t\bar{t}H$  production are yet unknown, but their effect should be covered by the size of the quoted QCD uncertainties.

As already mentioned above, suppressing the background to  $t\bar{t}H$  production is a real challenge, since the final state involves four b quarks, where three or four bottom quarks have to be tagged, and two out of the four have to be identified as  $H \rightarrow b\bar{b}$  decay products. To properly simulate this theoretically, precise predictions are required that take into account the decays of both the top quarks and the Higgs boson. At present, such predictions exist only at LO. Similar to the HW/HZ analysis, searching first for fat jets at high transverse momentum and a  $b\bar{b}$  substructure can lift the signal-to-background ratio to  $S/B \sim 1/2.4$ , assuming three b tags,  $M_H = 120 \text{ GeV}$ , and an integrated luminosity of  $100 \text{ fb}^{-1}$ , as shown in the parton-level study of Ref. [201]. The main background results from  $t\bar{t}b\bar{b}$  and  $t\bar{t}+2\text{jet}$  production within pure QCD, whose cross sections have recently been calculated at NLO in Refs. [259] and [260], respectively. However, the residual scale dependence of the background cross-section normalization is about  $\sim 20\%$ , and a careful study of the uncertainties of possible extrapolation procedure from signal-free control regions to signal regions has not yet been carried out. To this end, for the background the differential information on the top-quark decays has to be taken into account as well. The feasibility of the  $t\bar{t}H$  measurement is still not established.

### 6.3 Towards couplings analyses after discovery

Although the difficult hadronic environment of the LHC limits the precision of Higgs-boson studies, the global pattern of Higgs couplings could be tested at a qualitative level in a global fit to various channels with only mild theory assumptions. Assuming, for instance, that the Higgs-boson decay widths into weak gauge bosons are at most as large as their SM values,  $\Gamma_{H \rightarrow WW/ZZ} \leq \Gamma_{H \rightarrow WW/ZZ}^{\text{SM}}$ , which is the case in many models with extended Higgs sectors, the Higgs couplings of a not too heavy Higgs boson ( $110 \text{ GeV} < M_H < 190 \text{ GeV}$ ) to top quarks,  $\tau$ -leptons, and W and Z bosons could be determined to 10–40% in an LHC run at  $\sqrt{s} = 14 \text{ TeV}$  with an integrated luminosity of  $300 \text{ fb}^{-1}$  [261–263]. An increase of the integrated luminosity to  $3000 \text{ fb}^{-1}$  reduces the experimental uncertainties in the signal strengths  $\sigma/\sigma_{\text{SM}}$  by roughly a factor of 2 [262], so that the uncertainties of the Higgs-boson couplings should be reduced by a factor of about 1.5, since the couplings enter the signal strengths quadratically. Constraints on Higgs couplings might be even possible with lower luminosity or tighter constraints with the same luminosity if more and more sophisticated analysis techniques are exploited (see, e.g., Ref. [264]). Currently, the ATLAS [265] and CMS [266] collaborations follow the strategy of a first model-independent analysis of Higgs couplings, which has been put forward by the LHC Higgs Cross Section Working Group [267] and is based on a simple rescaling of SM cross sections. Ultimate precision Higgs coupling analyses, however, should go beyond such simple phenomenological studies, since their informative value is rather limited in the interesting case of significant discrepancies between SM and data. Proper model-independent non-standard coupling analyses should be thoroughly based on effective-field theories, including higher-order effects in a consistent way as much as possible. First steps into this direction are proposed in Ref. [268].

Among the various Higgs couplings, the self-interactions are of particular interest, since they determine the Higgs potential that drives EW symmetry breaking. As already explained for  $e^+e^-$  colliders, such studies require multiple-Higgs-boson production, e.g. Higgs-boson pair production to access the triple-Higgs coupling. The various channels for Higgs-boson pairs at hadron colliders are illustrated by some LO diagrams in Figure 17. The cross sections for (a) gluon fusion [269, 270], (b) Higgsstrahlung [271, 272], (c) vector-boson fusion [273, 274] are, however, very small and further suppressed by branching ratios of the many-particle final states. At present, it seems that only gluon fusion may

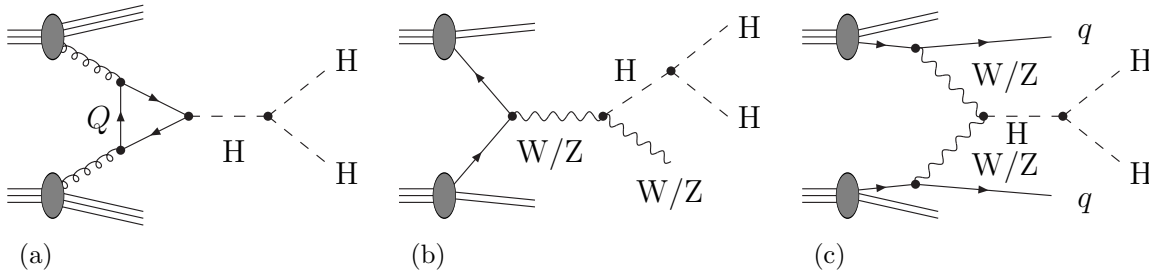


Figure 17: Representative LO diagrams for the main SM Higgs-boson pair production channels at hadron colliders, where  $q$  and  $Q$  denote light and heavy quarks, respectively: (a) gluon fusion, (b) Higgs-strahlung, (c) vector-boson fusion.

be able to establish a signal for Higgs-boson pairs and to allow for a qualitative measurement of the triple-Higgs coupling. Higher-order QCD corrections to  $gg \rightarrow HH$  are very similar to single-Higgs production  $gg \rightarrow H$ , though kinematically more complicated; the NLO QCD corrections to gluon fusion to Higgs-boson pairs, which are known in the heavy-top limit [270], confirm this expectation and yield a  $K$ -factor of the order of 2. Based on the HWW decays, a non-vanishing  $H^3$  coupling could be established for  $M_H = 150\text{--}200\text{ GeV}$  after collecting a high integrated luminosity of  $300\text{fb}^{-1}$  at the LHC with design the energy of 14 TeV [275]. Although the theoretical simulation [276] suggests that for a low mass of  $M_H \sim 120\text{ GeV}$  the rare decay  $HH \rightarrow b\bar{b}\gamma\gamma$  could establish the coupling for an integrated luminosity of  $600\text{fb}^{-1}$ , an experimental sensitivity study [262] for an integrated luminosity of  $3000\text{fb}^{-1}$  at a CM energy of 14 TeV indicates that more than one channel will be necessary to empirically establish a non-vanishing triple-Higgs-boson coupling.

Since triple-Higgs-boson production cross sections are way too small [277] at hadron colliders as well, an experimental test of quartic Higgs couplings at colliders is out of reach.

## 7 Searches at Tevatron

The Tevatron Run II started in 2001 with a pilot run at a new CM energy of 1.96 TeV. From spring 2002 until its shutdown in autumn 2011 it provided proton–antiproton collisions corresponding to a data set of up to  $10\text{ fb}^{-1}$  to the two experiments CDF and D0. In contrast to the searches at LEP, where the a priori signal-to-background ratio was at the level of  $10^{-4}$  to  $10^{-6}$  as both signal and background processes are mediated by the electroweak interaction, the huge total inelastic cross section due to processes mediated by the strong force is more than ten orders of magnitude higher than the cross section for Higgs-boson production (see Figure 6). Owing to the large cross section, the instantaneous luminosity of up to  $4 \times 10^{32}\text{ cm}^{-2}\text{s}^{-1}$  and the short time interval between bunch crossings of 396 ns not all interactions can be recorded. In order to limit the recorded data volume to a manageable size severe requirements on the presence and quality of final-state objects have to be imposed already at the trigger level. This online selection for Higgs-boson searches relies mostly on the presence of a colour-neutral object in the final state, i.e. photons, electrons, muons, or significant missing transverse momentum arising from neutrinos. Hence, although Higgs-boson topologies with fully hadronic final states, which comprise production in gluon fusion with subsequent decays via  $H \rightarrow b\bar{b}$  or  $H \rightarrow WW(ZZ) \rightarrow 4$  quarks, lead to the highest production rates, these cannot be exploited at Tevatron. Exceptions to this rule of thumb are the searches in the associated production  $WH(ZH) \rightarrow q\bar{q}b\bar{b}$  and in vector-boson fusion with the decay  $H \rightarrow b\bar{b}$  performed by CDF [278], where events were recorded by requiring multi-jets and a large scalar sum of transverse energies at the trigger level.

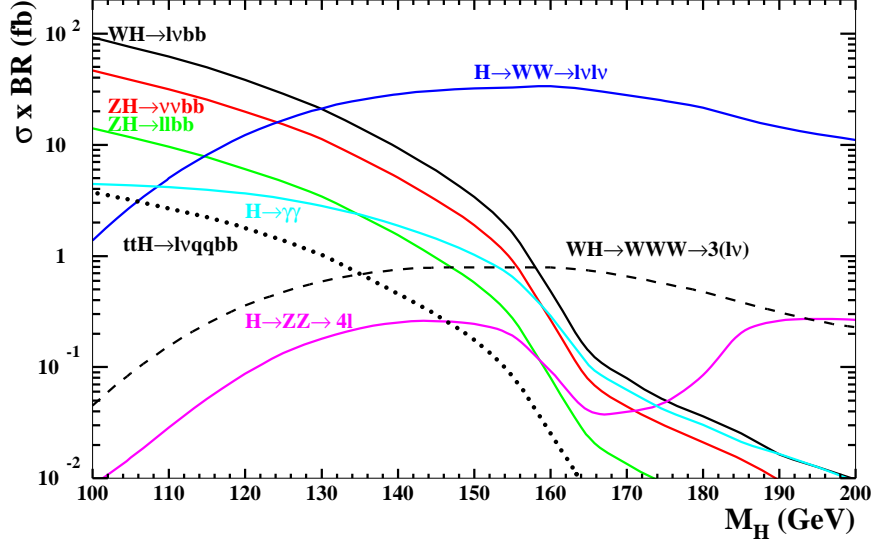


Figure 18: Production cross sections in the most sensitive search channels at the Tevatron. The numbers are extracted from Ref. [279].

## 7.1 Overview of search channels

Generically, the Higgs-boson mass range 100–200 GeV was investigated by both experiments CDF and D0. An overview of the production rates for most of the search channels considered at Tevatron is shown in Figure 18. For  $M_H \leq 130$  GeV the most abundant and most sensitive search channels are  $H \rightarrow b\bar{b}$  produced in association with a weak gauge boson  $W$  or  $Z$ , which decay leptonically via  $W \rightarrow \ell\nu$ ,  $Z \rightarrow \ell^+\ell^-$ , or  $Z \rightarrow \nu\bar{\nu}$ . Here and in the following  $\ell$  denotes an electron or muon. The relative magnitude of the rates is due to different couplings of the Higgs bosons to  $W$  and  $Z$  and the branching ratios  $\text{BR}(W \rightarrow \ell\nu) = 22\%$ ,  $\text{BR}(Z \rightarrow \ell^+\ell^-) = 6.7\%$ , and  $\text{BR}(Z \rightarrow \nu\bar{\nu}) = 20\%$ . For  $M_H$  in the range 130–200 GeV the sensitivity is dominated by the search for  $H \rightarrow W^+W^- \rightarrow \ell^+\nu\ell^-\bar{\nu}$  produced in gluon fusion. The discussion below focuses on these four final states. In addition to those high-sensitivity channels a plenitude of other channels was analyzed which yield cross-section limits for Higgs-boson production with a value of at best 7 times the SM prediction, and a sensitivity of a single channel (expressed in expected limits) of at least a factor 5 worse compared to a combination of the four channels mentioned above. Those channels include  $H \rightarrow \gamma\gamma$  (CDF [280] and D0 [281]),  $H \rightarrow ZZ \rightarrow \ell^+\ell^-\ell'^+\ell'^-$  (CDF [282]),  $q\bar{q}b\bar{b}$  from  $WH(ZH)$  and in VBF with the decay  $H \rightarrow b\bar{b}$  (CDF [278]),  $t\bar{t}H$  with  $H \rightarrow b\bar{b}$  (CDF [283]),  $H \rightarrow \tau^+\tau^-$  (CDF [284], D0 [285]),  $H \rightarrow W^+W^- \rightarrow \ell\nu q\bar{q}$  (D0 [286]) and  $W(Z)H \rightarrow W(Z)WW \rightarrow \ell^\pm\ell^\pm + X$  (CDF [287], and D0 [288]). Additional channels are included in the preliminary combinations in each experiment and the Tevatron combination. All those channels contribute to the overall sensitivity at the level of 10–20%. In most analyses the final discriminant is given by an event classifier based on the combination of multivariate techniques, which combines information from kinematical properties, such as observables sensitive to the Higgs-boson mass and topological information from flavour tagging. Usually the pre-selected event samples, where the presence of the basic physics objects of the final state under consideration are required, are divided in categories based on jet multiplicity, lepton flavour, multiplicity of  $b$ -tagged jets and the tightness of their selection requirements, and on additional kinematical properties, such as low or large missing transverse momentum. Often the selection strategy using multivariate techniques is a multi-step procedure. In the first step either



dominant reducible backgrounds are greatly reduced, or the events are divided in categories, in which a specific background is enriched or depleted. In the next selection step the signal can then be separated from the remaining backgrounds in a more efficient way. Sometimes a sequence of multivariate event classifiers is also applied, which one after the other try to suppress the dominant background classes. The final discriminants are then constructed from the responses of various multivariate techniques. This sophisticated selection procedure improves significantly the signal-to-background ratios in particular categories with respect to a more inclusive analysis and hence the overall sensitivity of the combined search. Higgs-boson production is simulated with PYTHIA [91, 92], to which a reweighting of the transverse-momentum spectrum of the Higgs boson is applied. QCD multi-jet production is estimated entirely using data-driven techniques. Other backgrounds are estimated from simulated events, which are generated with a variety of event generators such as ALPGEN [289], COMPHEP [290], HERWIG [291, 292], MC@NLO [225, 293], PYTHIA [91, 92], and SHERPA [294]. The misidentification probabilities for leptons and b-flavoured jets, as measured in data, are applied to the simulation.

## 7.2 Searches for $H \rightarrow b\bar{b}$

The searches for  $H \rightarrow b\bar{b}$  in the mass range 100–150 GeV are performed in three non-overlapping final-state topologies: (a) 1 lepton and large missing transverse momentum designed for  $WH \rightarrow \ell\nu b\bar{b}$ , but also selecting contributions from  $ZH \rightarrow \ell^+\ell^-b\bar{b}$ , where one lepton is not reconstructed and identified, (b) 2 leptons with an invariant mass consistent with  $M_Z$  optimized for  $ZH \rightarrow \ell^+\ell^-b\bar{b}$  production, and (c) 0 leptons and large missing transverse momentum designed for  $ZH \rightarrow \nu\bar{\nu}b\bar{b}$ , but also receiving contributions from  $WH \rightarrow \ell\nu b\bar{b}$  and  $ZH \rightarrow \ell^+\ell^-b\bar{b}$ , where one or two leptons are not reconstructed and identified. The suppression of background processes, in particular from  $W(Z)$ +light-flavour production, depends crucially on the performance of the algorithm to identify the b-flavoured jets from the Higgs-boson decay. Significant improvements were achieved over the last years, which greatly enhanced the sensitivity. The mass of the Higgs-boson candidate can be reconstructed from the invariant mass of the two jets assigned to the Higgs-boson decay with a mass resolution of 10–15%. This di-jet mass is an important observable to discriminate the signal process from background processes, in particular from di-boson production  $VZ$  with  $Z \rightarrow b\bar{b}$ . In addition to the multiplicity of leptons and the presence of missing transverse momentum exactly two or three jets are required with at least one being identified as b-flavoured. The events are further divided into categories depending on lepton flavour, lepton quality, b-tag multiplicity, and b-tag quality, in order to improve the signal-to-background ratio. For each category and Higgs-boson-mass hypothesis multivariate event classifiers are trained, which use the di-jet invariant mass and other kinematical quantities as input observables. The response of these multivariate techniques is used as the final discriminant. For the purpose of visualization of the sensitivity and results, especially when several channels and categories are combined, the bins of each final discriminating observable are ordered with respect to the expected signal-to-background (s/b) ratio. The expected and observed event yields in each  $\ln(s/b)$  bin are then added over the discriminating variables in all non-overlapping final states and event categories.

The expected and observed limits on the signal-strength parameter  $\mu = \sigma/\sigma_{\text{SM}}$  (called  $R$  in the Tevatron analyses), which relates the excluded cross section  $\sigma$  to the SM expectation  $\sigma_{\text{SM}}$  for Higgs-boson production, from the analysis of full data set collected during Run II at Tevatron (9.45 fb<sup>-1</sup> in CDF and 9.5–9.7 fb<sup>-1</sup> in D0) are summarized in Table 8. In both experiments and in all three search topologies the observed limit is weaker than the expected one over a broad mass range. The deviation is less than 1 standard deviation over the full mass range in the D0  $\ell\nu b\bar{b}$  [296] and  $\nu\nu b\bar{b}$  searches [298], and within 2 standard deviations in the D0  $\ell^+\ell^-b\bar{b}$  [300] search and the CDF  $\ell\nu b\bar{b}$  [295] and  $\nu\bar{\nu}b\bar{b}$  [299] searches. In the CDF  $\ell^+\ell^-b\bar{b}$  [299] search a maximum excess corresponding to a significance of 2.4 is observed at  $M_H = 135$  GeV, reduced to 2.1 when taking into account the “look-elsewhere effect” (LEE). When combining the three channels, CDF [302] observes a limit weaker than the expected by 2 standard

Table 8: Expected and observed limits on the signal-strength parameter  $\mu = \sigma/\sigma_{\text{SM}}$  in the search for  $H \rightarrow b\bar{b}$  in D0 and CDF. The entry “–” indicates that this information is not available.

channel	CDF	D0
	obs. (exp.) limit at $M_H = 115/125$ GeV	obs. (exp.) limit at $M_H = 115/125$ GeV
WH ( $H \rightarrow b\bar{b}$ , $W \rightarrow \ell\nu$ )	3.1 (2.0) / 4.9 (2.8) [295]	3.7 (3.2) / 5.2 (4.7) [296]
ZH ( $H \rightarrow b\bar{b}$ , $Z \rightarrow \nu\nu$ )	2.7 (2.7) / 6.7 (3.6) [297]	3.0 (2.7) / 4.3 (3.9) [298]
ZH ( $H \rightarrow b\bar{b}$ , $Z \rightarrow \ell\ell$ )	4.7 (2.7) / 7.1 (3.9) [299]	4.3 (3.7) / 7.1 (5.1) [300]
combined	– / –	1.9 (1.6) / 3.2 (2.3) [301]

deviations for  $M_H = 110\text{--}150$  GeV and a maximal deviation from the background-only hypothesis for  $M_H = 135$  GeV with a significance of 2.7 (2.5 after including the LEE in the mass range 115–150). In D0 [301] the combination yields a limit weaker than the expected by 1–1.7 standard deviations in the mass range 120–145 GeV and a maximal deviation from the background-only hypothesis for  $M_H = 135$  GeV with a significance of 1.7 (1.5 with LEE in the mass range 115–150 GeV). D0 excludes the mass range  $M_H = 100\text{--}102$  GeV. Both experiments conclude that the excess is compatible with the production of the SM Higgs boson with a mass of 125 GeV within large uncertainties. The best fit values for the signal strength at  $M_H = 125$  GeV is  $\mu = 1.2^{+1.2}_{-1.1}$  in D0, and in CDF  $\mu$  is approximately 2.5 consistent with the SM expectation of 1 within 2 standard deviations.

The combination of the observed event yields from CDF and D0 [303] in the  $\ln(s/b)$  distribution of  $H \rightarrow b\bar{b}$  searches after subtraction of the expected background in Figure 19 (top-left) shows a positive deviation from the expectation of zero for the background-only hypothesis in the bins of large signal-to-background ratio. The observed limit on the signal strength  $\mu$  is weaker than the expected by more than two standard deviations in the range 115–145 GeV, as shown in Figure 19 (top-right). Under the background-only hypothesis one expects to exclude the Higgs-boson-mass hypothesis in the range 100–116 GeV. Assuming a Higgs boson with mass of 125 GeV no excluded range is expected. The data allow the mass hypothesis below 106 GeV to be excluded. The local  $p$ -values in testing the background-only hypothesis as a function of  $M_H$  (see Figure 19 top-left) show deviations from the background-only hypothesis with a significance of larger than 2 in the mass range 115–145 GeV with the smallest  $p$ -value at 135 GeV corresponding to a local significance of 3.3 (2.8 at  $M_H = 125$  GeV). After taking into account the LEE in the mass range 115–150 GeV the significance is decreased to 3.1. The best fit value for the signal cross section obtained in data is compared to various types of expectations for signal+background hypothesis in Figure 19 (bottom-right). The fit values agree with the expectation for the SM Higgs boson at the 68 (95)% CL in the approximate mass ranges 112–120 GeV (105–132 GeV and 140–150 GeV). As  $M_H = 135$  GeV was already excluded by both LHC experiments and guided by the excess observed in each experiment at the LHC with a local significance of approximately 3 at  $M_H \approx 125$  GeV already in the analysis of the 2011 data, the Tevatron experiments quote a best fit value for the signal cross section  $(\sigma_{\text{WH}} + \sigma_{\text{ZH}}) \times \text{BR}(H \rightarrow b\bar{b})$  at  $M_H = 125$  GeV of  $0.23^{+0.09}_{-0.08}$  pb to be compared to the SM Higgs boson of  $0.12 \pm 0.01$  pb, consistent within 1.5 standard deviations. Despite having no sensitivity to exclude the SM Higgs boson hypothesis for masses larger than 116 GeV, the Tevatron observes a broad excess in the  $H \rightarrow b\bar{b}$  final state, consistent with a wide range of SM Higgs-boson-mass hypothesis. Based on these findings the Tevatron experiments reported evidence for the production of a new particle produced in association with weak bosons and decaying to a b-quark pair [303].

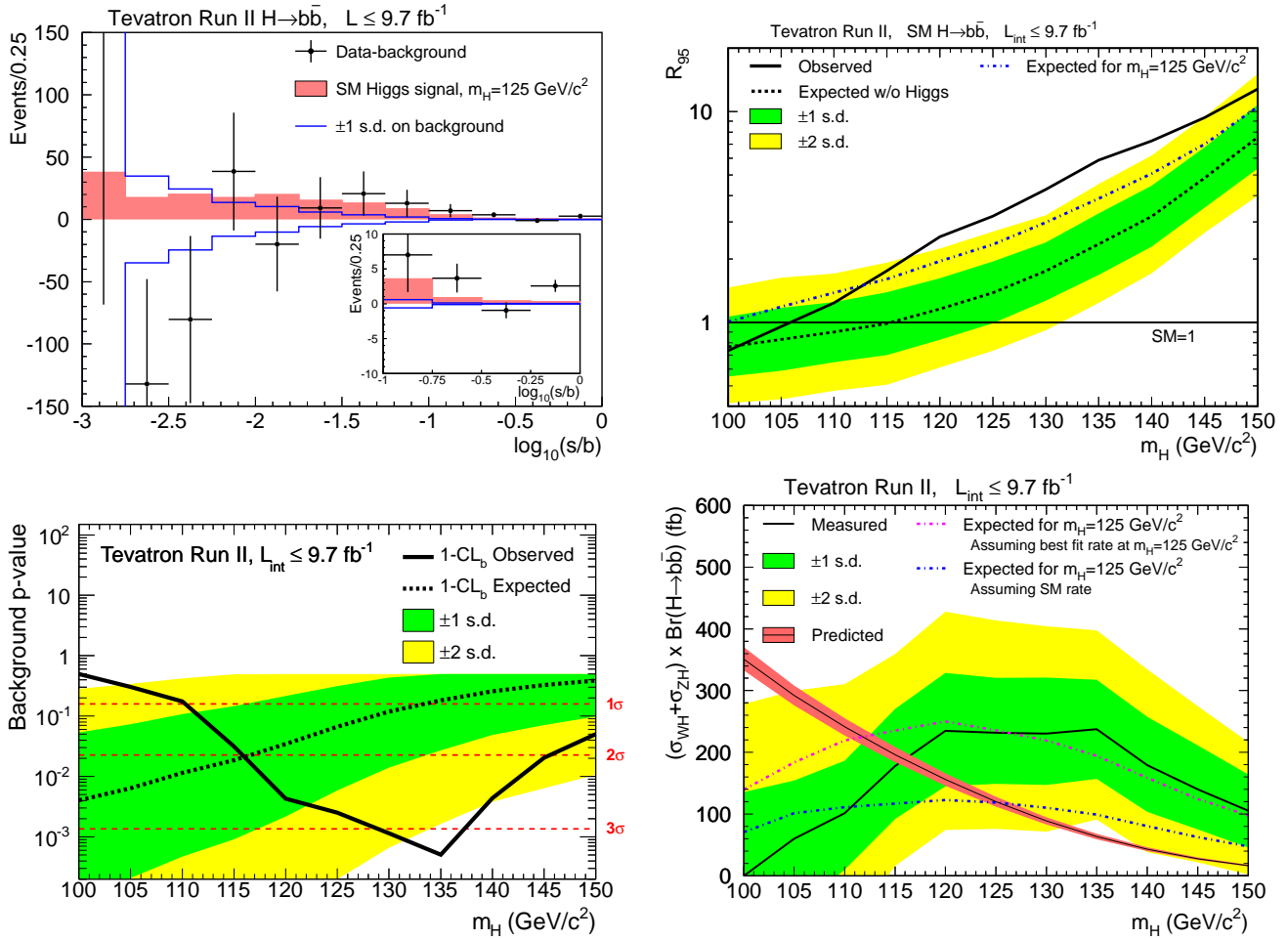


Figure 19: Results of the search for  $H \rightarrow b\bar{b}$  at Tevatron from the combination of CDF and D0 full Run II data [303]. Expected and observed event yields classified by signal-to-background ratio after background subtraction (top-left), exclusion limits on the signal strength  $R \equiv \mu = \sigma/\sigma_{\text{SM}}$  as function of  $M_H$  (top-right), local  $p$ -value for the background-only hypothesis as function of  $M_H$  (bottom-left), and best fit values for the signal cross section as a function of  $M_H$ , compared to the expectation for a SM Higgs boson as a function of  $M_H$  and the expectations for a SM Higgs boson with mass of 125 GeV evaluated at different  $M_H$  (bottom-right).

### 7.3 Searches for $H \rightarrow W^+W^- \rightarrow \ell^+\nu\ell^-\bar{\nu}$

The final-state topology is characterized by two isolated leptons of opposite charge and large missing transverse momentum. Due to the presence of two neutrinos in the final state the mass of the Higgs-boson candidates cannot be reconstructed and only the transverse mass of the di-lepton and missing-transverse-momentum system can be reconstructed. Observables that allow to suppress background processes comprise, among others, the di-lepton invariant mass, the transverse mass, and the azimuthal opening angle between the two leptons [304]. The latter observables exploit the scalar nature of the Higgs boson and the parity violating  $V - A$  structure of the  $W \rightarrow \ell\nu$  decay. Due to the spin correlations the signal accumulates at small values of the opening angle and di-lepton invariant mass. The search is optimized in different categories, distinguished, e.g., by lepton flavour and jet multiplicity (0, 1,  $\geq 2$ ). The latter aims to enhance the sensitivity for associated WH(ZH) and VBF production with two quarks in the final state. The composition of the remaining background is very different in the different jet categories: In the 0 (2) jet category the dominating background is given by WW ( $t\bar{t}$ ) production. The final discriminating observables based on multivariate techniques in each event topology, which are

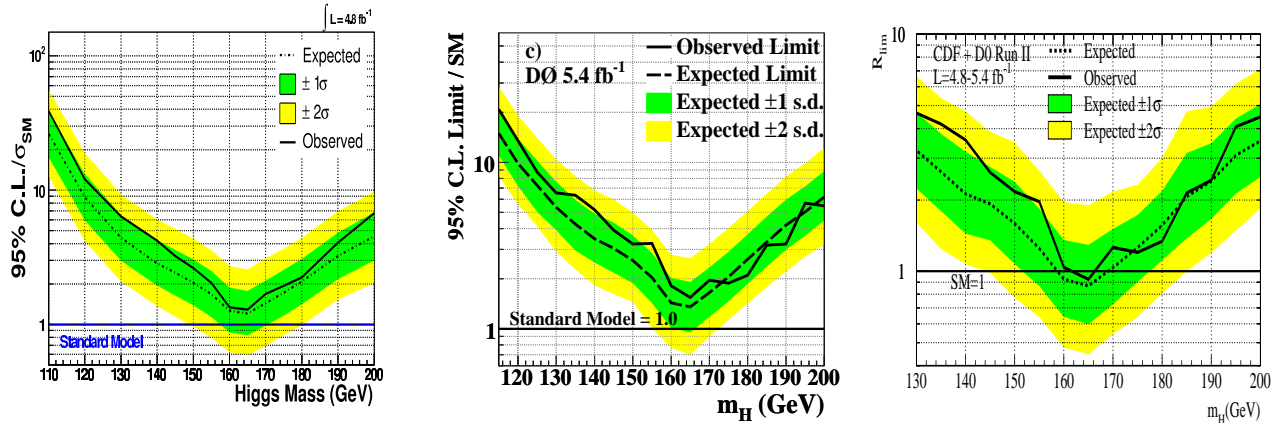


Figure 20: Cross-section limits with respect to the SM expectation for  $H \rightarrow W^+W^- \rightarrow \ell^+\nu\ell^-\bar{\nu}$  production in CDF [287] (left), in D0 [306] (middle), and in the first Tevatron combination [305] (right).

separately optimized for all Higgs-boson-mass hypotheses tested, are used as input for the statistical interpretation of the results. In addition searches for final states with two leptons with same electric charge or with three leptons were performed to enhance the sensitivity to WH(ZH) production, where the associated W(Z) boson decays to one (two) charged leptons. Due to the comparably large production rate,  $H \rightarrow W^+W^- \rightarrow \ell^+\nu\ell^-\bar{\nu}$  was the first channel to reach the sensitivity to exclude SM Higgs-boson cross sections in the vicinity of  $M_H = 160$  GeV. The only published combined Tevatron result [305] including  $H \rightarrow W^+W^- \rightarrow \ell^+\nu\ell^-\bar{\nu}$  search channels from spring 2010, which is based on a data sets of up to  $4.8 \text{ fb}^{-1}$  in CDF [287] and  $5.4 \text{ fb}^{-1}$  in D0 [306], excludes  $M_H = 162\text{--}166$  GeV with an expected exclusion of  $M_H = 159\text{--}169$  GeV (see Figure 20, right). This was the first time that Tevatron expected to exclude a Higgs-boson mass range. The individual experiments were not yet able to exclude a mass range, but gave observed (expected) limits on the signal-strength parameter at  $M_H = 165$  GeV of 1.29 (1.20) in CDF (see Figure 20, left) and 1.55 (1.36) in D0 (see Figure 20, middle), to be compared with the Tevatron combination 0.93 (0.87). Since then, many preliminary updates of searches for  $H \rightarrow W^+W^- \rightarrow \ell^+\nu\ell^-\bar{\nu}$  were performed extending the sensitivity for SM Higgs-boson production to a mass window of size of roughly 20 GeV around  $2M_W$ . Only D0 published a new result based on a data set of  $8.6 \text{ fb}^{-1}$  [307] yielding an expected excluded mass range of  $M_H = 159\text{--}169$  GeV. However, no mass range could be excluded due to an upwards fluctuation of the observed event yields by one standard deviation with respect to the background expectation.

## 7.4 Preliminary combined results

Over the years the findings in the plenitude of the decay channels and final-state topologies were combined regularly by CDF and D0 separately, and also in a common effort as the Tevatron combination. The correlations in the systematic uncertainties across channels and also across experiments were carefully taken into account. In the following the latest preliminary Tevatron combination (July 2012) [279] for the mass range  $M_H = 100\text{--}200$  GeV is briefly discussed. A comparison of the expected and observed event yields classified by signal-to-background ratios after background subtraction for  $M_H = 125$  GeV and  $M_H = 165$  GeV is shown in Figure 21 (top row). The Tevatron combination extends the exclusion sensitivity significantly with respect to the one in the individual experiments. The mass regions  $M_H = 100\text{--}120$  GeV and  $M_H = 139\text{--}184$  GeV are expected to be excluded as shown in Figure 21 (middle-left). The observed excluded mass ranges are significantly weaker and extend only over the mass ranges  $M_H = 100\text{--}103$  GeV and  $M_H = 147\text{--}180$  GeV. The largest deviation from the background-only hypothesis is observed for  $M_H = 120$  GeV with a local  $p$ -value of  $1.5 \times 10^{-3}$ , corre-

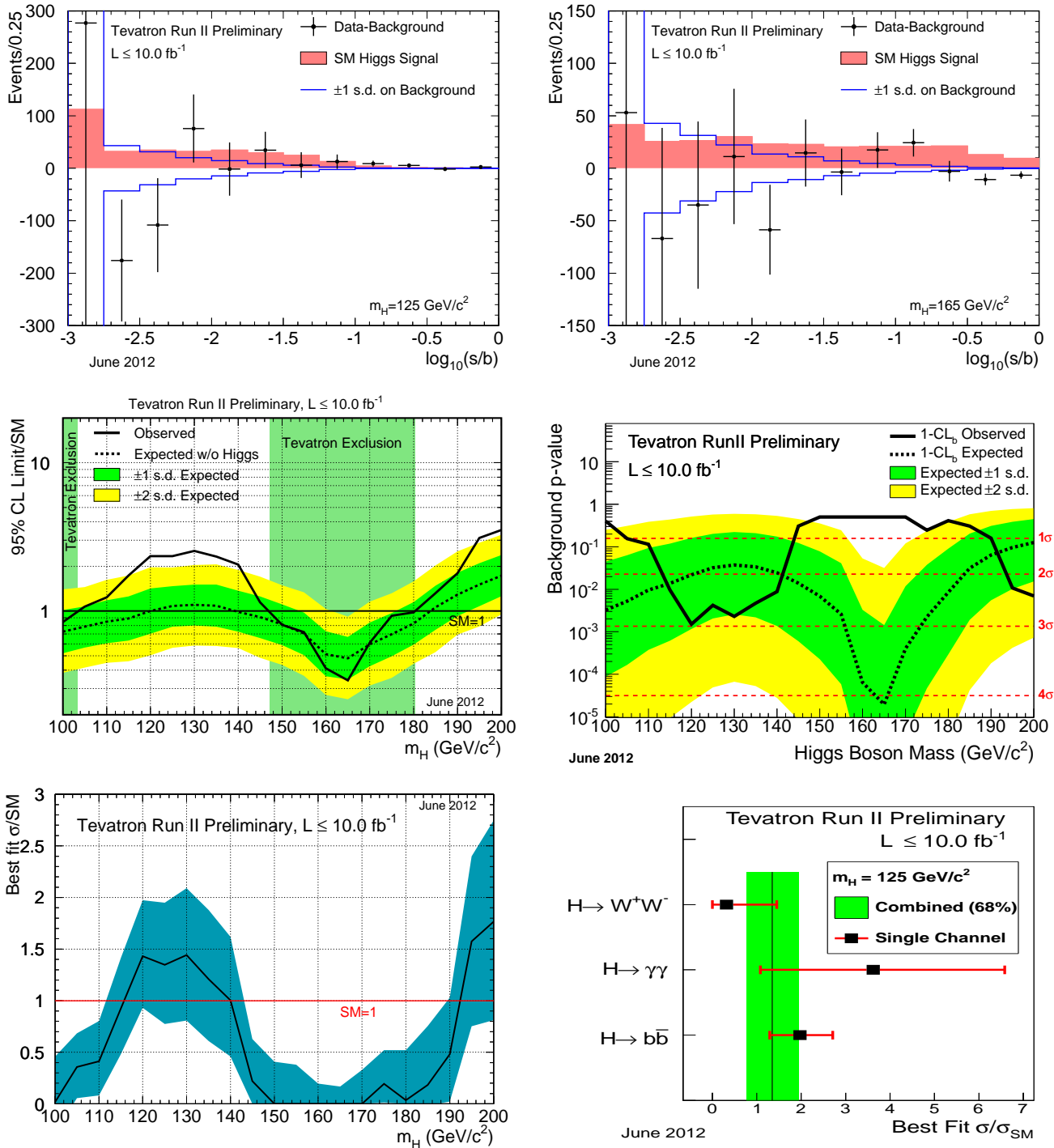


Figure 21: Preliminary results from the Tevatron combination in July 2012 [279]. Expected and observed event yields classified by the signal-to-background ratio after background subtraction for  $M_H = 125 \text{ GeV}$  (top-left) and  $M_H = 165 \text{ GeV}$  (top-right); exclusion limit on the signal strength  $\sigma/\sigma_{\text{SM}}$  as a function of  $M_H$  (middle-left), local  $p$ -value for the background-only hypothesis as a function of  $M_H$  (middle-right), best fit values of the signal strength as a function  $M_H$  (bottom-left), and best fit values for the signal strength in different decay modes for  $M_H = 125 \text{ GeV}$  (bottom-right).

sponding to a local significance of 3.0 as shown in Figure 21 (middle-right). The excess is dominated by the search for  $H \rightarrow b\bar{b}$  discussed above. Due to the limited mass resolution the significance is larger than 2 in the approximate mass range  $M_H = 115\text{--}145\text{ GeV}$ . Hence the influence of the LEE is also rather modest with a trial factor of approximately 2 yielding a global significance of 2.5. Another deviation from the background-only hypothesis with a significance of larger than 2 is observed for a Higgs-boson mass larger than 195 GeV, which was already excluded by the LHC experiments from 2011 data. The best fit value for the signal strength as a function of  $M_H$ , shown in Figure 21 (bottom-left), is consistent at 68% CL with the expectation for the SM Higgs boson in the mass ranges  $M_H = 110\text{--}140\text{ GeV}$  and approximately  $M_H = 190\text{--}200\text{ GeV}$ . Finally, the best signal-strength parameters in the different decay modes  $H \rightarrow b\bar{b}$ ,  $H \rightarrow WW$ , and  $H \rightarrow \gamma\gamma$  were determined for various fixed values of  $M_H$ . The result for  $M_H = 125\text{ GeV}$  is shown in Figure 21 (bottom-right).

## 8 Searches at the LHC

The design parameters of the LHC and the two multipurpose experiments ATLAS and CMS are chosen in such a way that the whole unexplored mass range, from the limit obtained at LEP up to the upper border of  $\lesssim 1\text{ TeV}$  demanded by unitarity (see Section 2.5), can be covered. On 30 March 2010, the LHC took first proton–proton collision data at the CM energy of 7 TeV, an energy unprecedented at accelerators at that time. Fully hadronic final states, arising from production in gluon fusion or weak-vector-boson fusion with subsequent decay via  $H \rightarrow b\bar{b}$  or  $H \rightarrow WW(ZZ) \rightarrow 4\text{ quarks}$  yielding the largest production rates, are not considered in the search. The overwhelming background and the limited trigger capabilities for these final states do not allow for performing a sensitive search. The large instantaneous luminosities of up to  $6.8 \times 10^{33}\text{ cm}^{-2}\text{s}^{-1}$  ( $3.7 \times 10^{33}\text{ cm}^{-2}\text{s}^{-1}$ ) reached in 2012 up to June (2011) together with the large total inelastic cross section and the interaction rate of 20 MHz lead to an average of 20 (10) overlaid proton–proton interactions in 2012 up to June (2011) often referred to as “pile-up”. This challenge, which was not of relevance at Tevatron, imposes additional challenges on the event reconstruction especially on isolation criteria and a precise determination of the missing transverse momentum. Only final states that contain at least one photon, electron, muon, or a hadronic tau-lepton decay in association with large missing transverse momentum are considered in the searches. The production rates for these topologies at the LHC and the ratio of cross sections at different CM energies are shown in Figure 22. In contrast to the searches at Tevatron channels with low branching ratios, such as  $H \rightarrow \gamma\gamma$  and  $H \rightarrow ZZ \rightarrow \ell^+\ell^-\ell'^+\ell'^-$  with branching ratios of 0.2% and 0.013% for a Higgs-boson mass of 125 GeV are also accessible due to the larger production cross section at the LHC. In fact these two channels provide the highest sensitivity over a large mass range.

The signal cross sections, the branching ratios, and their uncertainties are computed, as detailed in Sections 2.6 and 6, following the recommendations of the LHC Higgs Cross Section Working Group [25, 26]. Simulated events are generated using POWHEG interfaced to PYTHIA for the dominant production mechanisms in gluon fusion [226] and in weak-vector-boson fusion [239]. The associated production with a weak gauge boson and a pair of top quarks is mainly simulated with PYTHIA (CMS uses POWHEG for the decay channel  $H \rightarrow b\bar{b}$ ).

The dominant background processes, in particular the irreducible ones apart from a very few exceptions, are estimated at least partially with data-driven techniques. Only in some analyses the normalization and shape of the final discriminating distribution are completely estimated from data. Quite often the normalization is estimated in a control region, defined, e.g., by inverting some of the selection criteria, and the prediction for the ratio of the background expectations in the signal and control regions as well as the shape of the final discriminant are estimated from simulated events. The most advanced event generators are used to get as precise as possible predictions. Those include ALPGEN [289], MADGRAPH [309], MC@NLO [225, 293], and SHERPA [294], which perform a matching of

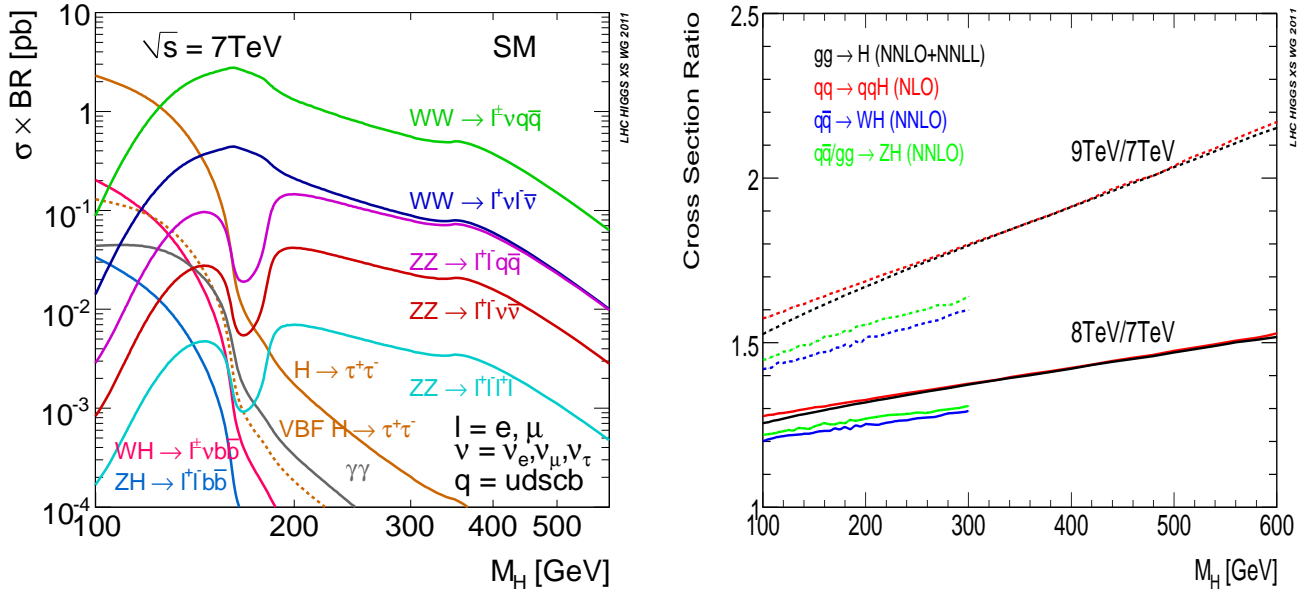


Figure 22: Higgs-boson production rates at the LHC for CM energies of 7 TeV in final states which are used to search for the Higgs boson (left) [25] and ratio of cross sections at different CM energies (right) [308].

matrix-element calculations and parton showers at NLO or LO in QCD, and dedicated programmes for gluon-induced di-boson production, such as GG2WW [310] and GG2ZZ [311] at LO. For cross checks and simulation of the parton shower, of the underlying event, and of pile-up the multipurpose event generators PYTHIA [91,92] and HERWIG [291,292] are used.

## 8.1 Search with data collected in 2010

The highest cross sections with final states involving at least one colour-neutral object are obtained in the mass range between 150 GeV and 170 GeV in the decay chains  $H \rightarrow W^+W^- \rightarrow \ell\nu q\bar{q}$  and  $H \rightarrow W^+W^- \rightarrow \ell^+\nu\ell^-\bar{\nu}$  (see l.h.s. of Figure 22). The semi-leptonic decay of the pair of W bosons is not usable in this low-mass interval due to the large background from W+jets production. The first sensitivity at the LHC hence stemmed from the  $H \rightarrow W^+W^- \rightarrow \ell^+\nu\ell^-\bar{\nu}$  final state. Both experiments performed a search in this final state with the data collected in 2010 at a CM energy of 7 TeV corresponding to integrated luminosities of 36 pb<sup>-1</sup> [312] and 35 pb<sup>-1</sup> [313]. The expected sensitivity in the mass range 150–170 GeV was at the level of 2–3 times the SM prediction (see Fig.23, middle and right). No significant deviation from the expected event yields from background processes was observed. ATLAS already investigated several other final states based on 2010 data:  $H \rightarrow \gamma\gamma$ ,  $H \rightarrow ZZ \rightarrow \ell^+\ell^-\ell'^+\ell'^-$ ,  $H \rightarrow ZZ \rightarrow \ell^+\ell^-\nu\nu$ ,  $H \rightarrow ZZ \rightarrow \ell^+\ell^-q\bar{q}$ , and  $H \rightarrow W^+W^- \rightarrow \ell\nu q\bar{q}$ . The individual sensitivities of each of these searches were at the best on the level of 15 times the SM prediction (Fig. 23, left).

## 8.2 Searches with data collected in 2011 and up to June in 2012

In 2011 each of the two experiments collected a data set corresponding to integrated luminosities of up to 5.1 fb<sup>-1</sup> at a CM energy of 7 TeV. In 2012 until June a data set corresponding to up to 5.9 fb<sup>-1</sup> per experiment was recorded at a CM energy of 8 TeV. An overview of the search channels considered, the considered mass range in each channel, and the integrated luminosities analyzed is given in Table 9. Three mass regions can be roughly distinguished: (a) 110 GeV ≤ M<sub>H</sub> ≤ 150 GeV, (b)



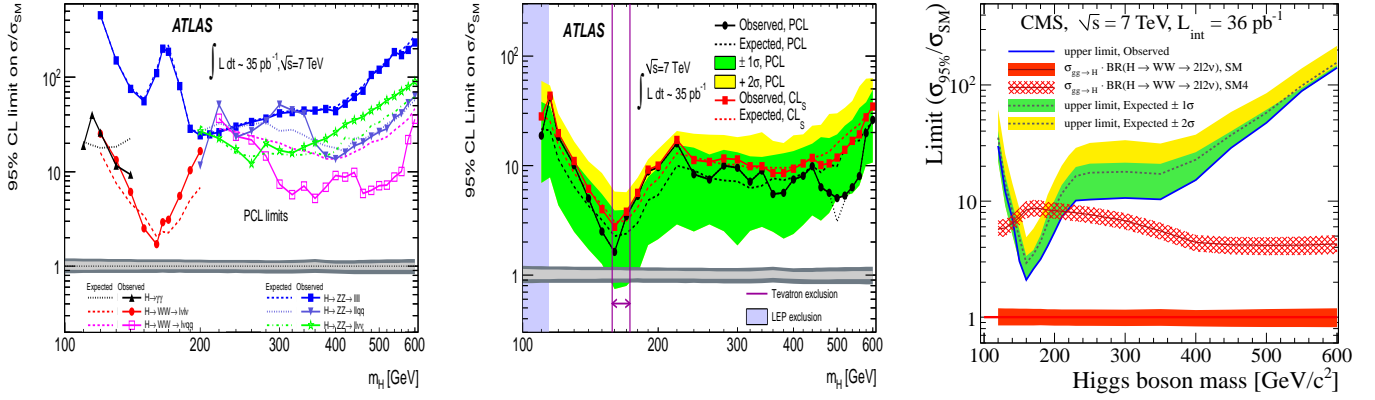


Figure 23: Observed and expected exclusion limits on the signal-strength parameter  $\mu$  obtained from 2010 collision data: individual channels (left), their combination (middle) in ATLAS [312], and the combination in CMS (right) [313].

Table 9: Search channels, mass ranges, integrated luminosities considered by ATLAS and CMS, and corresponding references. The results used in the combination of the 2011 data are documented in Ref. [314] for ATLAS and in Ref. [315] for CMS. An entry “–” indicates that this search channel was not considered for this data set. In 2012 CMS restricted the mass range for all published searches to values below 160 GeV. When two mass ranges are given, the search was performed in two disconnected ranges.

channel	ATLAS			CMS		
	mass range $M_H$ [GeV]	$\int L dt$ [ $\text{fb}^{-1}$ ]		mass range $M_H$ [GeV]	$\int L dt$ [ $\text{fb}^{-1}$ ]	
		2011	2012		2011	2012
$H \rightarrow \gamma\gamma$	110–150	4.8 [316]	5.9 [317]	110–150	5.1 [318]	5.3 [319]
$H \rightarrow \tau^+\tau^-$	110–150	4.7 [320]	–	110–145	4.9 [321]	5.1 [319]
$H \rightarrow b\bar{b}$	110–130	4.7 [322]	–	110–135	5.0 [323]	5.1 [319]
$H \rightarrow ZZ \rightarrow \ell^+\ell^-\ell'^+\ell'^-$	110–600	4.8 [324]	5.8 [317]	110–600/160	5.1 [325]	5.3 [319]
$H \rightarrow W^+W^- \rightarrow \ell^+\nu\ell^-\bar{\nu}$	110–600	4.7 [326]	5.8 [317]	110–600/160	4.9 [327]	5.1 [319]
$H \rightarrow ZZ \rightarrow \ell^+\ell^-\tau\tau$	–	–	–	190–600	4.7 [328]	–
$H \rightarrow ZZ \rightarrow \ell^+\ell^-q\bar{q}$	200–600	4.7 [329]	–	130–163,200–600	4.6 [330]	–
$H \rightarrow ZZ \rightarrow \ell^+\ell^-\nu\nu$	200–600	4.7 [331]	–	250–600	4.6 [332]	–
$H \rightarrow W^+W^- \rightarrow \ell\nu q\bar{q}$	300–600	4.7 [333]	–	–	–	–

$150 \text{ GeV} \leq M_H \leq 200 \text{ GeV}$ , and (c)  $200 \text{ GeV} \leq M_H \leq 600 \text{ GeV}$ .

The mass range above 600 GeV, which is highly disfavoured by electroweak precision measurements, was not considered, because the theoretical tools or recipes described in Refs. [25, 26, 54, 55] (see also references therein) for a proper description of the extremely broad Higgs-boson lineshape and their interference with irreducible background for such large masses were not available to the experiments until June 2012.

Both experiments published their findings based on the complete 2011 data set [314, 315]. These data were partially reanalyzed with better reconstruction and identification tools, and optimized analysis techniques, resulting in a significantly increased sensitivity. In combination with the analysis of the data



set collected in 2012 up to June, the reanalyzed 2011 data are published in Refs. [317,319]. CMS only considered the mass region below 160 GeV in the 2012 data analysis and reanalyzed the 2011 data in the channels  $H \rightarrow \gamma\gamma$ ,  $H \rightarrow b\bar{b}$ ,  $H \rightarrow \tau^+\tau^-$ , and  $H \rightarrow ZZ \rightarrow \ell^+\ell^-\ell'^+\ell'^-$ . ATLAS reanalyzed the channels  $H \rightarrow \gamma\gamma$  and  $H \rightarrow ZZ \rightarrow \ell^+\ell^-\ell'^+\ell'^-$  in the 2011 data, and so far has only investigated those two channels and the  $H \rightarrow W^+W^- \rightarrow e\mu\nu\bar{\nu}$  decay mode in 2012 data.

In the low-mass region 110–150 GeV the decays to photons, to a pair of tau leptons or bottom quarks, and to a pair of weak gauge bosons (WW and ZZ), which decay to four leptons, were considered by both experiments. The decays  $H \rightarrow \gamma\gamma$  and  $H \rightarrow ZZ \rightarrow \ell^+\ell^-\ell'^+\ell'^-$ , with very low rate, provide an excellent resolution for the reconstruction of the invariant mass of the decay products of the Higgs-boson candidate with an accuracy of about 1–2%. In the decay mode  $H \rightarrow W^+W^- \rightarrow \ell^+\nu\ell^-\bar{\nu}$ , which has a comparably high production rate, only the transverse mass can be reconstructed. The decays  $H \rightarrow \tau^+\tau^-$  and  $H \rightarrow b\bar{b}$  allow for reconstructing the mass of the Higgs-boson candidate with limited resolution in the range of 10–30%, due to the presence of several neutrinos in the final state or the limited energy resolution for the reconstruction of jets compared to charged leptons and photons. CMS also considered the decay  $H \rightarrow ZZ \rightarrow \ell^+\ell^-q\bar{q}$  for mass values larger than 130 GeV, where the mass can be reconstructed with an accuracy of roughly 10%.

In the intermediate-mass region 150–200 GeV the sensitivity of the search is dominated by the decay mode  $H \rightarrow W^+W^- \rightarrow \ell^+\nu\ell^-\bar{\nu}$ , which has a large production rate, but allows only for reconstructing the transverse mass. The search for  $H \rightarrow ZZ \rightarrow \ell^+\ell^-\ell'^+\ell'^-$  with low rate, but excellent mass reconstruction capabilities provides a sensitivity that is roughly one order of magnitude smaller.

In the high-mass region 200–600 GeV various final states arising from the decay of the Higgs boson into a pair of electroweak gauge bosons are considered. In addition to the final states that dominate the sensitivity in the intermediate-mass region, the decays  $H \rightarrow ZZ \rightarrow \ell^+\ell^-q\bar{q}$ ,  $H \rightarrow ZZ \rightarrow \ell^+\ell^-\nu\nu$  are searched for by both experiments as well, while  $H \rightarrow ZZ \rightarrow \ell^+\ell^-\tau\tau$  is analyzed only by CMS, and  $H \rightarrow W^+W^- \rightarrow \ell\nu q\bar{q}$  only by ATLAS. The signal rates for  $H \rightarrow ZZ \rightarrow \ell^+\ell^-\ell'^+\ell'^-$  and  $H \rightarrow W^+W^- \rightarrow \ell^+\nu\ell^-\bar{\nu}$  get quite small for large  $M_H$ , and hence the sensitivity is increased by including decay modes of the weak gauge bosons with larger branching ratios. These final states are not considered for smaller masses as the backgrounds, dominated by W and Z production in association with jets, increase in importance in this region and cannot be suppressed sufficiently or cannot be estimated with sufficient precision from control regions in data to the required level. Additionally the width of the reconstructed Higgs-boson mass distribution is no longer dominated by the experimental resolution, but by the natural width in the  $H \rightarrow ZZ \rightarrow \ell^+\ell^-\ell'^+\ell'^-$  channels for masses above 350 GeV. Hence the relative sensitivity to the other decay modes, which have a worse mass resolution or only allow an approximate mass observable to be reconstructed, gets weaker.

The channels  $H \rightarrow W^+W^- \rightarrow \ell^+\nu\ell^-\bar{\nu}$  and  $H \rightarrow ZZ \rightarrow \ell^+\ell^-\ell'^+\ell'^-$  contribute significantly to the overall sensitivity over the full mass range. For small values of  $M_H$  it is important to lower the threshold for the transverse momenta of the selected leptons as much as possible, limited often by trigger rate requirements, and to retain simultaneously a low misidentification rate.

- In the  $H \rightarrow W^+W^- \rightarrow \ell^+\nu\ell^-\bar{\nu}$  analysis an excess of events with two leptons of opposite charge and large missing transverse momentum is searched for. Events are divided into separate categories according to jet multiplicity and lepton flavours, where the two-jet category has selection criteria designed to enhance sensitivity to the VBF production process. ATLAS so far has only considered the  $e\mu$  final state for the 2012 data analysis due to the higher pile-up conditions with worse resolution for the missing transverse momentum and the correspondingly increased background from Drell–Yan production in the same-lepton-flavour final state. In events with no jets, the main background stems from non-resonant WW production; in events with one jet, the dominant backgrounds are from WW and top-quark production, and in events with two jets from top-quark production. In CMS in the analysis of the 2011 data MVA classifiers are trained for a number of

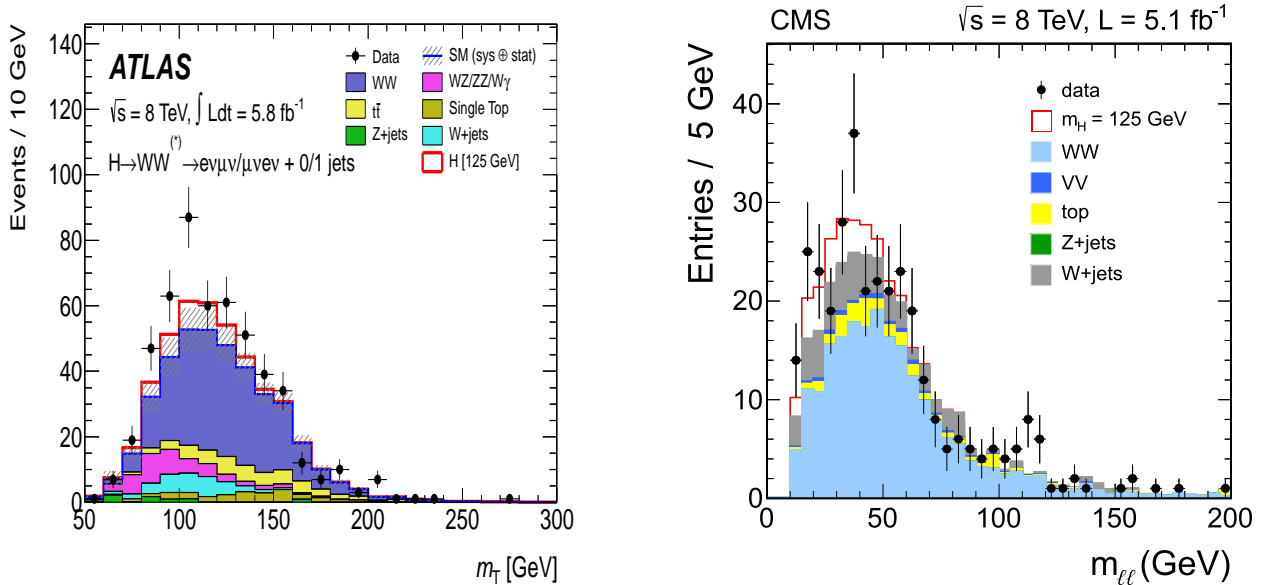


Figure 24: Distributions of the final discriminant in the  $H \rightarrow W^+W^- \rightarrow \ell^+\nu\ell^-\bar{\nu}$  search at 8 TeV in 2012 in ATLAS [317] (left) and CMS [319] (right).

Higgs-boson masses to improve the separation of signal from backgrounds, and a search is made for an excess of events in the output distributions of the classifiers. In the 2012 analysis CMS uses sequential cuts, and the di-lepton invariant mass is used as final discriminant. ATLAS performs a cut-based analysis, optimized for different  $M_H$  ranges, and the WW transverse-mass distribution is used as the final discriminant. All background rates, except for very small contributions from WZ, ZZ, and  $W\gamma^*$  are evaluated from data. The distribution of the final discriminants in the analysis of the 8 TeV data show a clear broad excess in ATLAS and a less significant broad one in CMS (see Figure 24).

- In the  $H \rightarrow ZZ \rightarrow \ell^+\ell^-\ell'^+\ell'^-$  channel an excess in the invariant-mass spectrum of the four isolated leptons over a small continuum background is searched for. The  $4e$ ,  $4\mu$ ,  $2e2\mu$  final states are analyzed separately, since there are differences in the four-lepton mass resolutions and the background rates arising from jets misidentified as leptons. The main irreducible background from non-resonant ZZ production is mainly estimated from simulation. The smaller reducible backgrounds from Z+jets production, which mostly impacts the low four-lepton invariant-mass region, and top-quark pair production are estimated from control regions in data, or at least the normalization is validated in dedicated control regions. The final discriminant in ATLAS is the four-lepton invariant-mass spectrum. CMS exploits the different kinematics and angular correlations to discriminate further the signal process from the irreducible ZZ background. The information from the five angles, which describe the production and decay kinematics in the Higgs-boson candidate rest frame, are combined in the so-called MELA observable [334]. CMS uses a two-dimensional final discriminant consisting of the four-lepton invariant mass and the MELA output ( $K_D$ ). A clear excess in the four-lepton invariant-mass spectra is observed in both experiments at masses of 125 GeV in ATLAS and 126 GeV in CMS, respectively (see Figure 25).

In addition to the two channels discussed above, where the full mass range is covered, the channel  $H \rightarrow ZZ \rightarrow \ell^+\ell^-\nu\nu$  provides the largest sensitivity in the high-mass range and dominates the sensitivity for  $M_H$  values larger than 300 GeV.

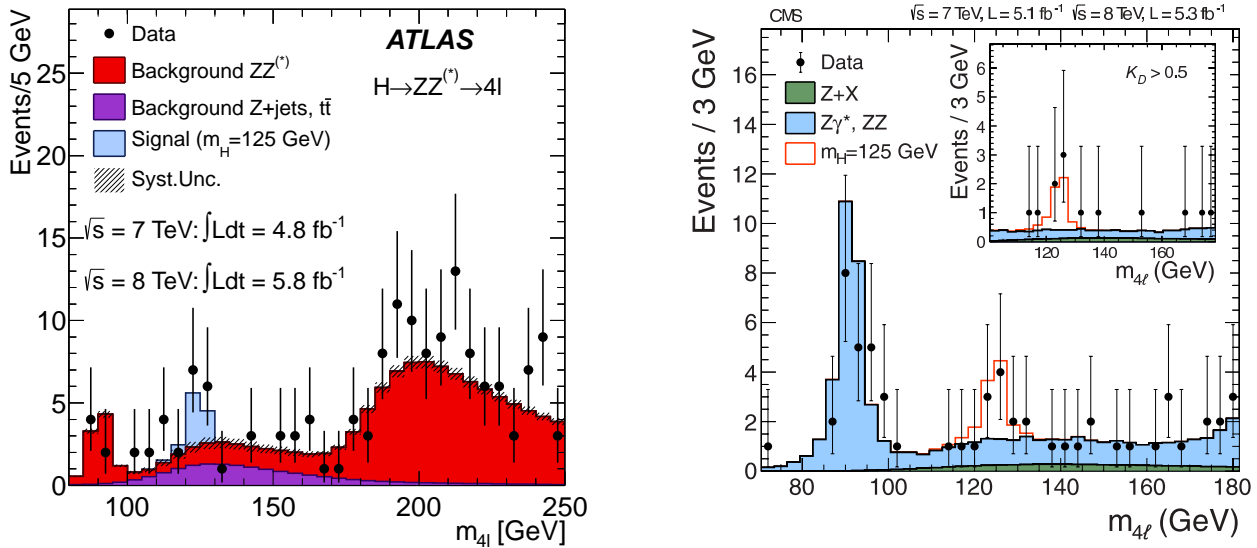


Figure 25: Four-lepton invariant-mass spectra in ATLAS [317] (left) and CMS [319] (right) for the combination of the 2011 and 2012 data.

- In the search for  $H \rightarrow ZZ \rightarrow \ell^+ \ell^- \nu \bar{\nu}$  events with a pair of electrons or muons with opposite charge, consistent with the decay of an on-shell Z, and large missing transverse momentum are selected. After applying additional kinematical requirements, which depend on the Higgs-boson mass hypothesis, a transverse-mass observable is used as the final discriminant. The background predictions for weak-gauge-boson pair production are obtained from simulation, whereas the other backgrounds are determined from control samples in collision data. A significant fraction of the selected signal events stems from the decay  $H \rightarrow W^+ W^- \rightarrow \ell^+ \nu \ell^- \bar{\nu}$  especially for lower masses. In order to avoid double counting of signal yields, the selection is designed to have no overlap with the dedicated  $H \rightarrow W^+ W^- \rightarrow \ell^+ \nu \ell^- \bar{\nu}$  analysis. The normalization of most background processes is estimated from control regions in data.
- In the search for  $H \rightarrow ZZ \rightarrow \ell^+ \ell^- q \bar{q}$  events with a pair of electron or muons and a pair of jets, which each have an invariant mass consistent with  $M_Z$ , are selected. The events are categorized according to the number of b-tagged jets in the final state (none or at least one in ATLAS; 0, 1, or 2 in CMS), in order to profit from the relatively large rate of b-jets from Z-boson decays present in the signal compared to the rate of b-jets found in the Z+jets background. Additional kinematical requirements are applied depending on the Higgs-boson mass hypothesis. CMS also exploits the different angular correlations between the final-state objects for the signal process compared to the background processes. The final discriminating variable is given by the invariant mass of the two leptons and two jets. CMS also searches in the mass range below  $2M_Z$ , where the mass-window criteria on the di-lepton mass is replaced by an upper bound. The dominant background from Z+jet production is estimated from control samples in data, defined by sidebands in the di-jet invariant mass.
- The search for  $H \rightarrow W^+ W^- \rightarrow \ell \nu q \bar{q}$  (only ATLAS) requires events with an isolated lepton and missing transverse momentum and two jets with an invariant mass compatible with a W boson. The mass of the Higgs-boson candidate can be constructed by solving a quadratic equation to solve for the component of the neutrino momentum along the beam axis exploiting the W mass constraint for the lepton plus neutrino system. The analysis further classifies events by lepton flavour and by the number of additional jets (0, 1, or 2), where the two-jet channel is optimized for the VBF production process. The final discriminant is given by invariant mass of the  $\ell \nu q \bar{q}$

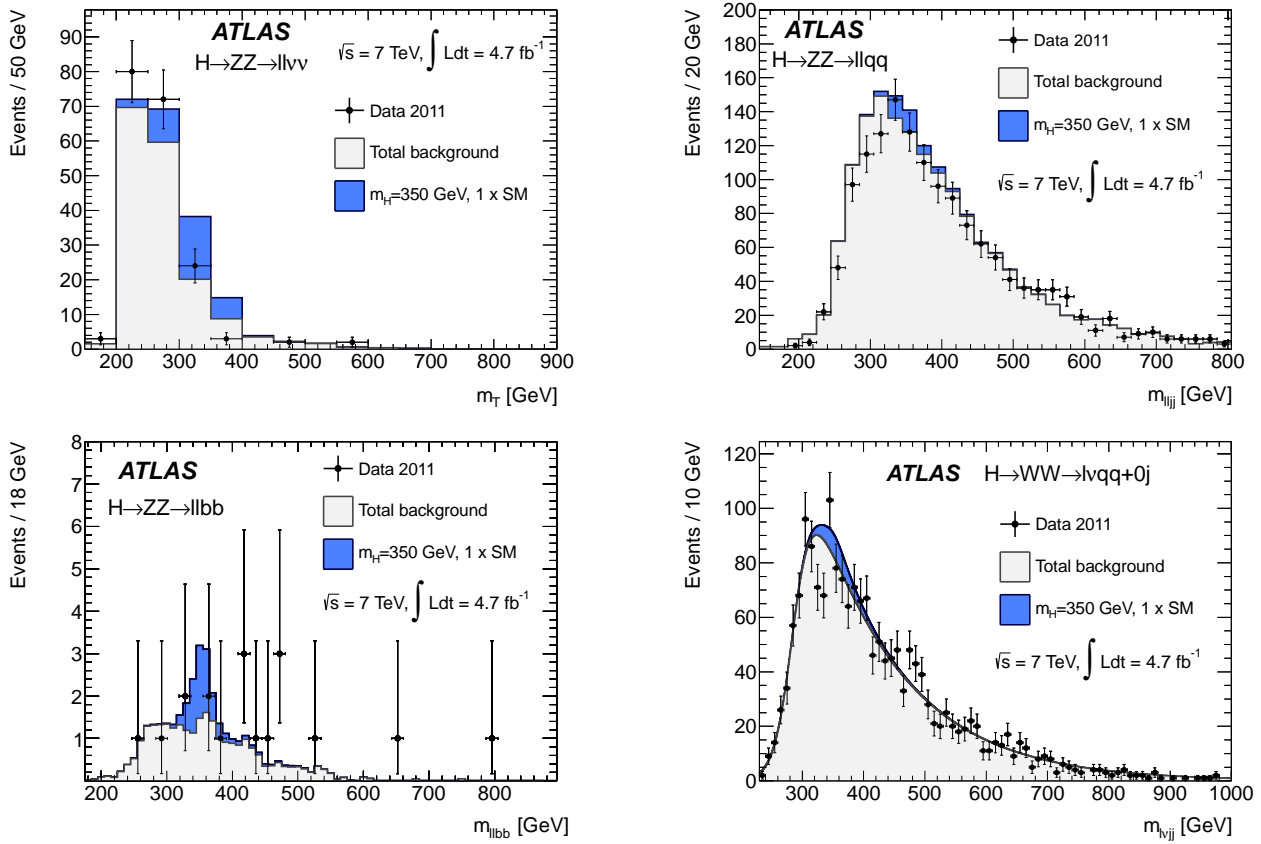


Figure 26: Distributions of the final discriminants in the ATLAS searches [335] in the high- $M_H$  region:  $H \rightarrow ZZ \rightarrow \ell^+ \ell^- \nu \nu$  (top-left),  $H \rightarrow ZZ \rightarrow \ell^+ \ell^- q \bar{q}$  (top-right),  $H \rightarrow ZZ \rightarrow \ell^+ \ell^- b \bar{b}$  (bottom-left), and  $H \rightarrow W^+ W^- \rightarrow \ell \nu q \bar{q}$  (bottom-right).

system. The background is modeled with a smooth function.

- The search for  $H \rightarrow ZZ \rightarrow \ell^+ \ell^- \tau \tau$  (only CMS) selects events with electron or muon pairs, which are consistent with stemming from the decay of an on-shell  $Z$  boson, and a pair of tau-lepton candidates, which either decay hadronically or into an electron or muon. Final states with only electrons or muons are not considered, as they are already included in the dedicated  $H \rightarrow ZZ \rightarrow \ell^+ \ell^- \ell'^+ \ell'^-$  search. The final discriminant is given by the distribution of the di-lepton–di-tau invariant mass, constructed from the visible products of the tau-lepton decays, neglecting the effect of the accompanying neutrinos. The mass resolution for Higgs-boson candidates is 10–15%. The dominant background from  $ZZ$  production is estimated from simulation. Other backgrounds are estimated from control regions in data.

The final mass distributions (examples from ATLAS are shown in Figure 26) agree with the expectations from background processes.

In the low-mass range in addition to  $H \rightarrow W^+ W^- \rightarrow \ell^+ \nu \ell^- \bar{\nu}$  and  $H \rightarrow ZZ \rightarrow \ell^+ \ell^- \ell'^+ \ell'^-$  the search is performed for  $H \rightarrow \gamma \gamma$ ,  $H \rightarrow \tau^+ \tau^-$ , and  $H \rightarrow b \bar{b}$ .

- The  $H \rightarrow \gamma \gamma$  analysis selects events with two isolated photons with large transverse momenta. The dominant reducible backgrounds are multi-jet production and single-photon production in association with jets with cross sections several orders of magnitude larger than the signal cross section. These backgrounds can be suppressed to a level of less than 25% due to the excellent discrimination capabilities of the LHC detectors between photon and jets. The irreducible background

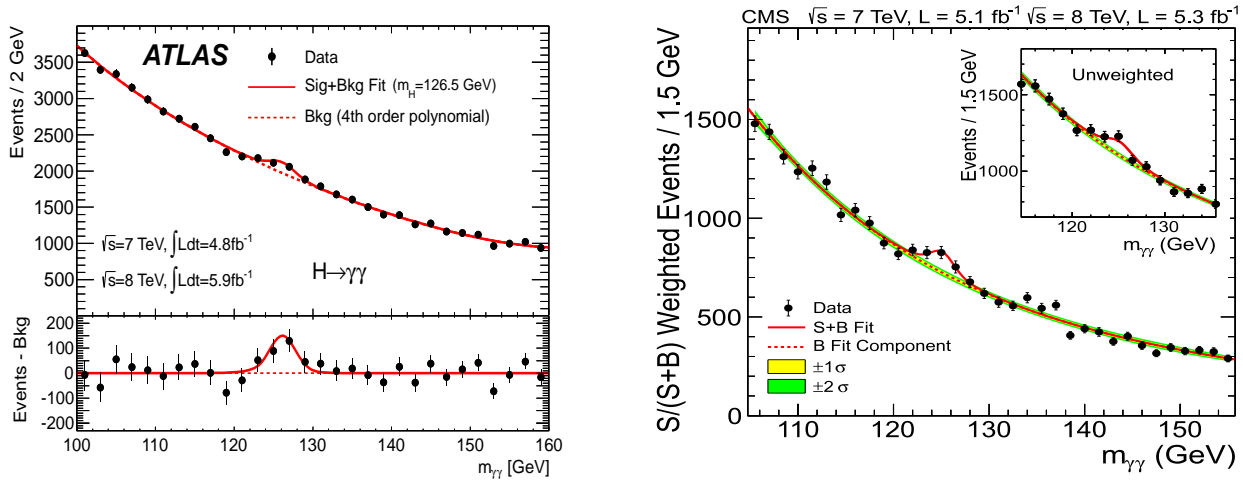


Figure 27: Di-photon invariant-mass spectra after the inclusive selection in ATLAS [317] (left) and CMS [319] (right) for the combination of the 2011 and 2012 data.

from di-photon production can only be discriminated from the signal process by an excellent reconstruction of the invariant mass of the di-photon system, which depends on the measurement of the energies of the photons and their opening angle. In both experiments the contribution from the resolution in the measurement of the opening angle was found to be negligible. The di-photon mass spectra after requiring two isolated photon candidates for the data from 2011 and 2012 are shown in Figure 27. The sensitivity of the search can be enhanced by splitting the event sample in various categories with different ratios of expected signal over background event yields and different signal mass resolutions. Both experiments consider event classes exploiting the typical VBF signature of two additional jets with large separation in pseudorapidity and large di-jet invariant mass. ATLAS uses nine additional categories based on the pseudorapidity of each photon, whether it is reconstructed as a converted or unconverted photon, and the momentum component of the di-photon system transverse to the di-photon thrust axis. CMS uses four additional categories depending on the score of a boosted decision tree. The background in the signal region is estimated from a fit to the observed di-photon mass distribution in data. A clear excess in the invariant di-photon mass spectra is observed in both experiments at masses of 126 GeV in ATLAS and 125 GeV in CMS, respectively.

- The  $H \rightarrow \tau^+\tau^-$  analysis searches for a broad excess in the reconstructed di-tau invariant-mass distribution, where the mass reconstruction is mostly based on the ideas in Refs. [336, 337] with a resolution between 10–30%. Events are classified according to the tau-lepton decay modes (into an electron, a muon, or hadrons plus neutrinos). ATLAS considers all decay-mode combinations, whereas CMS has not investigated yet the double electron and double hadronic final state. Depending on the final state the event samples are further divided into exclusive subcategories, which are optimized for the sensitivity to a particular production mode. The category optimized for the VBF signature provides the largest sensitivity. Events failing these selection requirements are separated further, e.g., in a category with two jets optimized for associated production  $HW(HZ)$ , with one jet with large transverse momentum for associated production and production in gluon fusion, and with either no jets or with one with a small transverse momentum aiming at the gluon-fusion production process. The main irreducible background arises from  $Z \rightarrow \tau\tau$  production, whose di-tau invariant-mass distribution is derived from data by selecting  $Z \rightarrow \mu\mu$  events, in which the reconstructed muons are replaced with reconstructed particles from the decay of simulated  $\tau$  leptons of the same momenta. The reducible backgrounds from  $W$ +jets, Drell–Yan,

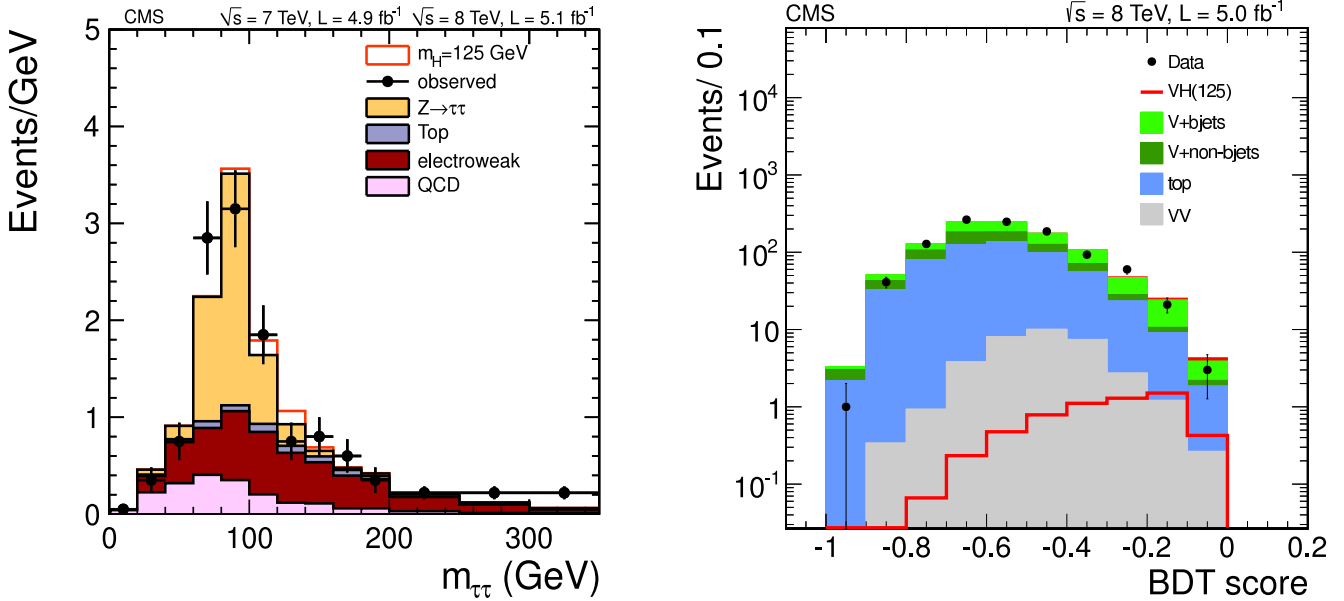


Figure 28: Distributions of the final discriminant for the search in  $H \rightarrow \tau^+\tau^-$  combined for 2011 and 2012 data (left) and  $H \rightarrow b\bar{b}$  for 2012 data (right) in CMS [319].

and multi-jet production are also evaluated from control samples in data. The distribution of the di-tau mass distribution for 2011 and 2012 data in CMS is shown in Figure 28 (left). No significant deviation from the background expectation is observed.

- The  $H \rightarrow b\bar{b}$  analysis selects events produced in association with a  $W$  or  $Z$  decaying via  $Z \rightarrow \ell^+\ell^-$ ,  $Z \rightarrow \nu\bar{\nu}$ , or  $W \rightarrow \ell\nu$ . The selection requires two  $b$ -tagged jets and either two leptons, one lepton and missing transverse momentum, or large missing transverse momentum. CMS selects events with a high transverse momentum of the di-jet system in order to improve the mass resolution and to suppress background processes. A multivariate classifier is trained for different  $M_H$  values and its output is used as the final discriminant in CMS (see Figure 28, right). ATLAS subdivides the events in categories according to the transverse momentum of the weak gauge boson and uses the di-jet invariant mass of the  $b$ -tagged jets as the final discriminant. No significant deviation from the background expectation is observed.

### 8.3 Excluded mass ranges

In most search channels and over almost the full investigated mass range from 110–600 GeV no significant excess with respect to the background-only hypothesis is observed. This allows for the exclusion of a large part in the mass range of the SM Higgs boson. In the combination of the different search channels the ratio of the cross section for the different production modes and the ratio of the decay branching ratios are taken from the SM prediction. Upper limits on the signal strength  $\mu$ , which relates the excluded cross section to that for Higgs-boson production in the SM, are derived based on the profile likelihood ratio [109] as test statistic using the  $CL_s$  technique [106] to avoid exclusion of parameter space where no sensitivity is expected. Correlations in the theoretical and systematic uncertainties, which are included via nuisance parameters in the likelihood function, among the various search channels and event categories are taken into account (see Refs. [114,314,315] for details). The exclusion limits obtained in both experiments in the various search channels and their combination from the first analysis of the full 2011 data set are shown in Figure 29, for the combination in each experiment from the (re-)analysis of 2011 and 2012 data in Figure 30, and both are summarized in Table 10.



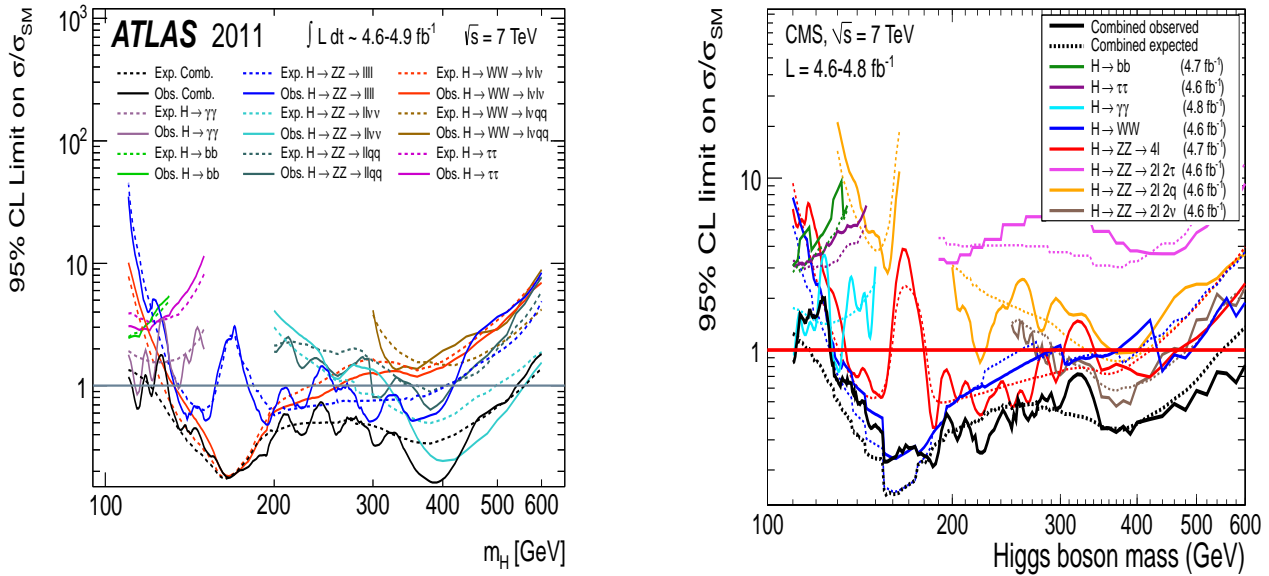


Figure 29: Exclusion limits on the signal-strength parameter  $\mu$  as a function of the hypothetical Higgs-boson mass in the individual channels and their combination obtained from the analysis of 2011 data by ATLAS [314] (left) and CMS [315] (right).

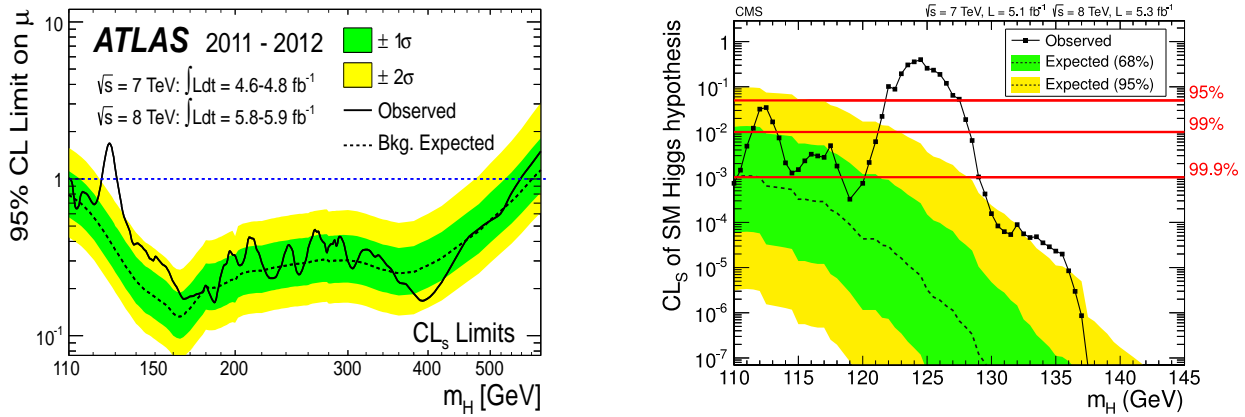


Figure 30: Exclusion limits on the signal-strength parameter  $\mu$  as a function of the hypothetical Higgs-boson mass obtained from the analysis of 2011 and 2012 data by ATLAS [317] (left) and confidence level  $CL_s$  for rejecting the signal+background hypothesis as a function of the hypothetical Higgs-boson mass by CMS [319] (right).

Already with the data set from 2011 a large mass range is excluded. However, in the low-mass range the observed limit is weaker than the expected one, which extends from 118–560 GeV (by applying a simple “or” of the two experiments). After adding the 2012 data set and re-analyzing the 2011 data the expected exclusion sensitivity extends over the mass range of 110–582 GeV. The mass range that is excluded neither by ATLAS nor by CMS, is the interval from 122–127 GeV. The large deviations of the observed from the expected limits are caused by the observed excesses of events discussed above. For a large mass range, reduced production cross sections of 20% of the SM prediction are excluded as well, and the SM Higgs-boson hypothesis can be excluded with very high confidence level.

Table 10: Mass ranges for the SM Higgs boson excluded by the combination of all searches of ATLAS and CMS: observed excluded range, expected excluded range for 2011 data alone [314,315], and combination of reanalyzed 2011 data and 2012 data [317,319].

	2011 data		2011+2012 data	
	excl. $M_H$ [GeV]	exp. excl. $M_H$ [GeV]	excl. $M_H$ [GeV]	exp. excl. $M_H$ [GeV]
ATLAS	111.4–116.6, 119.4–122.1 129.2–541	120–560	111–122, 131–559	110–582
CMS	127–600	118–543	110–121.5, 127–600	110–543

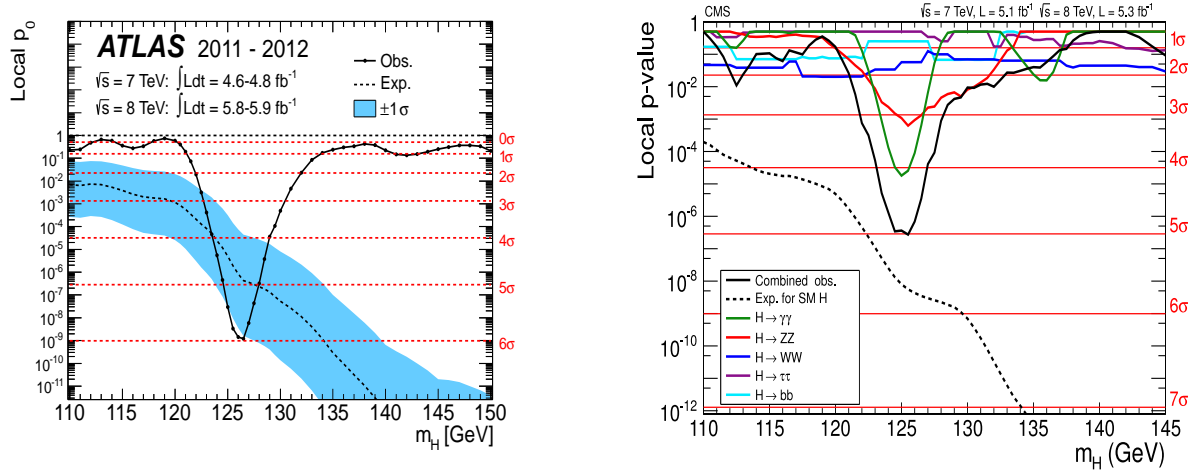


Figure 31: Local  $p$ -values as function of the hypothetical Higgs-boson mass in ATLAS [317] (left) and CMS [319] (right).

## 8.4 Observation of a new particle

When testing the compatibility with the background-only hypothesis, already in the 2011 data, tantalizing hints for the possible production of a new particle were observed, which corresponded to local significance of 2.9 at a mass of 126 GeV in ATLAS [314] and a local significance of 3.1 at a mass of 124 GeV in CMS [315]. These local significances are already larger than the ones shown by the individual Tevatron experiments and quite similar to the combined significance published by CDF and D0. When taking into account the “look-elsewhere effect” in the whole mass range considered from 110–600 GeV the global significances were found to be roughly 1 in ATLAS and 1.5 in CMS. After adding the 2012 data available up to June to the analysis the local significances ( $p$ -values) increased (decreased) to  $5.9$  ( $1.7 \times 10^{-9}$ ) at 126.5 GeV in ATLAS and  $5.0$  ( $2.8 \times 10^{-7}$ ) in CMS (see Figure 31). An overview of the observed and expected significances in the various search channels and their combination is given in Table 11, ordered by the size of the excess. The observed significance is due to the excesses observed in the channels with high mass resolution  $H \rightarrow \gamma\gamma$ ,  $H \rightarrow ZZ \rightarrow \ell^+ \ell^- \ell'^+ \ell'^-$  and with large production rate  $H \rightarrow W^+ W^- \rightarrow \ell^+ \nu \ell^- \bar{\nu}$ . No hints for the decay into a pair of fermions are observed yet, though the expected significance in the combination of  $H \rightarrow \tau^+ \tau^-$  and  $H \rightarrow b\bar{b}$  is equal to the expected one in  $H \rightarrow W^+ W^- \rightarrow \ell^+ \nu \ell^- \bar{\nu}$  in the CMS analysis. Assuming that the observed signal is due to the SM Higgs boson, ATLAS observes an upwards fluctuation of roughly one standard deviation compared to the expectation at a mass of 126.5 GeV and CMS observes a downwards fluctuation of roughly one standard deviation at a mass of 125.5 GeV. The global significance is 5.1 (5.3) in ATLAS for the mass



Table 11: Local significances in different search channels in ATLAS [317] and CMS [319].  $Z$  denotes the maximum significance observed at the mass value  $M_{\max, Z}$  when scanning the hypothetical Higgs-boson mass in the hypothesis test, and  $Z_{\text{exp.}}$  is the median expected significance for a SM Higgs boson at the same mass value. An entry “–” means that the information is not publicly available.

channel	ATLAS			CMS		
	$Z$	$Z_{\text{exp.}}$	$M_{\max, Z}$	$Z$	$Z_{\text{exp.}}$	$M_{\max, Z}$
$H \rightarrow \gamma\gamma$	4.5	2.5	126.5 GeV	4.1	2.8	125 GeV
$H \rightarrow ZZ \rightarrow \ell^+\ell^-\ell'^+\ell'^-$	3.6	2.7	125.0 GeV	3.2	3.8	125.6 GeV
$H \rightarrow W^+W^- \rightarrow \ell^+\nu\ell^-\bar{\nu}$	2.8	2.3	125.0 GeV	1.6	2.4	–
$H \rightarrow b\bar{b}+H \rightarrow \tau^+\tau^-$	–	–	–	0.4	2.4	–
combined	5.9	4.9	126.5 GeV	5.0	5.8	125.5 GeV

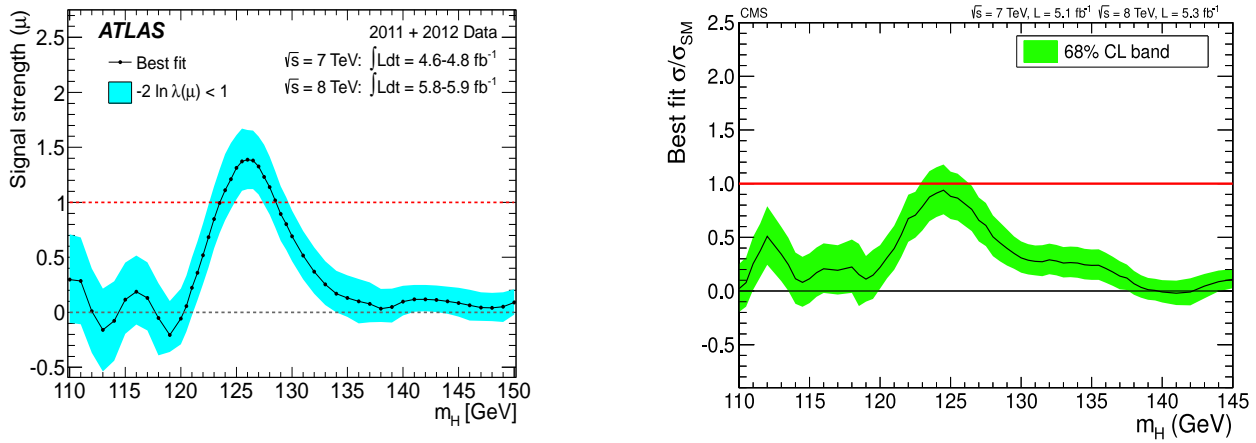


Figure 32: Best fit values for the signal strength  $\mu$  as function of the hypothetical Higgs-boson mass in ATLAS [317] (left) and CMS [319] (right).

range 110–600 (110–150) GeV and 4.5 (4.6) in CMS for the mass range 110–145 (110–130) GeV. These findings encouraged the two experiments ATLAS and CMS to proclaim the discovery of a new particle and to entitle their publications [317,319] with “Observation of a new particle / boson”.

## 8.5 Anatomy of the new particle

From the observation of the decay into a pair of particles with identical spin and with vanishing sum of the electric charges it can be concluded that the particle is electrically neutral, has integer spin, and hence is a neutral boson. The observation of the decay in two massless identical vector bosons,  $H \rightarrow \gamma\gamma$ , excludes the hypothesis of a spin-1 particle according to the Landau–Yang theorem [338].

A first crucial test of the compatibility of the observed event yields with the prediction for the SM Higgs boson is provided by a fit of the signal-strength parameter  $\mu$ . The overall signal strength relative to the SM prediction  $\mu$ , which assumes the ratio of production cross sections and ratio of branching ratios as predicted by the SM, is shown in Figure 32 as function of the hypothetical Higgs-boson mass. In both experiments the largest signal strengths of  $1.4 \pm 0.3$  observed at a mass of 126.0 GeV (ATLAS) and of  $0.87 \pm 0.23$  observed at a mass of 125.5 GeV (CMS) are compatible with unity. In a next step the best signal strength is determined for each decay mode of the new boson, which only assumes

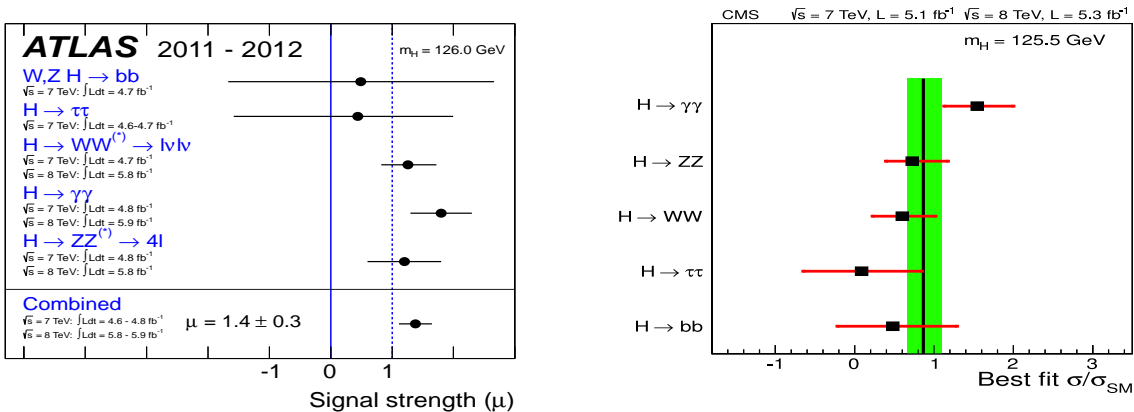


Figure 33: Best fit values for the signal strength  $\mu$  in the different decay modes as function of the hypothetical Higgs-boson mass in ATLAS [317] (left) and CMS [319] (right).

that the different production modes contribute as predicted by the SM. The fit results for the different decay modes, where the hypothetical Higgs-boson mass is fixed to the value that yields the largest overall signal strength, are also consistent with the SM prediction (Figure 33) within the still large uncertainties.

The compatibility of a simultaneous determination of the best signal strength  $\mu$  and the best mass value  $M_H$  in several final states is demonstrated in Figure 34. The best mass value  $M_H$  is determined in both experiments from the observed mass spectra in the  $H \rightarrow \gamma\gamma$  and  $H \rightarrow ZZ \rightarrow \ell^+\ell^-\ell'^+\ell'^-$  final states. The signal strengths in each final state (decay modes and classification categories) are treated as independent nuisance parameters. The results for the mass of the new boson, as obtained by the two collaborations are

ATLAS:  $126.0 \pm 0.4(\text{stat.}) \pm 0.4(\text{sys.})$  GeV [317] and CMS:  $125.3 \pm 0.4(\text{stat.}) \pm 0.5(\text{sys.})$  GeV [319].

In both experiments the systematic uncertainty is dominated by the knowledge of the absolute energy scale of photons and to a lesser extent of that of electrons. The mass values determined in the different final states within one experiment as well as the mass values determined in the two experiments are consistent with each other. Already now the precision of the determination of the mass is better than one percent. Note that the measured mass value is perfectly compatible with the  $M_H$  range preferred by the fit of the SM to electroweak precision measurements (see Section 2.5). The particle discovery, thus, is not only a triumph of the interplay of LHC measurements and corresponding theoretical predictions, but also a spectacular success of electroweak precision physics—assuming the new particle is in fact the Higgs boson of the SM.

## 9 Conclusions and outlook

Almost 50 years after the postulate of an elementary scalar boson, which in the standard theory of electroweak interactions—the Glashow–Salam–Weinberg model—is the companion of the mechanism to describe the spontaneous breaking of the electroweak symmetry, a new neutral boson with a mass of 126 GeV has been discovered in the search for the SM Higgs boson at the LHC. So far all observed event yields in the different final states are consistent with the expectations for the SM Higgs boson, but also with predictions for a Higgs boson in several extended models. Assuming that the excess observed at Tevatron in the  $b\bar{b}$  final state is not due to a statistical fluctuation, but due to the production of the particle discovered at the LHC, the decay of the new particle into a pair of b-quarks and probably also into a pair of tau leptons should be observed at LHC in the near future.

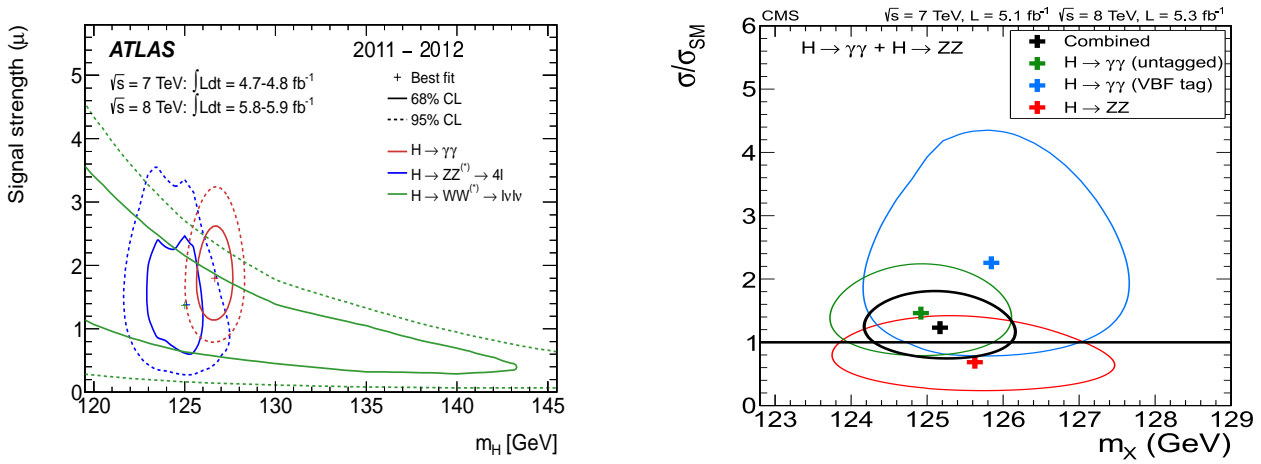


Figure 34: Best fit values for the signal strength  $\mu$  versus hypothetical Higgs-boson mass  $M_H$  in ATLAS [317] (left) and CMS [319] (right).

The allowed mass range for the Higgs boson could be confined unambiguously by the tremendous and challenging efforts in the searches at the colliders LEP, Tevatron, and LHC during the last decades: The combination of ALEPH, DELPHI, L3, and OPAL results exclude  $M_H = 0-114.4$  GeV, the preliminary combination of CDF and D0 results additionally exclude  $M_H = 147-180$  GeV (and  $M_H = 100-103$  GeV), and finally at least one of ATLAS and CMS excludes the SM Higgs boson in the ranges  $M_H = 110-122$  GeV and  $M_H = 127-600$  GeV. In significant parts of the excluded mass ranges a Higgs boson with reduced couplings with respect to the SM prediction is also excluded.

The role of the Higgs boson in the zoo of elementary particles is rather special. It is the only elementary spin-0 boson and shows a very distinctive interaction pattern with all other particles. The scalar nature of the new boson can be affirmed by excluding the alternative integer-spin hypotheses from the measurement of angular correlations in production and decay of the new boson. Assuming it is a spin-0 boson this will probably be possible with the data collected at LHC until the end of 2012. In order to verify the consistency with being a Higgs boson, the Lorentz structure of the interactions with all particles to which a coupling has been or will be observed, in particular to the massive gauge bosons, has to be determined. This includes the determination of its CP nature, which in the SM is predicted to be CP even. In models with extended Higgs sectors CP-odd states or states of mixed CP nature are often predicted.

The idea of the Higgs mechanism interprets particle masses as an interaction strength of each elementary massive particle to the vacuum expectation value of the Higgs field, whose particle excitation represents the Higgs boson. As a result, all massive elementary particles couple to the Higgs boson proportional to their masses. In a first approach, the coupling strengths can be determined from the measurement of the products of production cross section times branching ratio, which can be extracted from the observed event yields in the different final states. Later, more sophisticated coupling analyses based on effective field theories, quantifying non-standard effects in a model-independent way, may be carried out with higher precision. For a mass of 126 GeV, for which the SM predicts the total Higgs-boson width to be 4 MeV, the total width cannot be determined at the LHC with sufficient precision. As a consequence only ratios of couplings can be determined at the LHC in a completely model-independent way. However, with mild assumptions, e.g. that the couplings to massive weak gauge bosons are not larger than predicted by the SM (valid in many extended Higgs sectors), absolute coupling strengths can be measured as well. At a future  $e^+e^-$  collider absolute coupling values can be determined in a completely model-independent way and probably with a significantly better precision. Finally, a determination of the trilinear Higgs-boson self-coupling would be highly desirable in order to

at least partially reconstruct the Higgs potential. Owing to the low signal rates that are expected for Higgs-boson pair production this will be very challenging at the LHC, both in its run at a CM energy of 14 TeV and in its high-luminosity phase, but also future  $e^+e^-$  colliders will have to be pushed to their limits to this end.

Assuming the observed particle will be identified as a Higgs boson, the power to discriminate the SM Higgs boson from Higgs bosons in extended models depends on the achievable precision in the coupling determination. The possibly observed qualitative or quantitative differences between SM theory predictions and experiment in Higgs-boson observables could indicate the way, how the SM may have to be extended, and tell which models are clearly disfavoured or can be ruled out. In addition, the future research programme includes the search for additional Higgs bosons in non-standard scalar sectors, the search for other new particles, and the investigation of processes like weak-gauge-boson scattering that are most sensitive to the mechanism of electroweak symmetry breaking.

Any model for the unification of the fundamental strong and electroweak forces will predict new heavy particles, which in turn receive their mass most likely via spontaneous symmetry breaking. Accepting the Higgs mechanism as the correct modelling of electroweak symmetry breaking, it is, thus, reasonable to expect that new Higgs bosons arise in SM extensions. Conversely, precision measurements of *the* or more Higgs bosons serve as a window to non-standard theories or even grand unification. Supersymmetric theories are typical examples sharing this feature.

Apart from these general considerations, there are at least two known phenomena where our established theoretical world, which consists of the Standard Model of particle physics and general relativity, finds its limitations: The unknown constitution of *Dark Matter* and the enigmatical role and size of *Dark Energy* in the universe. Clarifying the nature and profile of the new particle is of utmost importance especially in the light of those conundrums, since extended Higgs models can accommodate Dark Matter candidates and Higgs fields could in fact play a key role in the inflationary phase of the cosmological expansion that is driven by Dark Energy.

Particle physics has reached a crossroad, and Higgs precision physics will probably contribute a lot to steer the field in future directions.

## References

- [1] S. L. Glashow, Nucl. Phys. **22** (1961) 579;  
S. Weinberg, Phys. Rev. Lett. **19** (1967) 1264;  
A. Salam, In the Proceedings of 8th Nobel Symposium, Lerum, Sweden, 19-25 May 1968, p. 367;  
S. L. Glashow, J. Iliopoulos, L. Maiani, Phys. Rev. D **2** (1970) 1285.
- [2] Y. Nambu, Phys. Rev. Lett. **4** (1960) 380;  
J. Goldstone, Nuovo Cim. **19** (1961) 154;  
J. Goldstone, A. Salam, S. Weinberg, Phys. Rev. **127** (1962) 965.
- [3] F. Englert, R. Brout, Phys. Rev. Lett. **13** (1964) 321.
- [4] P. W. Higgs, Phys. Lett. **12** (1964) 132 and Phys. Rev. Lett. **13** (1964) 508.
- [5] G. S. Guralnik, C. R. Hagen, T. W. B. Kibble, Phys. Rev. Lett. **13** (1964) 585.
- [6] D. J. Gross, F. Wilczek, Phys. Rev. Lett. **30** (1973) 1343 and Phys. Rev. D **8** (1973) 3633;  
H. D. Politzer, Phys. Rev. Lett. **30** (1973) 1346;  
H. Fritzsche, M. Gell-Mann, H. Leutwyler, Phys. Lett. B **47** (1973) 365;  
H. Fritzsche, M. Gell-Mann, eConf C **720906V2** (1972) 135 [hep-ph/0208010].
- [7] G. 't Hooft, M. J. G. Veltman, Nucl. Phys. B **50** (1972) 318.
- [8] B. W. Lee, J. Zinn-Justin, Phys. Rev. D **5** (1972) 3121, Phys. Rev. D **5** (1972) 3137 [Erratum-ibid. D **8** (1973) 4654] and Phys. Rev. D **7** (1973) 1049.

- [9] S. Weinberg, *The Quantum Theory of Fields – Vol. 2: Modern Applications*, Cambridge University Press, 1996.
- [10] M. Böhm, A. Denner, H. Joos, *Gauge Theories of the Strong and Electroweak Interaction*, B.G. Teubner Stuttgart/Leipzig/Wiesbaden, 2001.
- [11] G. Sterman, *An Introduction to Quantum Field Theory*, Cambridge University Press, 1993.
- [12] R.K. Ellis, W.J. Stirling, B.R. Webber, *QCD and Collider Physics*, Cambridge University Press, 1996.
- [13] J. Collins, *Foundations of Perturbative QCD*, Cambridge University Press, 2011.
- [14] D. A. Ross, M. J. G. Veltman, Nucl. Phys. B **95** (1975) 135.
- [15] [ALEPH, DELPHI, L3, OPAL and SLD Collaborations, LEP Electroweak Working Group and SLD Electroweak Group and SLD Heavy Flavour Group], Phys. Rept. **427** (2006) 257 [arXiv:hep-ex/0509008].
- [16] P. Sikivie, L. Susskind, M. B. Voloshin, V. I. Zakharov, Nucl. Phys. B **173** (1980) 189.
- [17] S. Dittmaier, M. Krämer, Phys. Rev. D **65** (2002) 073007 [hep-ph/0109062].
- [18] H. -L. Lai *et al.*, Phys. Rev. D **82** (2010) 074024 [arXiv:1007.2241 [hep-ph]].
- [19] A. D. Martin, W. J. Stirling, R. S. Thorne, G. Watt, Eur. Phys. J. C **63** (2009) 189 [arXiv:0901.0002 [hep-ph]].
- [20] R. D. Ball *et al.*, Nucl. Phys. B **849** (2011) 296 [arXiv:1101.1300 [hep-ph]].
- [21] S. Alekhin, J. Blümlein, S. Moch, Phys. Rev. D **86** (2012) 054009 [arXiv:1202.2281 [hep-ph]].
- [22] M. Glück, P. Jimenez-Delgado, E. Reya, C. Schuck, Phys. Lett. B **664** (2008) 133 [arXiv:0801.3618 [hep-ph]].
- [23] A. Cooper-Sarkar [for the H1 and ZEUS Collaboration], arXiv:1012.1438 [hep-ph].
- [24] M. Botje *et al.*, arXiv:1101.0538 [hep-ph];  
PDF4LHC steering committee, <http://www.hep.ucl.ac.uk/pdf4lh/>, 2010.
- [25] S. Dittmaier, G. Passarino, C. Mariotti, R. Tanaka *et al.* [LHC Higgs Cross Section Working Group], CERN-2011-002, arXiv:1101.0593 [hep-ph].
- [26] S. Dittmaier, G. Passarino, C. Mariotti, R. Tanaka *et al.* [LHC Higgs Cross Section Working Group], CERN-2012-002, arXiv:1201.3084 [hep-ph].
- [27] A. D. Martin, R. G. Roberts, W. J. Stirling, R. S. Thorne, Eur. Phys. J. C **39** (2005) 155 [hep-ph/0411040].
- [28] H. Spiesberger, Phys. Rev. D **52** (1995) 4936 [hep-ph/9412286];  
M. Roth, S. Weinzierl, Phys. Lett. B **590** (2004) 190 [hep-ph/0403200].
- [29] B. W. Lee, J. Zinn-Justin, Phys. Rev. D **5** (1972) 3155.
- [30] T. Appelquist, C. W. Bernard, Phys. Rev. D **22** (1980) 200;  
A. C. Longhitano, Nucl. Phys. B **188** (1981) 118.
- [31] J. M. Cornwall, D. N. Levin, G. Tiktopoulos, Phys. Rev. D **10** (1974) 1145 [Erratum-ibid. D **11** (1975) 972].
- [32] M. J. Herrero, E. Ruiz Morales, Nucl. Phys. B **418** (1994) 431 [hep-ph/9308276] and Nucl. Phys. B **437** (1995) 319 [hep-ph/9411207];  
D. Espriu, J. Matias, Phys. Lett. B **341** (1995) 332 [hep-ph/9407292];  
S. Dittmaier, C. Grosse-Knetter, Nucl. Phys. B **459** (1996) 497 [hep-ph/9505266];  
A. Nyffeler, A. Schenk, Phys. Rev. D **62** (2000) 113006 [hep-ph/9907294].
- [33] J. van der Bij, M. J. G. Veltman, Nucl. Phys. B **231** (1984) 205;  
R. Barbieri, P. Ciafaloni, A. Strumia, Phys. Lett. B **317** (1993) 381.

- [34] R. Boughezal, J. B. Tausk, J. J. van der Bij, Nucl. Phys. B **713** (2005) 278 [hep-ph/0410216].
- [35] C. E. Vayonakis, Lett. Nuovo Cim. **17** (1976) 383;  
M. S. Chanowitz, M. K. Gaillard, Nucl. Phys. B **261** (1985) 379;  
G. J. Gounaris, R. Kögerler, H. Neufeld, Phys. Rev. D **34** (1986) 3257.
- [36] Y. -P. Yao, C. P. Yuan, Phys. Rev. D **38** (1988) 2237;  
J. Bagger, C. Schmidt, Phys. Rev. D **41** (1990) 264;  
H. -J. He, Y. -P. Kuang, X. -y. Li, Phys. Rev. Lett. **69** (1992) 2619 and Phys. Rev. D **49** (1994) 4842;  
A. Denner, S. Dittmaier, Phys. Rev. D **54** (1996) 4499 [hep-ph/9603341].
- [37] C. Grosse-Knetter, Z. Phys. C **67** (1995) 261 [hep-ph/9405412].
- [38] B. W. Lee, C. Quigg, H. B. Thacker, Phys. Rev. D **16** (1977) 1519.
- [39] T. Hambye, K. Riesselmann, Phys. Rev. D **55** (1997) 7255 [hep-ph/9610272].
- [40] L. Maiani, G. Parisi, R. Petronzio, Nucl. Phys. B **136** (1978) 115;  
M. Lindner, Z. Phys. C **31** (1986) 295.
- [41] Z. Fodor, K. Holland, J. Kuti, D. Nogradi, C. Schroeder, PoS LAT **2007** (2007) 056 [arXiv:0710.3151 [hep-lat]];  
P. Gerhold, K. Jansen, JHEP **0907** (2009) 025 [arXiv:0902.4135 [hep-lat]].
- [42] S. R. Coleman, E. J. Weinberg, Phys. Rev. D **7** (1973) 1888.
- [43] M. Lindner, M. Sher, H. W. Zaglauer, Phys. Lett. B **228** (1989) 139;  
M. Sher, Phys. Rept. **179** (1989) 273;  
G. Altarelli, G. Isidori, Phys. Lett. B **337** (1994) 141;  
J. A. Casas, J. R. Espinosa, M. Quiros, Phys. Lett. B **342** (1995) 171 [hep-ph/9409458] and Phys. Lett. B **382** (1996) 374 [hep-ph/9603227].
- [44] J. Ellis *et al.*, Phys. Lett. B **679** (2009) 369 [arXiv:0906.0954 [hep-ph]].
- [45] The LEP Electroweak Working Group, <http://lepewwg.web.cern.ch/LEPEWWG/> .
- [46] M. Baak *et al.*, Eur. Phys. J. C **72** (2012) 2205 [arXiv:1209.2716 [hep-ph]].
- [47] A. B. Arbuzov *et al.*, Comput. Phys. Commun. **174** (2006) 728 [hep-ph/0507146].
- [48] G. Montagna, O. Nicrosini, F. Piccinini, G. Passarino, Comput. Phys. Commun. **117** (1999) 278 [hep-ph/9804211].
- [49] D. Bardin, G. Passarino, *The Standard Model in the Making: Precision Study of the Electroweak Interactions* Oxford University Press, 1999.
- [50] O. Eberhardt *et al.*, Phys. Rev. Lett. **109** (2012) 241802 [arXiv:1209.1101 [hep-ph]].
- [51] A. Djouadi, J. Kalinowski, M. Spira, Comput. Phys. Commun. **108** (1998) 56 [arXiv:hep-ph/9704448];  
A. Djouadi, J. Kalinowski, M. Mühlleitner, M. Spira, in *Proceedings of 6th Les Houches Workshop: Physics at TeV Colliders*, Les Houches, 2009, arXiv:1003.1643 [hep-ph].
- [52] A. Denner *et al.*, Eur. Phys. J. C **71** (2011) 1753 [arXiv:1107.5909 [hep-ph]].
- [53] N. Kauer, G. Passarino, JHEP **1208** (2012) 116 [arXiv:1206.4803 [hep-ph]].
- [54] G. Passarino, C. Sturm, S. Uccirati, Nucl. Phys. B **834** (2010) 77 [arXiv:1001.3360 [hep-ph]];  
S. Gorla, G. Passarino, D. Rosco, Nucl. Phys. B **864** (2012) 530 [arXiv:1112.5517 [hep-ph]].
- [55] C. Anastasiou, S. Buehler, F. Herzog, A. Lazopoulos, JHEP **1204** (2012) 004 [arXiv:1202.3638 [hep-ph]].
- [56] L. Resnick, M. K. Sundaresan, P. J. S. Watson, Phys. Rev. D **8** (1973) 172.
- [57] J. R. Ellis, M. K. Gaillard, D. V. Nanopoulos, Nucl. Phys. B **106** (1976) 292.

- [58] E. Braaten, J. P. Leveille, Phys. Rev. D **22** (1980) 715;  
 N. Sakai, Phys. Rev. D **22** (1980) 2220;  
 T. Inami, T. Kubota, Nucl. Phys. B **179** (1981) 171;  
 M. Drees, K. -i. Hikasa, Phys. Lett. B **240** (1990) 455 [Erratum-ibid. B **262** (1991) 497].
- [59] M. Drees, K. -i. Hikasa, Phys. Rev. D **41** (1990) 1547.
- [60] S. G. Gorishnii, A. L. Kataev, S. A. Larin, Sov. J. Nucl. Phys. **40** (1984) 329 [Yad. Fiz. **40** (1984) 517];  
 S. G. Gorishnii, A. L. Kataev, S. A. Larin, L. R. Surguladze, Mod. Phys. Lett. A **5** (1990) 2703 and Phys. Rev. D **43** (1991) 1633;  
 L. R. Surguladze, Phys. Lett. B **341** (1994) 60 [hep-ph/9405325];  
 A. L. Kataev, V. T. Kim, Mod. Phys. Lett. A **9** (1994) 1309. K. G. Chetyrkin, A. Kwiatkowski, Nucl. Phys. B **461** (1996) 3 [hep-ph/9505358];  
 S. A. Larin, T. van Ritbergen, J. A. M. Vermaseren, Phys. Lett. B **362** (1995) 134 [hep-ph/9506465];  
 K. G. Chetyrkin, Phys. Lett. B **390** (1997) 309 [hep-ph/9608318];  
 K. G. Chetyrkin, M. Steinhauser, Phys. Lett. B **408** (1997) 320 [hep-ph/9706462];  
 P. A. Baikov, K. G. Chetyrkin, J. H. Kühn, Phys. Rev. Lett. **96** (2006) 012003 [hep-ph/0511063].
- [61] C. Anastasiou, F. Herzog, A. Lazopoulos, JHEP **1203** (2012) 035 [arXiv:1110.2368 [hep-ph]].
- [62] A. Djouadi, P. Gambino, Phys. Rev. D **51** (1995) 218 [Erratum-ibid. D **53** (1996) 4111] [hep-ph/9406431].
- [63] K. Melnikov, Phys. Rev. D **53** (1996) 5020 [hep-ph/9511310];  
 R. Harlander, M. Steinhauser, Phys. Rev. D **56** (1997) 3980 [hep-ph/9704436].
- [64] W. Bernreuther, A. Brandenburg, M. Flesch, Phys. Rev. D **56** (1997) 90 [hep-ph/9701347].
- [65] J. Fleischer, F. Jegerlehner, Phys. Rev. D **23** (1981) 2001.
- [66] B. A. Kniehl, Nucl. Phys. B **376** (1992) 3;  
 D. Y. Bardin, B. M. Vilensky, P. K. Khristova, Sov. J. Nucl. Phys. **53** (1991) 152 [Yad. Fiz. **53** (1991) 240];  
 A. Dabelstein, W. Hollik, Z. Phys. C **53** (1992) 507.
- [67] B. A. Kniehl, Phys. Rev. D **50** (1994) 3314 [hep-ph/9405299];  
 A. Kwiatkowski, M. Steinhauser, Phys. Lett. B **338** (1994) 66 [Erratum-ibid. B **342** (1995) 455] [hep-ph/9405308];  
 A. Djouadi, P. Gambino, Phys. Rev. D **51** (1995) 218 [Erratum-ibid. D **53** (1996) 4111] [hep-ph/9406431];  
 B. A. Kniehl, M. Spira, Nucl. Phys. B **432** (1994) 39 [hep-ph/9410319]. B. A. Kniehl, M. Steinhauser, Phys. Lett. B **365** (1996) 297 [hep-ph/9507382] and , Nucl. Phys. B **454** (1995) 485 [hep-ph/9508241].
- [68] A. Ghinculov, Phys. Lett. B **337** (1994) 137 [Erratum-ibid. B **346** (1995) 426] [hep-ph/9405394];  
 L. Durand, B. A. Kniehl, K. Riesselmann, Phys. Rev. D **51** (1995) 5007 [hep-ph/9412311].
- [69] A. Djouadi, Phys. Rept. **457** (2008) 1 [arXiv:hep-ph/0503172].
- [70] T. G. Rizzo, Phys. Rev. D **22** (1980) 178 [Addendum-ibid. D **22** (1980) 1824].
- [71] T. Inami, T. Kubota, Y. Okada, Z. Phys. C **18** (1983) 69;  
 A. Djouadi, M. Spira, P. M. Zerwas, Phys. Lett. B **264** (1991) 440.
- [72] M. Spira, A. Djouadi, D. Graudenz, P. M. Zerwas, Nucl. Phys. B **453** (1995) 17 [hep-ph/9504378].
- [73] K. G. Chetyrkin, B. A. Kniehl, M. Steinhauser, Phys. Rev. Lett. **79** (1997) 353 [hep-ph/9705240] and Nucl. Phys. B **510** (1998) 61 [hep-ph/9708255];  
 M. Schreck, M. Steinhauser, Phys. Lett. B **655** (2007) 148 [arXiv:0708.0916 [hep-ph]].

- [74] S. Actis, G. Passarino, C. Sturm, S. Uccirati, Phys. Lett. B **669** (2008) 62 [arXiv:0809.1302 [hep-ph]].
- [75] S. Actis, G. Passarino, C. Sturm, S. Uccirati, Nucl. Phys. B **811** (2009) 182 [arXiv:0809.3667 [hep-ph]].
- [76] M. Steinhauser, Phys. Rev. D **59** (1999) 054005 [hep-ph/9809507].
- [77] M. A. Shifman, A. I. Vainshtein, M. B. Voloshin, V. I. Zakharov, Sov. J. Nucl. Phys. **30** (1979) 711 [Yad. Fiz. **30** (1979) 1368].
- [78] H.-Q. Zheng, D.-D. Wu, Phys. Rev. D **42** (1990) 3760;  
A. Djouadi, M. Spira, J. J. van der Bij, P. M. Zerwas, Phys. Lett. B **257** (1991) 187;  
S. Dawson, R. P. Kauffman, Phys. Rev. D **47** (1993) 1264.
- [79] K. Melnikov, O. I. Yakovlev, Phys. Lett. B **312** (1993) 179 [hep-ph/9302281];  
M. Inoue, R. Najima, T. Oka, J. Saito, Mod. Phys. Lett. A **9** (1994) 1189;  
J. Fleischer, O. V. Tarasov, V. O. Tarasov, Phys. Lett. B **584** (2004) 294 [hep-ph/0401090].
- [80] K. Melnikov, M. Spira, O. I. Yakovlev, Z. Phys. C **64** (1994) 401 [hep-ph/9405301].
- [81] U. Aglietti, R. Bonciani, G. Degrassi, A. Vicini, Phys. Lett. B **595** (2004) 432 [hep-ph/0404071].
- [82] M. Steinhauser, hep-ph/9612395.
- [83] M. Spira, A. Djouadi, P. M. Zerwas, Phys. Lett. B **276** (1992) 350.
- [84] C. A. Nelson, Phys. Rev. D **37** (1988) 1220;  
A. Soni, R. M. Xu, Phys. Rev. D **48** (1993) 5259 [hep-ph/9301225];  
D. Chang, W. Y. Keung, I. Phillips, Phys. Rev. D **48** (1993) 3225 [hep-ph/9303226];  
A. Skjold, P. Osland, Phys. Lett. B **311** (1993) 261 [hep-ph/9303294];  
V.D. Barger *et al.*, Phys. Rev. D **49** (1994) 79 [hep-ph/9306270];  
T. Arens, L. M. Sehgal, Z. Phys. C **66** (1995) 89 [hep-ph/9409396];  
C. P. Buszello, I. Fleck, P. Marquard, J. J. van der Bij, Eur. Phys. J. C **32** (2004) 209 [hep-ph/0212396];  
S. Y. Choi, D. J. Miller, M. M. Mühlleitner, P. M. Zerwas, Phys. Lett. B **553** (2003) 61 [hep-ph/0210077].
- [85] B.A. Kniehl, Nucl. Phys. B **352** (1991) 1 and Nucl. Phys. B **357** (1991) 439;  
D.Y. Bardin, P.K. Khristova, B.M. Vilensky, Sov. J. Nucl. Phys. **54** (1991) 833 [Yad. Fiz. **54** (1991) 1366].
- [86] A. Bredenstein, A. Denner, S. Dittmaier, M. M. Weber, Phys. Rev. D **74** (2006) 013004 [arXiv:hep-ph/0604011] and JHEP **0702** (2007) 080 [arXiv:hep-ph/0611234].
- [87] A. Ghinculov, Nucl. Phys. B **455** (1995) 21 [hep-ph/9507240];  
A. Frink, B.A. Kniehl, D. Kreimer, K. Riesselmann, Phys. Rev. D **54** (1996) 4548 [hep-ph/9606310].
- [88] A. Denner, S. Dittmaier, M. Roth, D. Wackerroth, Nucl. Phys. B **560** (1999) 33 [arXiv:hep-ph/9904472];  
A. Denner, S. Dittmaier, M. Roth, L. H. Wieders, Nucl. Phys. B **724** (2005) 247 [arXiv:hep-ph/0505042].
- [89] M. Spira, Fortsch. Phys. **46** (1998) 203 [arXiv:hep-ph/9705337].
- [90] J. Baglio, A. Djouadi, JHEP **1103** (2011) 055 [arXiv:1012.0530 [hep-ph]].
- [91] T. Sjöstrand, S. Mrenna, P. Z. Skands, JHEP **0605** (2006) 026 [hep-ph/0603175].
- [92] T. Sjöstrand, S. Mrenna, P. Z. Skands, Comput. Phys. Commun. **178** (2008) 852 [arXiv:0710.3820 [hep-ph]].
- [93] F. Abe *et al.* [CDF Collaboration], Phys. Rev. D **41** (1990) 1717.
- [94] G. P. Yost *et al.* [Particle Data Group Collaboration], Phys. Lett. B **204** (1988) 1.



- [95] A. S. Schwarz, *Phys. Scripta* **33** (1986) 5.
- [96] J. F. Gunion, H. E. Haber, G. L. Kane, S. Dawson, *Front. Phys.* **80** (2000) 1.
- [97] R. N. Cahn, *Nucl. Phys. Proc. Suppl.* **13** (1990) 155.
- [98] E. Gross, P. Yepes, *Int. J. Mod. Phys. A* **8** (1993) 407.
- [99] M. M. Kado, C. G. Tully, *Ann. Rev. Nucl. Part. Sci.* **52** (2002) 65.
- [100] C. Cowan. “Statistics” in J. Beringer *et al.* [Particle Data Group Collaboration], *Phys. Rev. D* **86** (2012) 010001.
- [101] G. Cowan, “Statistical Data analysis”, Oxford University Press (1997). [113]
- [102] O. Helene, *Nucl. Instrum. Meth.* **212** (1983) 319.
- [103] G. Zech, *Nucl. Instrum. Meth. A* **277** (1989) 608.
- [104] V. F. Obraztsov, *Nucl. Instrum. Meth. A* **4316** (1992) 388;  
A. Favara, M. Pieri, hep-ex/9706016;  
P. Bock, *JHEP* **0701** (2007) 080, [hep-ex/0405072].
- [105] J. Neyman and E. S. Pearson, *Phil. Trans. R. Soc. Lond. A* **231** (1933), 289.
- [106] A. L. Read, *J. Phys. G G* **28** (2002) 2693.
- [107] T. Junk, *Nucl. Instrum. Meth. A* **434** (1999) 435, [hep-ex/9902006].
- [108] R. D. Cousins, V. L. Highland, *Nucl. Instrum. Meth. A* **320** (1992) 331.
- [109] G. Cowan, K. Cranmer, E. Gross, O. Vitells, *Eur. Phys. J. C* **71** (2011) 1554, [arXiv:1007.1727 [physics.data-an]].
- [110] S. S. Wilks, *Ann. Math. Statist.* **9** (1938) 60.
- [111] A. Wald, *Transactions of the American Mathematical Society*, Vol. 54, No. 3 (1943), 426.
- [112] E. Gross, O. Vitells, *Eur. Phys. J. C* **70** (2010) 525 [arXiv:1005.1891 [physics.data-an]].
- [113] O. J. Dunn, *J. Am. Statist. Assoc.* **56** (1961) 52.
- [114] ATLAS Collaboration, CMS Collaboration and the LHC Higgs Combination Group, “Procedure for the LHC Higgs boson search combination in Summer 2011”, ATL-PHYS-PUB-2011-11, CMS NOTE-2011/005.
- [115] M. S. Carena *et al.*, in *Physics at LEP2*, eds. G. Altarelli, T. Sjöstrand and F. Zwirner (CERN 96-01, Geneva, 1996), Vol. 1, p. 351, [hep-ph/9602250].
- [116] W. Kilian, M. Krämer, P. M. Zerwas, *Phys. Lett. B* **373** (1996) 135 [hep-ph/9512355].
- [117] F. Boudjema *et al.*, eConf C **050318** (2005) 0601 [hep-ph/0510184].
- [118] W. Bernreuther *et al.*, in *Z Physics at LEP1*, eds. G. Altarelli, R. Kleiss, C. Verzegnassi (CERN 89-08, Geneva, 1989), Vol. 2, p. 1.
- [119] E. Accomando *et al.* [ECFA/DESY LC Physics Working Group Collaboration], *Phys. Rept.* **299** (1998) 1 [hep-ph/9705442];  
J. A. Aguilar-Saavedra *et al.* [ECFA/DESY LC Physics Working Group Collaboration], hep-ph/0106315;  
T. Abe *et al.* [American Linear Collider Working Group Collaboration], hep-ex/0106056;  
G. Aarons *et al.* [ILC Collaboration], arXiv:0709.1893 [hep-ph].
- [120] W. Beenakker *et al.*, in *Physics at LEP2* (Report CERN 96-01, Geneva, 1996), eds. A. Altarelli, T. Sjöstrand, F. Zwirner, Vol. 1, p.3, hep-ph/9602351.
- [121] R. N. Cahn, M. S. Chanowitz, N. Fleishon, *Phys. Lett. B* **82** (1979) 113;  
L. Bergstrom, G. Hulth, *Nucl. Phys. B* **259** (1985) 137 [Erratum-ibid. B **276** (1986) 744];  
A. Barroso, J. Pulido, J. C. Romao, *Nucl. Phys. B* **267** (1986) 509.

- [122] A. Abbasabadi, D. Bowser-Chao, D. A. Dicus, W. W. Repko, Phys. Rev. D **52** (1995) 3919 [hep-ph/9507463];  
A. Djouadi, V. Driesen, W. Hollik, J. Rosiek, Nucl. Phys. B **491** (1997) 68 [hep-ph/9609420].
- [123] D. R. T. Jones, S. T. Petcov, Phys. Lett. B **84** (1979) 440.
- [124] J. Fleischer, F. Jegerlehner, Nucl. Phys. B **216** (1983) 469;  
B. A. Kniehl, Z. Phys. C **55** (1992) 605;  
A. Denner, J. Küblbeck, R. Mertig, M. Böhm, Z. Phys. C **56** (1992) 261.
- [125] F. Jegerlehner, K. Kolodziej, T. Westwanski, Eur. Phys. J. C **44** (2005) 195 [hep-ph/0503169].
- [126] S. Dawson, J. L. Rosner, Phys. Lett. B **148** (1984) 497.
- [127] K. -i. Hikasa, Phys. Lett. B **164** (1985) 385 [Erratum-ibid. **195B** (1987) 623].
- [128] D. A. Dicus, S. S. D. Willenbrock, Phys. Rev. D **32** (1985) 1642.
- [129] G. Altarelli, B. Mele, F. Pitolli, Nucl. Phys. B **287** (1987) 205.
- [130] G. Belanger *et al.*, Phys. Lett. B **559** (2003) 252 [hep-ph/0212261].
- [131] A. Denner, S. Dittmaier, M. Roth, M. M. Weber, Phys. Lett. B **560** (2003) 196 [hep-ph/0301189]  
and Nucl. Phys. B **660** (2003) 289 [hep-ph/0302198].
- [132] F. Boudjema *et al.*, Phys. Lett. B **600** (2004) 65 [hep-ph/0407065].
- [133] A. Djouadi, J. Kalinowski, P. M. Zerwas, Z. Phys. C **54** (1992) 255.
- [134] J. F. Gunion, B. Grzadkowski, X. -G. He, Phys. Rev. Lett. **77** (1996) 5172 [hep-ph/9605326].
- [135] H. Baer, S. Dawson, L. Reina, Phys. Rev. D **61** (2000) 013002 [hep-ph/9906419];  
A. Juste, G. Merino, hep-ph/9910301.
- [136] M. Battaglia, K. Desch, AIP Conf. Proc. **578** (2001) 163 [hep-ph/0101165].
- [137] S. Dittmaier *et al.*, Phys. Lett. B **441** (1998) 383 [hep-ph/9808433];  
S. Dawson, L. Reina, Phys. Rev. D **59** (1999) 054012 [arXiv:hep-ph/9808443].
- [138] Y. You *et al.*, Phys. Lett. B **571** (2003) 85 [hep-ph/0306036];  
G. Belanger *et al.*, Phys. Lett. B **571** (2003) 163 [hep-ph/0307029];  
A. Denner, S. Dittmaier, M. Roth, M. M. Weber, Phys. Lett. B **575** (2003) 290 [hep-ph/0307193]  
and Nucl. Phys. B **680** (2004) 85 [hep-ph/0309274].
- [139] C. Farrell, A. H. Hoang, Phys. Rev. D **72** (2005) 014007 [hep-ph/0504220] and Phys. Rev. D **74**  
(2006) 014008 [hep-ph/0604166].
- [140] S. Moretti, Phys. Lett. B **452** (1999) 338 [hep-ph/9902214];  
C. Schwinn, hep-ph/0412028;  
K. Kolodziej, S. Szczypinski, Nucl. Phys. B **801** (2008) 153 [arXiv:0803.0887 [hep-ph]] and Eur.  
Phys. J. C **64** (2009) 645 [arXiv:0903.4606 [hep-ph]].
- [141] G. J. Gounaris, D. Schildknecht, F. M. Renard, Phys. Lett. B **83** (1979) 191.
- [142] F. Boudjema, E. Chopin, Z. Phys. C **73** (1996) 85 [hep-ph/9507396];  
V. A. Ilyin *et al.*, Phys. Rev. D **54** (1996) 6717 [hep-ph/9506326];  
A. Djouadi, W. Kilian, M. Mühlleitner, P. M. Zerwas, Eur. Phys. J. C **10** (1999) 27 [hep-ph/9903229];  
D. J. Miller, S. Moretti, Eur. Phys. J. C **13** (2000) 459 [hep-ph/9906395];  
U. Baur, Phys. Rev. D **80** (2009) 013012 [arXiv:0906.0028 [hep-ph]].
- [143] G. Belanger *et al.*, Phys. Lett. B **576** (2003) 152 [hep-ph/0309010];  
R. -Y. Zhang *et al.*, Phys. Lett. B **578** (2004) 349 [hep-ph/0308203].
- [144] M. Davier, H. Nguyen Ngoc, Phys. Lett. B **229** (1989) 150.
- [145] G. Altarelli, R. Kleiss, C. Verzegnassi, (Eds.), CERN-89-08-V-2.

- [146] D. Decamp *et al.* [ALEPH Collaboration], Phys. Lett. B **236** (1990) 233.
- [147] P. Abreu *et al.* [DELPHI Collaboration], Nucl. Phys. B **342** (1990) 1.
- [148] B. Adeva *et al.* [L3 Collaboration], Phys. Lett. B **248** (1990) 203.
- [149] P. D. Acton *et al.* [OPAL Collaboration], Phys. Lett. B **268** (1991) 122.
- [150] D. Decamp *et al.* [ALEPH Collaboration], Phys. Lett. B **246** (1990) 306.
- [151] P. Abreu *et al.* [DELPHI Collaboration], Z. Phys. C **51** (1991) 25.
- [152] B. Adeva *et al.* [L3 Collaboration], Phys. Lett. B **252** (1990) 518.
- [153] M. Z. Akrawy *et al.* [OPAL Collaboration], Z. Phys. C **49** (1991) 1.
- [154] P. Abreu *et al.* [DELPHI Collaboration], Nucl. Phys. B **373** (1992) 3.
- [155] B. Adeva *et al.* [L3 Collaboration], Phys. Lett. B **283** (1992) 454.
- [156] M. Z. Akrawy *et al.* [OPAL Collaboration], Phys. Lett. B **253** (1991) 511.
- [157] D. Buskulic *et al.* [ALEPH Collaboration], Phys. Lett. B **384** (1996) 427.
- [158] P. Abreu *et al.* [DELPHI Collaboration], Nucl. Phys. B **421** (1994) 3.
- [159] M. Acciarri *et al.* [L3 Collaboration], Phys. Lett. B **385** (1996) 454.
- [160] G. Alexander *et al.* [OPAL Collaboration], Z. Phys. C **73** (1997) 189.
- [161] D. Decamp *et al.* [ALEPH Collaboration], Phys. Lett. B **241** (1990) 141.
- [162] D. Decamp *et al.* [ALEPH Collaboration], Phys. Lett. B **245** (1990) 289.
- [163] D. Decamp *et al.* [ALEPH Collaboration], Phys. Rept. **216** (1992) 253.
- [164] D. Buskulic *et al.* [ALEPH Collaboration], Phys. Lett. B **313** (1993) 299.
- [165] B. Adeva *et al.* [L3 Collaboration], Phys. Lett. B **257** (1991) 450.
- [166] O. Adriani *et al.* [L3 Collaboration], Phys. Lett. B **303** (1993) 391.
- [167] M. Z. Akrawy *et al.* [OPAL Collaboration], Phys. Lett. B **236** (1990) 224.
- [168] M. Z. Akrawy *et al.* [OPAL Collaboration], Phys. Lett. B **251** (1990) 211.
- [169] R. Akers *et al.* [OPAL Collaboration], Phys. Lett. B **327** (1994) 397.
- [170] J. F. Grivaz, F. Le Diberder, Nucl. Instrum. Meth. A **333** (1993) 320;
- [171] R. Barate *et al.* [ALEPH Collaboration], Phys. Lett. B **412** (1997) 155.
- [172] R. Barate *et al.* [ALEPH Collaboration], Phys. Lett. B **495** (2000) 1 [hep-ex/0011045].
- [173] P. Janot “HZHA”, in *Physics at LEP2*, eds. G. Altarelli, T. Sjöstrand and F. Zwirner (CERN 96-01, Geneva, 1996), Vol. 2, p. 299, [hep-ph/9602203].
- [174] K. Ackerstaff *et al.* [OPAL Collaboration], Phys. Lett. B **393** (1997) 231.
- [175] P. Abreu *et al.* [DELPHI Collaboration], Eur. Phys. J. C **2** (1998) 1.
- [176] M. Acciarri *et al.* [L3 Collaboration], Phys. Lett. B **411** (1997) 373.
- [177] K. Ackerstaff *et al.* [OPAL Collaboration], Eur. Phys. J. C **1** (1998) 425 [hep-ex/9709003].
- [178] R. Barate *et al.* [ALEPH Collaboration], Phys. Lett. B **440** (1998) 403 [Phys. Lett. B **447** (1999) 336] [hep-ex/9811032].
- [179] P. Abreu *et al.* [DELPHI Collaboration], Eur. Phys. J. C **10** (1999) 563.
- [180] M. Acciarri *et al.* [L3 Collaboration], Phys. Lett. B **431** (1998) 437.
- [181] G. Abbiendi *et al.* [OPAL Collaboration], Eur. Phys. J. C **7** (1999) 407 [hep-ex/9811025].
- [182] R. Barate *et al.* [ALEPH Collaboration], Eur. Phys. J. C **17** (2000) 223.
- [183] P. Abreu *et al.* [DELPHI Collaboration], Eur. Phys. J. C **17** (2000) 187 [Addendum-ibid. C **17** (2000) 549] [hep-ex/0104020].

- [184] M. Acciarri *et al.* [L3 Collaboration], Phys. Lett. B **461** (1999) 376 [hep-ex/9909004].
- [185] G. Abbiendi *et al.* [OPAL Collaboration], Eur. Phys. J. C **12** (2000) 567 [hep-ex/9908002].
- [186] R. Barate *et al.* [ALEPH Collaboration], Phys. Lett. B **499** (2001) 53 [hep-ex/0010062].
- [187] J. Abdallah *et al.* [DELPHI Collaboration], Eur. Phys. J. C **23** (2002) 409 [hep-ex/0201022].
- [188] M. Acciarri *et al.* [L3 Collaboration], Phys. Lett. B **508** (2001) 225 [hep-ex/0012019].
- [189] P. Abreu *et al.* [DELPHI Collaboration], Phys. Lett. B **499** (2001) 23 [hep-ex/0102036].
- [190] G. Abbiendi *et al.* [OPAL Collaboration], Phys. Lett. B **499** (2001) 38 [hep-ex/0101014].
- [191] A. Heister *et al.* [ALEPH Collaboration], Phys. Lett. B **526** (2002) 191 [hep-ex/0201014].
- [192] J. Abdallah *et al.* [DELPHI Collaboration], Eur. Phys. J. C **32** (2004) 145 [hep-ex/0303013].
- [193] P. Achard *et al.* [L3 Collaboration], Phys. Lett. B **517** (2001) 319 [hep-ex/0107054].
- [194] G. Abbiendi *et al.* [OPAL Collaboration], Eur. Phys. J. C **26** (2003) 479 [hep-ex/0209078].
- [195] S. Jin, Peter McNamara, Nucl. Instrum. Meth. A **462** (2001) 561.
- [196] M. Acciarri *et al.* [L3 Collaboration], Phys. Lett. B **495** (2000) 18 [hep-ex/0011043].
- [197] R. Barate *et al.* [ALEPH and DELPHI and L3 and OPAL Collaborations and LEP Working Group for Higgs boson searches], Phys. Lett. B **565** (2003) 61 [hep-ex/0306033].
- [198] U. Aglietti *et al.*, hep-ph/0612172.
- [199] J. Baglio, A. Djouadi, JHEP **1010** (2010) 064 [arXiv:1003.4266 [hep-ph], arXiv:1009.1363 [hep-ph]];  
 J. Baglio, A. Djouadi, S. Ferrag, R. M. Godbole, Phys. Lett. B **699** (2011) 368 [Erratum-ibid. B **702** (2011) 105] [arXiv:1101.1832 [hep-ph]];  
 J. Baglio, A. Djouadi, R. Godbole, arXiv:1107.0281 [hep-ph].
- [200] J. M. Butterworth, A. R. Davison, M. Rubin, G. P. Salam, Phys. Rev. Lett. **100** (2008) 242001. [arXiv:0802.2470 [hep-ph]];  
 J. M. Butterworth *et al.*, ATL-PHYS-PUB-2009-088.
- [201] T. Plehn, G. P. Salam, M. Spannowsky, Phys. Rev. Lett. **104** (2010) 111801 [arXiv:0910.5472 [hep-ph]].
- [202] H. M. Georgi, S. L. Glashow, M. E. Machacek, D. V. Nanopoulos, Phys. Rev. Lett. **40** (1978) 692.
- [203] D. Graudenz, M. Spira, P. M. Zerwas, Phys. Rev. Lett. **70** (1993) 1372.
- [204] R. V. Harlander, Phys. Lett. B **492** (2000) 74 [hep-ph/0007289];  
 S. Catani, D. de Florian, M. Grazzini, JHEP **0105** (2001) 025 [hep-ph/0102227];  
 R. V. Harlander, W. B. Kilgore, Phys. Rev. D **64** (2001) 013015 [hep-ph/0102241] and Phys. Rev. Lett. **88** (2002) 201801 [hep-ph/0201206];  
 C. Anastasiou, K. Melnikov, Nucl. Phys. B **646** (2002) 220 [hep-ph/0207004];  
 V. Ravindran, J. Smith, W. L. van Neerven, Nucl. Phys. B **665** (2003) 325 [hep-ph/0302135];  
 J. Blümlein, V. Ravindran, Nucl. Phys. B **716** (2005) 128 [hep-ph/0501178].
- [205] S. Marzani *et al.*, Nucl. Phys. B **800** (2008) 127 [arXiv:0801.2544 [hep-ph]];  
 R. V. Harlander, K. J. Ozeren, Phys. Lett. B **679** (2009) 467 [arXiv:0907.2997 [hep-ph]] and JHEP **0911** (2009) 088 [arXiv:0909.3420 [hep-ph]];  
 R. V. Harlander, H. Mantler, S. Marzani, K. J. Ozeren, Eur. Phys. J. C **66** (2010) 359 [arXiv:0912.2104 [hep-ph]];  
 A. Pak, M. Rogal, M. Steinhauser, Phys. Lett. B **679** (2009) 473 [arXiv:0907.2998 [hep-ph]] and JHEP **1002** (2010) 025 [arXiv:0911.4662 [hep-ph]].

- [206] S. Catani, D. de Florian, M. Grazzini, P. Nason, JHEP **0307** (2003) 028 [hep-ph/0306211];  
S. Moch, A. Vogt, Phys. Lett. B **631** (2005) 48 [hep-ph/0508265];  
E. Laenen, L. Magnea, Phys. Lett. B **632** (2006) 270 [hep-ph/0508284];  
A. Idilbi, X. -d. Ji, J. -P. Ma, F. Yuan, Phys. Rev. D **73** (2006) 077501 [hep-ph/0509294];  
V. Ravindran, Nucl. Phys. B **746** (2006) 58 [hep-ph/0512249].
- [207] V. Ahrens, T. Becher, M. Neubert, L. L. Yang, Phys. Rev. D **79** (2009) 033013 [arXiv:0808.3008 [hep-ph]], Eur. Phys. J. C **62** (2009) 333 [arXiv:0809.4283 [hep-ph]] and Phys. Lett. B **698** (2011) 271 [arXiv:1008.3162 [hep-ph]].
- [208] G. Degrossi, F. Maltoni, Phys. Lett. B **600** (2004) 255 [hep-ph/0407249].
- [209] S. Actis, G. Passarino, C. Sturm, S. Uccirati, Phys. Lett. B **670** (2008) 12 [arXiv:0809.1301 [hep-ph]].
- [210] C. Anastasiou, R. Boughezal, F. Petriello, JHEP **0904** (2009) 003 [arXiv:0811.3458 [hep-ph]].
- [211] W. -Y. Keung, F. J. Petriello, Phys. Rev. D **80** (2009) 013007 [arXiv:0905.2775 [hep-ph]];  
O. Brein, Phys. Rev. D **81** (2010) 093006 [arXiv:1003.4438 [hep-ph]].
- [212] E. Accomando, Phys. Lett. B **661** (2008) 129 [arXiv:0709.1364 [hep-ph]];  
T. Binoth, M. Ciccolini, N. Kauer, M. Krämer, JHEP **0612** (2006) 046 [hep-ph/0611170];  
J. M. Campbell, R. K. Ellis, C. Williams, JHEP **1110** (2011) 005 [arXiv:1107.5569 [hep-ph]];  
G. Passarino, JHEP **1208** (2012) 146 [arXiv:1206.3824 [hep-ph]].
- [213] D. de Florian, M. Grazzini, Phys. Lett. B **674** (2009) 291 [arXiv:0901.2427 [hep-ph]].
- [214] D. de Florian, M. Grazzini, Z. Kunszt, Phys. Rev. Lett. **82** (1999) 5209 [hep-ph/9902483];  
V. Ravindran, J. Smith, W. L. Van Neerven, Nucl. Phys. B **634** (2002) 247 [hep-ph/0201114];  
C. J. Glosser, C. R. Schmidt, JHEP **0212** (2002) 016 [hep-ph/0209248].
- [215] G. Bozzi, S. Catani, D. de Florian, M. Grazzini, Nucl. Phys. B **737** (2006) 73 [hep-ph/0508068].  
Q. -H. Cao, C. -R. Chen, C. Schmidt, C. -P. Yuan, arXiv:0909.2305 [hep-ph].
- [216] D. de Florian, G. Ferrera, M. Grazzini, D. Tommasini, JHEP **1111** (2011) 064 [arXiv:1109.2109 [hep-ph]].
- [217] C. F. Berger *et al.*, JHEP **1104** (2011) 092 [arXiv:1012.4480 [hep-ph]];  
I. W. Stewart, F. J. Tackmann, Phys. Rev. D **85** (2012) 034011 [arXiv:1107.2117 [hep-ph]];  
T. Becher, M. Neubert, JHEP **1207** (2012) 108 [arXiv:1205.3806 [hep-ph]];  
X. Liu, F. Petriello, arXiv:1210.1906 [hep-ph].
- [218] C. Anastasiou, K. Melnikov, F. Petriello, Phys. Rev. Lett. **93** (2004) 262002 [hep-ph/0409088]  
and Nucl. Phys. B **724** (2005) 197 [hep-ph/0501130];  
C. Anastasiou, G. Dissertori, F. Stöckli, JHEP **0709** (2007) 018 [arXiv:0707.2373 [hep-ph]].
- [219] S. Catani, M. Grazzini, Phys. Rev. Lett. **98** (2007) 222002 [hep-ph/0703012];  
M. Grazzini, JHEP **0802** (2008) 043 [arXiv:0801.3232 [hep-ph]].
- [220] C. Anastasiou, S. Buehler, F. Herzog, A. Lazopoulos, JHEP **1112** (2011) 058 [arXiv:1107.0683 [hep-ph]].
- [221] D. de Florian, G. Ferrera, M. Grazzini, D. Tommasini, JHEP **1206** (2012) 132 [arXiv:1203.6321 [hep-ph]].
- [222] J. Campbell, K. Ellis, MCFM, <http://mcfm.fnal.gov>, 2010.
- [223] C. F. Berger, V. Del Duca, L. J. Dixon, Phys. Rev. D **74** (2006) 094021 [Erratum-ibid. D **76** (2007) 099901] [hep-ph/0608180];  
S. D. Badger, E. W. N. Glover, K. Risager, JHEP **0707** (2007) 066 [arXiv:0704.3914 [hep-ph]];  
E. W. N. Glover, P. Mastrolia, C. Williams, JHEP **0808** (2008) 017 [arXiv:0804.4149 [hep-ph]];  
S. Badger, E. W. N. Glover, P. Mastrolia, C. Williams, JHEP **1001** (2010) 036 [arXiv:0909.4475 [hep-ph]].

- L. J. Dixon, Y. Sofianatos, JHEP **0908** (2009) 058 [arXiv:0906.0008 [hep-ph]];  
 S. Badger, J. M. Campbell, R. K. Ellis, C. Williams, JHEP **0912** (2009) 035 [arXiv:0910.4481 [hep-ph]].
- [224] J. M. Campbell, R. K. Ellis, G. Zanderighi, JHEP **0610** (2006) 028 [hep-ph/0608194];  
 J. M. Campbell, R. K. Ellis, C. Williams, Phys. Rev. D **81** (2010) 074023 [arXiv:1001.4495 [hep-ph]].
- [225] S. Frixione, B. R. Webber, JHEP **0206** (2002) 029 [hep-ph/0204244].
- [226] E. Bagnaschi, G. Degrossi, P. Slavich, A. Vicini, JHEP **1202** (2012) 088 [arXiv:1111.2854 [hep-ph]].
- [227] A. Banfi, G. P. Salam, G. Zanderighi, JHEP **1206** (2012) 159 [arXiv:1203.5773 [hep-ph]];  
 A. Banfi, P. F. Monni, G. P. Salam, G. Zanderighi, Phys. Rev. Lett. **109** (2012) 202001 [arXiv:1206.4998 [hep-ph]].
- [228] R. N. Cahn, S. Dawson, Phys. Lett. B **136** (1984) 196 [Erratum-ibid. B **138** (1984) 464].
- [229] V. D. Barger, R. J. N. Phillips, D. Zeppenfeld, Phys. Lett. B **346** (1995) 106 [hep-ph/9412276];  
 D. L. Rainwater, D. Zeppenfeld, JHEP **9712** (1997) 005 [hep-ph/9712271] and Phys. Rev. D **60** (1999) 113004 [Erratum-ibid. D **61** (2000) 099901] [hep-ph/9906218];  
 D. L. Rainwater, D. Zeppenfeld, K. Hagiwara, Phys. Rev. D **59** (1998) 014037 [hep-ph/9808468];  
 V. Del Duca *et al.*, JHEP **0610** (2006) 016 [hep-ph/0608158].
- [230] V. Del Duca *et al.*, Nucl. Phys. B **616** (2001) 367 [hep-ph/0108030].
- [231] A. Nikitenko, M. L. Vazquez Acosta, arXiv:0705.3585 [hep-ph].
- [232] T. Han, G. Valencia, S. Willenbrock, Phys. Rev. Lett. **69** (1992) 3274 [hep-ph/9206246].
- [233] T. Figy, C. Oleari, D. Zeppenfeld, Phys. Rev. D **68** (2003) 073005 [hep-ph/0306109];  
 T. Figy, D. Zeppenfeld, Phys. Lett. B **591** (2004) 297 [hep-ph/0403297].
- [234] M. Ciccolini, A. Denner, S. Dittmaier, Phys. Rev. Lett. **99** (2007) 161803 [arXiv:0707.0381 [hep-ph]] and Phys. Rev. D **77** (2008) 013002 [arXiv:0710.4749 [hep-ph]].
- [235] R. V. Harlander, J. Vollinga, M. M. Weber, Phys. Rev. D **77** (2008) 053010 [arXiv:0801.3355 [hep-ph]].
- [236] P. Bolzoni, F. Maltoni, S. -O. Moch, M. Zaro, Phys. Rev. Lett. **105** (2010) 011801 [arXiv:1003.4451 [hep-ph]].
- [237] P. Bolzoni, F. Maltoni, S. -O. Moch, M. Zaro, Phys. Rev. D **85** (2012) 035002 [arXiv:1109.3717 [hep-ph]].
- [238] J. R. Andersen, T. Binoth, G. Heinrich, J. M. Smillie, JHEP **0802** (2008) 057 [arXiv:0709.3513 [hep-ph]];  
 A. Bredenstein, K. Hagiwara, B. Jäger, Phys. Rev. D **77** (2008) 073004 [arXiv:0801.4231 [hep-ph]].
- [239] P. Nason, C. Oleari, JHEP **1002** (2010) 037 [arXiv:0911.5299 [hep-ph]].
- [240] T. Figy, S. Palmer, G. Weiglein, JHEP **1202** (2012) 105 [arXiv:1012.4789 [hep-ph]].
- [241] K. Arnold *et al.*, VBFNLO, <http://www-itp.particle.uni-karlsruhe.de/vbfnloweb>, 2009.
- [242] A. Denner, S. Dittmaier, S. Kallweit, A. Mück, HAWK, <http://omnibus.uni-freiburg.de/sd565/programs/hawk/hawk.html>, 2010.
- [243] P. Bolzoni, F. Maltoni, S. Moch, M. Zaro, VBF@NNLO, <http://vbf-nnlo.phys.ucl.ac.be/vbf.html>, 2011.
- [244] S. L. Glashow, D. V. Nanopoulos, A. Yildiz, Phys. Rev. D **18** (1978) 1724;  
 J. Finjord, G. Girardi, P. Sorba, Phys. Lett. B **89** (1979) 99.

- [245] T. Han, S. Willenbrock, Phys. Lett. **B273** (1991) 167;  
H. Baer, B. Bailey, J. F. Owens, Phys. Rev. **D47** (1993) 2730;  
J. Ohnemus, W. J. Stirling, Phys. Rev. **D47** (1993) 2722.
- [246] O. Brein, A. Djouadi, R. Harlander, Phys. Lett. **B579** (2004) 149 [hep-ph/0307206].
- [247] G. Ferrera, M. Grazzini, F. Tramontano, Phys. Rev. Lett. **107** (2011) 152003 [arXiv:1107.1164 [hep-ph]].
- [248] L. Altenkamp *et al.*, JHEP **1302** (2013) 078 [arXiv:1211.5015 [hep-ph]].
- [249] O. Brein, R. Harlander, M. Wiesemann, T. Zirke, Eur. Phys. J. C **72** (2012) 1868 [arXiv:1111.0761 [hep-ph]].
- [250] M. L. Ciccolini, S. Dittmaier, M. Krämer, Phys. Rev. **D68** (2003) 073003 [hep-ph/0306234].
- [251] A. Denner, S. Dittmaier, S. Kallweit, A. Mück, JHEP **1203** (2012) 075 [arXiv:1112.5142 [hep-ph]].
- [252] A. Banfi, J. Cancino, Phys. Lett. B **718** (2012) 499 [arXiv:1207.0674 [hep-ph]].
- [253] O. Brein, R. V. Harlander, T. J. E. Zirke, Comput. Phys. Commun. **184** (2013) 998 [arXiv:1210.5347 [hep-ph]].
- [254] M. Spira, V2HV, <http://people.web.psi.ch/spira/v2hv>, 2007.
- [255] R. Raitio, W. W. Wada, Phys. Rev. D **19** (1979) 941;  
Z. Kunszt, Nucl. Phys. B **247** (1984) 339;  
J. N. Ng, P. Zakarauskas, Phys. Rev. D **29** (1984) 876.
- [256] W. Beenakker *et al.*, Phys. Rev. Lett. **87** (2001) 201805 [hep-ph/0107081] and Nucl. Phys. B **653** (2003) 151 [hep-ph/0211352];  
L. Reina, S. Dawson, Phys. Rev. Lett. **87** (2001) 201804 [arXiv:hep-ph/0107101];  
L. Reina, S. Dawson, D. Wackerroth, Phys. Rev. D **65** (2002) 053017 [arXiv:hep-ph/0109066];  
S. Dawson, L. H. Orr, L. Reina, D. Wackerroth, Phys. Rev. D **67** (2003) 071503 [arXiv:hep-ph/0211438];  
S. Dawson *et al.*, Phys. Rev. D **68** (2003) 034022 [arXiv:hep-ph/0305087].
- [257] R. Frederix *et al.*, Phys. Lett. B **701** (2011) 427 [arXiv:1104.5613 [hep-ph]].
- [258] M. V. Garzelli, A. Kardos, C. G. Papadopoulos, Z. Trocsanyi, Europhys. Lett. **96** (2011) 11001 [arXiv:1108.0387 [hep-ph]].
- [259] A. Bredenstein, A. Denner, S. Dittmaier, S. Pozzorini, JHEP **0808** (2008) 108 [arXiv:0807.1248 [hep-ph]], Phys. Rev. Lett. **103** (2009) 012002 [arXiv:0905.0110 [hep-ph]] and JHEP **1003** (2010) 021 [arXiv:1001.4006 [hep-ph]];  
G. Bevilacqua *et al.*, JHEP **0909** (2009) 109 [arXiv:0907.4723 [hep-ph]].
- [260] G. Bevilacqua, M. Czakon, C. G. Papadopoulos, M. Worek, Phys. Rev. Lett. **104** (2010) 162002 [arXiv:1002.4009 [hep-ph]] and Phys. Rev. D **84** (2011) 114017 [arXiv:1108.2851 [hep-ph]].
- [261] M. Dührssen *et al.*, Phys. Rev. D **70** (2004) 113009 [hep-ph/0406323].
- [262] ATLAS Collaboration, ATL-PHYS-PUB-2012-004.
- [263] CMS Collaboration, CMS-NOTE-2012-006.
- [264] R. Lafaye *et al.*, JHEP **0908** (2009) 009 [arXiv:0904.3866 [hep-ph]].
- [265] ATLAS Collaboration, ATLAS-CONF-2012-127.
- [266] CMS Collaboration, CMS PAS HIG-12-045.
- [267] LHC Higgs Cross Section Working Group, A. David *et al.*, arXiv:1209.0040 [hep-ph].
- [268] G. Passarino, Nucl. Phys. B **868** (2013) 416 [arXiv:1209.5538 [hep-ph]].

- [269] E. W. N. Glover, J. J. van der Bij, Nucl. Phys. B **309** (1988) 282;  
D. A. Dicus, C. Kao, S. S. D. Willenbrock, Phys. Lett. B **203** (1988) 457;  
T. Plehn, M. Spira, P. M. Zerwas, Nucl. Phys. B **479** (1996) 46 [Erratum-ibid. B **531** (1998) 655] [hep-ph/9603205].
- [270] S. Dawson, S. Dittmaier, M. Spira, Phys. Rev. D **58** (1998) 115012 [hep-ph/9805244].
- [271] V. D. Barger, T. Han, R. J. N. Phillips, Phys. Rev. D **38** (1988) 2766;  
M. Moretti *et al.*, JHEP **1011** (2010) 097 [arXiv:1008.0820 [hep-ph]].
- [272] A. Djouadi, W. Kilian, M. Mühlleitner, P. M. Zerwas, Eur. Phys. J. C **10** (1999) 45 [hep-ph/9904287].
- [273] W. -Y. Keung, Mod. Phys. Lett. A **2** (1987) 765;  
O. J. P. Eboli, G. C. Marques, S. F. Novaes, A. A. Natale, Phys. Lett. B **197** (1987) 269;  
D. A. Dicus, K. J. Kallianpur, S. S. D. Willenbrock, Phys. Lett. B **200** (1988) 187;  
A. Abbasabadi, W. W. Repko, D. A. Dicus, R. Vega, Phys. Lett. B **213** (1988) 386.
- [274] T. Figy, Mod. Phys. Lett. A **23** (2008) 1961 [arXiv:0806.2200 [hep-ph]].
- [275] U. Baur, T. Plehn, D. L. Rainwater, Phys. Rev. D **67** (2003) 033003 [hep-ph/0211224].
- [276] U. Baur, T. Plehn, D. L. Rainwater, Phys. Rev. D **69** (2004) 053004 [hep-ph/0310056].
- [277] T. Plehn, M. Rauch, Phys. Rev. D **72** (2005) 053008 [hep-ph/0507321];  
T. Binoth, S. Karg, N. Kauer, R. Rückl, Phys. Rev. D **74** (2006) 113008 [hep-ph/0608057].
- [278] T. Aaltonen *et al.* [CDF Collaboration], JHEP **1302** (2013) 004 [arXiv:1208.6445 [hep-ex]].
- [279] Tevatron New Physics Higgs Working Group and CDF and D0 Collaborations, arXiv:1207.0449 [hep-ex].
- [280] T. Aaltonen *et al.* [CDF Collaboration], Phys. Lett. B **717** (2012) 173 [arXiv:1207.6386 [hep-ex]].
- [281] V. M. Abazov *et al.* [D0 Collaboration], Phys. Rev. Lett. **107** (2011) 151801 [arXiv:1107.4587 [hep-ex]].
- [282] T. Aaltonen *et al.* [CDF Collaboration], Phys. Rev. D **86** (2012) 072012 [arXiv:1207.5016 [hep-ex]].
- [283] T. Aaltonen *et al.* [CDF Collaboration], Phys. Rev. Lett. **109** (2012) 181802 [arXiv:1208.2662 [hep-ex]].
- [284] T. Aaltonen *et al.* [CDF Collaboration], Phys. Rev. Lett. **108** (2012) 181804 [arXiv:1201.4880 [hep-ex]].
- [285] V. M. Abazov *et al.* [D0 Collaboration], Phys. Lett. B **714** (2012) 237 [arXiv:1203.4443 [hep-ex]].
- [286] V. M. Abazov *et al.* [D0 Collaboration], Phys. Rev. Lett. **106** (2011) 171802 [arXiv:1101.6079 [hep-ex]].
- [287] T. Aaltonen *et al.* [CDF Collaboration], Phys. Rev. Lett. **104** (2010) 061803, [arXiv:1001.4468 [hep-ex]].
- [288] V. M. Abazov *et al.* [D0 Collaboration], Phys. Rev. D **84** (2011) 092002 [arXiv:1107.1268 [hep-ex]].
- [289] M. L. Mangano *et al.*, JHEP **0307** (2003) 001 [hep-ph/0206293].
- [290] E. Boos *et al.* [CompHEP Collaboration], Nucl. Instrum. Meth. A **534** (2004) 250 [hep-ph/0403113].
- [291] G. Corcella *et al.*, JHEP **0101** (2001) 010 [hep-ph/0011363].
- [292] M. Bahr *et al.*, Eur. Phys. J. C **58** (2008) 639 [arXiv:0803.0883 [hep-ph]].
- [293] S. Frixione *et al.*, arXiv:1010.0819 [hep-ph].
- [294] T. Gleisberg *et al.*, JHEP **0902** (2009) 007 [arXiv:0811.4622 [hep-ph]].
- [295] T. Aaltonen *et al.* [CDF Collaboration], Phys. Rev. Lett. **109** (2012) 111804 [arXiv:1207.1703 [hep-ex]].



- [296] V. M. Abazov *et al.* [D0 Collaboration], Phys. Rev. Lett. **109** (2012) 121804 [arXiv:1208.0653 [hep-ex]].
- [297] T. Aaltonen *et al.* [CDF Collaboration], Phys. Rev. Lett. **109** (2012) 111805 [arXiv:1207.1711 [hep-ex]].
- [298] V. M. Abazov *et al.* [D0 Collaboration], Phys. Lett. B **716** (2012) 285 [arXiv:1207.5689 [hep-ex]].
- [299] T. Aaltonen *et al.* [CDF Collaboration], Phys. Rev. Lett. **109** (2012) 111803 [arXiv:1207.1704 [hep-ex]].
- [300] V. M. Abazov *et al.* [D0 Collaboration], Phys. Rev. Lett. **109** (2012) 121803 [arXiv:1207.5819 [hep-ex]].
- [301] V. M. Abazov *et al.* [D0 Collaboration], Phys. Rev. Lett. **109** (2012) 121802 [arXiv:1207.6631 [hep-ex]].
- [302] T. Aaltonen *et al.* [CDF Collaboration], Phys. Rev. Lett. **109** (2012) 111802 [arXiv:1207.1707 [hep-ex]].
- [303] T. Aaltonen *et al.* [CDF and D0 Collaborations], Phys. Rev. Lett. **109** (2012) 071804, [arXiv:1207.6436 [hep-ex]].
- [304] M. Dittmar, H. K. Dreiner, Phys. Rev. D **55** (1997) 167 [hep-ph/9608317].
- [305] T. Aaltonen *et al.* [CDF and D0 Collaborations], Phys. Rev. Lett. **104** (2010) 061802 [arXiv:1001.4162 [hep-ex]].
- [306] V. M. Abazov *et al.* [D0 Collaboration],
- [307] V. M. Abazov *et al.* [D0 Collaboration], Phys. Rev. D **86** (2012) 032010 [arXiv:1207.1041 [hep-ex]].
- [308] The LHC Higgs Cross Section Working Group,  
<https://twiki.cern.ch/twiki/bin/view/LHCPhysics/CrossSections> .
- [309] J. Alwall *et al.*, JHEP **1106** (2011) 128 [arXiv:1106.0522 [hep-ph]].
- [310] T. Binoth, M. Ciccolini, N. Kauer, M. Krämer, JHEP **0503** (2005) 065 [hep-ph/0503094].
- [311] T. Binoth, N. Kauer, P. Mertsch, arXiv:0807.0024 [hep-ph].
- [312] ATLAS Collaboration, Eur. Phys. J. C **71** (2011) 1728 [arXiv:1106.2748 [hep-ex]].
- [313] CMS Collaboration, Phys. Lett. B **699** (2011) 25
- [314] ATLAS Collaboration, Phys. Rev. D **86** (2012) 032003 [arXiv:1207.0319 [hep-ex]].
- [315] CMS Collaboration, Phys. Lett. B **710** (2012) 26 [arXiv:1202.1488 [hep-ex]].
- [316] ATLAS Collaboration, Phys. Rev. Lett. **108** (2012) 111803 [arXiv:1202.1414 [hep-ex]].
- [317] ATLAS Collaboration, Phys. Lett. B **716** (2012) 1 [arXiv:1207.7214 [hep-ex]].
- [318] CMS Collaboration, Phys. Lett. B **710** (2012) 403 [arXiv:1202.1487 [hep-ex]].
- [319] CMS Collaboration, Phys. Lett. B **716** (2012) 30 [arXiv:1207.7235 [hep-ex]].
- [320] ATLAS Collaboration, JHEP **1209** (2012) 070 [arXiv:1206.5971 [hep-ex]].
- [321] CMS Collaboration, Phys. Lett. B **713** (2012) 68 [arXiv:1202.4083 [hep-ex]].
- [322] ATLAS Collaboration, Phys. Lett. B **718** (2012) 369 [arXiv:1207.0210 [hep-ex]].
- [323] CMS Collaboration, Phys. Lett. B **710** (2012) 284 [arXiv:1202.4195 [hep-ex]].
- [324] ATLAS Collaboration, Phys. Lett. B **710** (2012) 383 [arXiv:1202.1415 [hep-ex]].
- [325] CMS Collaboration, Phys. Rev. Lett. **108** (2012) 111804 [arXiv:1202.1997 [hep-ex]].
- [326] ATLAS Collaboration, Phys. Lett. B **716** (2012) 62 [arXiv:1206.0756 [hep-ex]].
- [327] CMS Collaboration, Phys. Lett. B **710** (2012) 91 [arXiv:1202.1489 [hep-ex]].
- [328] CMS Collaboration, JHEP **1203** (2012) 081 [arXiv:1202.3617 [hep-ex]].

- [329] ATLAS Collaboration, Phys. Lett. B **717** (2012) 70 [arXiv:1206.2443 [hep-ex]].
- [330] CMS Collaboration, JHEP **1204** (2012) 036 [arXiv:1202.1416 [hep-ex]].
- [331] ATLAS Collaboration, Phys. Lett. B **717** (2012) 29 [arXiv:1205.6744 [hep-ex]].
- [332] CMS Collaboration, JHEP **1203** (2012) 040 [arXiv:1202.3478 [hep-ex]].
- [333] ATLAS Collaboration, Phys. Lett. B **718** (2012) 391 [arXiv:1206.6074 [hep-ex]].
- [334] Y. Gao *et al.*, Phys. Rev. D **81** (2010) 075022 [arXiv:1001.3396 [hep-ph]].
- [335] ATLAS Collaboration, Phys. Lett. B **710** (2012) 49 [arXiv:1202.1408 [hep-ex]].
- [336] R. K. Ellis, I. Hinchliffe, M. Soldate, J. J. van der Bij, Nucl. Phys. B **297** (1988) 221.
- [337] A. Elagin, P. Murat, A. Pranko, A. Safonov, Nucl. Instrum. Meth. A **654** (2011) 481 [arXiv:1012.4686 [hep-ex]].
- [338] L. D. Landau, Dokl. Akad. Nauk USSR **60** (1948) 207,  
C. N. Yang, Phys. Rev. **77** (1950) 242.